DROP-ON-DEMAND INKJET DEPOSITION

OF COMPLEX FLUID ON TEXTILES

A Dissertation
Presented to
The Academic Faculty

by

Xi Wang

In Partial Fulfillment
of the Requirements for the Degree
Doctor of Philosophy in the
School of Polymer, Textile and Fiber Engineering

Georgia Institute of Technology
December 2008

DROP-ON-DEMAND INKJET DEPOSITION

OF COMPLEX FLUID ON TEXTILES

Approved by:

Dr. Wallace W. Carr, Advisor
School of Polymer, Textile and Fiber Engineering
Georgia Institute of Technology

Dr. Anselm Griffin
School of Polymer, Textile and Fiber Engineering
Georgia Institute of Technology

Dr. David G. Bucknall
School of Polymer, Textile and Fiber Engineering
Georgia Institute of Technology

Dr. Carson J. Meredith
School of Chemical and Biomolecular Engineering
Georgia Institute of Technology

Dr. Jeffrey F. Morris
Benjamin Levich Institute and Department of Chemical Engineering
City College of New York

Date Approved: [07 28, 2008]

To My Parents and Wenzhan

ACKNOWLEDGEMENTS

I would like to thank my father and mother (Zhaochuan Wang and Guolan Li) for all of their moral and financial support throughout these years. It is merely possible for me to accomplish this task without them. I would also like to thank Wenzhan for her encouragement and support without which I could not have started this journey.

Especially, I would like to thank my advisor (Dr. Wallace W. Carr) for his patience, discipline, guidance and encouragement. It is through his great effort and willingness to spend time with me that I could take the road to the Ph.D. I have learned a lot from him over the years in research and living my life. I would also like to thank Dr. Bucknall and Dr. Morris for all of their scientific and technical advices and great suggestions on my research work. I would also like to thank Dr. Griffin and Dr. Meredith for serving on my committee and providing helpful advices throughout this Ph.D. process. I would like to thank Dr. Hongming Dong, Dr. Heungsup Park, Dr. Hyunyoung Ok, and Mr. Dan Brooks for their valuable cooperation and discussion.

Thanks also to the members of the North Avenue Presbyterian Church for their love, support, and prayer and all my friends for the happy time we spent together.

TABLE OF CONTENTS

LIST OF TABLES

LIST OF FIGURES

SUMMARY

The objective of the research was to develop fundamental understanding of the process of deposition of complex mixtures by the inkjet method. Motivation for this work resulted from the requirement that "inks" in a growing number of textile applications contain solid particles, typically also requiring additives including dispersants. Such inks are likely to be highly solids-laden and non-Newtonian, and predictions of behavior based on existing understanding of drop formation from Newtonian liquids may be unsatisfactory. The formulation of high performance / high value-added treatments in the form of inks for textiles greatly affects deposition and ink-substrate interaction. Characterization of the effects of the various components of the solids-laden inks on drop formation and substrate interaction is crucial to utilization.

In the first part of the research, the rheological properties and DOD drop formation dynamics of carbon black pigmented inkjet inks were investigated. It was found that the suspension microstructure responds to bulk motions, leading to shear rate and time dependent shear viscosity. However, DOD drop formation dynamics of highly pigmented inkjet ink and pure Newtonian fluid was similar even though shear rate up to 2×10^{5} s^{-1} exists during inkjet jetting process. A proposed explanation for these observations is that the shearing time during DOD drop ejection is insufficient for changing and stabilizing the microstructure of the suspension.

The second part of the research contributes to the understanding of DOD drop formation dynamics of pure Newtonian fluids and builds on the work done previously in our group. The focus was on the effects of signal amplitude and jetting frequency on

DOD drop formation dynamics. Higher signal amplitude led to higher speeds of primary drop and satellites and larger liquid volume ejected. The reproducibility of evolution of the secondary liquid thread was very low once voltage amplitude was increased to a level where the wave-like instability breakup occurred. Jetting frequency was found to affect the volume and speed of ejected liquid body when it is sufficiently high. When the nozzle went from idle to jetting, the drop triggered by the first pulse was found to be identical and independent of jetting frequency. However, at sufficiently high jetting frequency, DOD drop formation varied over the first four pulses after idle. A modulating pulse added before the first pulse eliminated the variation in drop formation at the higher jetting frequencies.

The last part of the thesis was a qualitative investigation of DOD drop impaction and post-impaction on inkjet paper and textiles. Dynamics of DOD drop accumulation and spreading on the substrates and final ink distribution show drastic differences between these two substrates. The final ink distributions on inkjet paper resembled irregular circles, with their size increasing as the number of drops increased. The final ink distribution on fabric was greatly affected by the fabric structure, that is, the yarn direction and intersections. The ink tended to stay on one yarn as drops accumulated until excess ink moved to neighboring yarns. As the number of drops increased, the primary change in the ink distribution on the cotton fabric was the increasing distance over which the ink spread along the yarns. Fibers protrude from the surface of the cotton yarns, creating a "hairy" fabric. These fibers can affect the distribution of ink on the fabric.

CHAPTER 1

INTRODUCTION

Inkjet printing is a non-impact printing technology in which drops of tens of picoliter are jetted from a small capillary orifice (usually less than 100-μm diameter) onto a designated position on a substrate such as inkjet paper. Historically, two micro-drop formation techniques, continuous inkjet printing and drop-on-demand (DOD) inkjet printing, were developed during the same period of time. In 1965, Sweet reported how drops with uniform size and distance can be formed at high frequency by applying a pressure wave to an orifice [3], which is now called continuous inkjet printing technology. After reliably and continuously generating drops through liquid breakup, selected drops are electrically charged so that when they pass through an electric field, they are deflected to a collection chamber and recirculated. The uncharged drops are unaffected by the electric field and fly onto the media for imaging purposes.

Drop-on-demand (DOD) inkjet printing technology was developed in the 1970's. As indicated by its name, DOD inkjet printing involves devices which eject drops only when demanded. This approach reduces the complexity of continuous inkjet printing since the electric field and recirculation system are not required. Rapid development and commercialization of DOD inkjet printing was started in mid-1970s [6, 7]. At the early stage, the major type of devices for generating DOD drops involved piezoelectric ceramic. By applying electric pulses to a piezoelectric material, mechanical motions are produced which induce pressure waves in the capillary tube, causing ink to be squeezed out of the nozzle opening. A second mode of DOD inkjet printing is called thermal inkjet printing. Instead of using piezoelectric material to generate mechanical motion, thermal inkjet printing utilizes a small heater inside the nozzle chamber to generate a vapor bubble. The growth and collapse of the bubble induce pressure variations and cause DOD drop

formation. The mechanism may constrain potential applications due to the high temperature generated by the heater which may degrade materials dissolved or dispersed in the inkjet inks.

As DOD inkjet technology offers the opportunities of constructing macroscopic objects from microscopic elements [8], it has received great attention from both industry and academy in utilizing this technology to fabricate functional objects. By defining the formation of one drop as "1" and no drop as "0", inkjet printing can be considered a binary material delivery system. If the drop volume formed by the DOD drop formation process can be reduced to 5 picoliter, line resolution of 10 μm is possible in the future. By dissolving and/or dispensing functional materials in a solvent to form complex fluids and tuning rheological and physiochemical properties to achieve jettability, in principle, a 3D printer [9] can be developed to allow digital fabrication processing. The ultimate goal of developing this technology could be *digitally* transporting fluids containing polymers, particles, cells, etc. in the form of picoliter-size droplets precisely onto desired substrates to, for example, construct three dimensional objects with feature resolution of as small as 10 μm.

Figure 1-1 shows the number of publications with topics related to inkjet printing technology versus time based on data from ISI Web of Knowledge^{SM}. Attention to both developing inkjet printing technology and applying it to delivery varied materials such as polymers has increased sharply over last ten years. The applications of inkjet printing technology are being expanded from monochromatic and color printing on flat substrate to textile printing [10-18], fabrication of complex shapes of ceramic structures [19-25], fabrication of electronics [25-29], maskless lithography [29-31], rapid prototyping and tooling (RPT) [31-33], and transporting bio-materials [1, 34-36]. De Gans *et al*. [2] gave an excellent review on the application of inkjet printing on delivering polymeric materials.

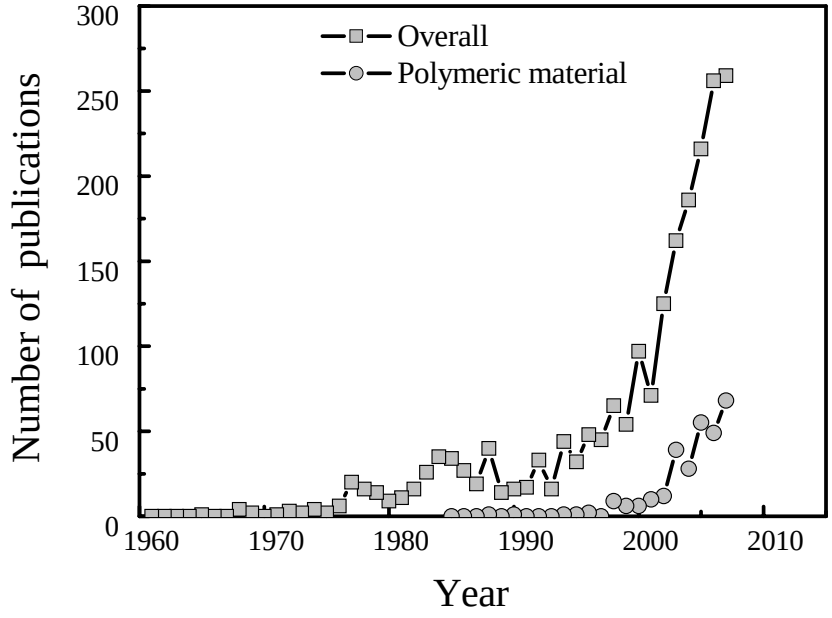

Figure 1-1: Number of publications with topics related to inkjet printing technology versus time (data were obtained by using ISI Web of Knowledge^{SM}).

Despite of all the research conducted, fundamental understanding of DOD drop formation and impaction is still lacking. Considering the complexity of inkjet nozzle design and actuating mechanism, rheological and physiochemical properties of the inkjet inks, variety of the substrates, and interactions among them, making inkjet printing an industrial fabrication tool is challenging.

Several of the existing/potential problems in applying inkjet printing technology will be discussed next. The first issue is that the content of functional materials in inkjet inks is often low because shear viscosity must be kept below a threshold limit to ensure jettability. The utilization of inkjet inks with high material loading could increase the efficiency of material delivery and thus be beneficial in increasing the penetration of inkjet printing technology into various fabrication processes. Inkjet inks with high

volume fraction of functional materials are being developed with shear viscosity at elevated jetting temperature in the range suitable for commercially available inkjet printheads [20-24]. However, little effort has been made to understand the role of rheological properties of inkjet inks in the DOD drop formation process.

With high volume fraction of functional materials such as colloidal particles and polymeric materials, inkjet inks may exhibit various non-Newtonian behaviors, such as dependence of viscosity on shear rate and/or shearing time, viscoelasticity, and varying extensional viscosity [4]. Even though ultra-high shear rates (up to 10^6 s^{-1}) occur during the emergence of liquid thread from the inkjet nozzle as indicated by data discussed in Chapter 4, apparent shear viscosity measured at low shear rates is currently being used throughout the inkjet industry to characterize inkjet inks containing these functional materials. Thus the characterization of the flow properties of inkjet inks in terms of shear-rate dependent, temperature dependent, and time dependent viscosity is badly needed. The understanding of the structural response of the colloidal/non-colloidal particles and particle agglomerates, polymeric materials, cells, etc. to a high shear flow field is also very important.

For DOD drop formation process, the length scale is ~ O(100 μm), confined by the nozzle size, and the time scale is ~ O(100 μs), depending on the jetting frequency. In this process, the shear rate can be as high as 10^6 s^{-1} and the rate of surface dilatational deformation can be as high as 10^5 s^{-1}. Understanding of how the interactions among particles, surfactants and polymeric materials are affected by the strong shearing field is needed to explain and predict DOD drop formation performance of varied inkjet inks and ink/nozzle compatibility. Due to the extremely small temporal and spatial scales, investigation to reveal the response of particles (colloidal and non-colloidal, rigid and deformable, individual and aggregated, steric dispersed and electrostatic dispersed), surfactants, and dissolved polymers (various molecular weight, chain structure, etc.) to

the strong hydrodynamic motion and drastic free surface evolution is extremely difficult to conduct.

Another issue needed to be addressed is how micron-size drops interact with substrates with roughness, porosity, and/or chemical heterogeneity. For these substrates, there is competition between spreading and penetration. After the drying process, the distribution of functional materials is non-axisymmetric and three dimensional.

In Figure 1-2, the complexity of DOD drop deposition of functional materials is illustrated using steric-dispersed rigid colloidal particles. The whole DOD drop deposition process, including drop formation, impaction, and drying, takes less than 1 s [5] and involves physical and chemical processes which will be selectively discussed in this thesis.

In this dissertation research, the DOD drop formation dynamics and rheological properties of surface-modified-carbon-black pigmented water-based inkjet inks have been studied. To facilitate the rheological study, a capillary viscometer was developed to measure the apparent shear viscosity of inkjet inks at shear rate up to 2×10^5 s^{-1}. Impaction of Newtonian fluids on inkjet paper and textiles were also investigated. A high-resolution high-speed continuous imaging system was developed and used for studying multi-DOD drop impaction.

In each of the chapters 2-6, the following sections are included: background and literature review, objective, experimental, results and discussion, and conclusions. Rheological properties of inkjet inks, DOD drop formation, and DOD drop impaction are covered in these chapters. Chapter 7 contains a summary of conclusions and recommendations for future work.

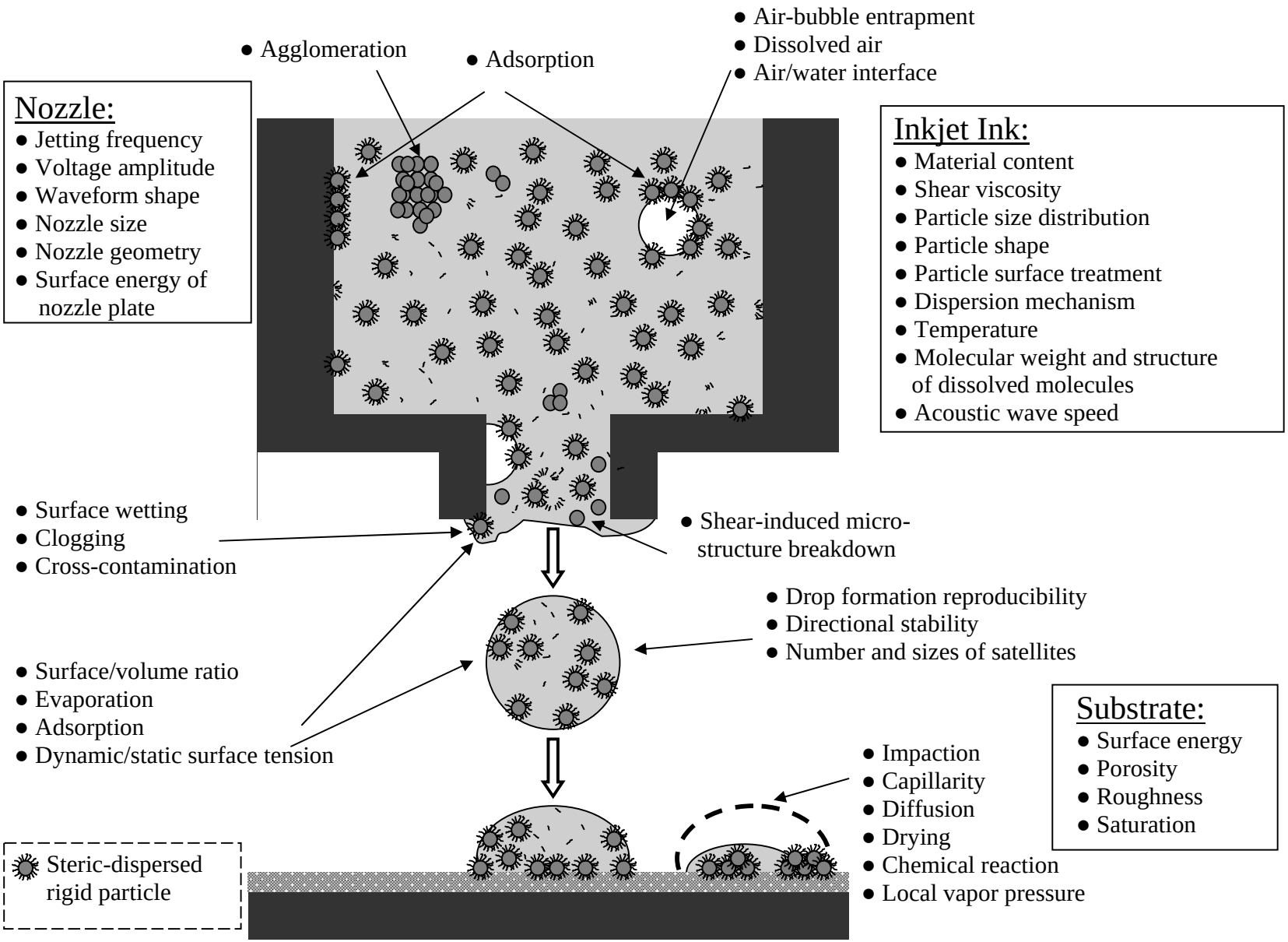

Figure 1-2: Important factors related to DOD deposition of steric-dispersed rigid colloidal particles. Concept for this schematic was taken from Figure 4 in reference 34.

1.1 References

1. Sumerel, J., Lewis, J., Doraiswamy, A., et al., Biotech. J. 1, 976 (2006).
2. De Gans, B.J., Duineveld, P.C., and Schubert, U.S., Adv. Mater.16, 203 (2004).
3. Sweet, R. G., Rev. Sci. Instrum. 36, 131-136 (1965).
4. Macosko, C. W., Rheology: principles, measurements, and applications, New York: VCH, (1994).
5. Dong, H., Drop-on-demand inkjet drop formation and deposition, Doctorial dissertation, Georgia Institute of Technology, Atlanta, (2006).
6. Zoltan, S. L., U. S. Patent 3683212 (1974).
7. Kyser, E. L. and Sears, S. B., U. S. Patent 3946398 (1976).
8. Gershenfeld, N., FAB: the coming revolution on your desktop – from personal computers to personal fabrication, Basic Books, New York, (2005).
9. http://www.livescience.com/technology/top10-transform-tech-1.html, (08/2008)
10. Tyler, D. J., Textile Prog. 37, 66 (2005).
11. Tippett, B.G., International Conference on Digital Production Printing and Industrial Applications: Final Program and Proceedings, 276 (2003).
12. Sarma, D., Textile World 154, 42 (2004).
13. Hees, U., Freche, M., Kluge, M., Provost, J., and Weiser, J., Final Program and Proceedings of IS&T's NIP 19, 626 (2003).
14. Kiatkamjornwong, S., Putthimai, P., and Noguchi, H., Surface Coatings International Part B: Coatings Transactions 88, 25 (2005).
15. Sarma, D. and Liker, S., Final Program and Proceedings of IS&T's NIP 21, 245 (2005).
16. Le, H., International Conference on Digital Production Printing and Industrial Applications: Final Program and Proceedings, 159 (2005).

17. Kruger, C., Dieleman, C., Kluge, M., Provost, J., and Weiser, J., Final Program and Proceedings of IS&T's NIP20, 610 (2004).
18. El-Molla, M. M., Dyes and Pigments 74, 371 (2007).
19. Derby, B. and Reis N., MRS Bull. 28, 815 (2003).
20. Lee, D. H. and Derby, B., J. Eur. Ceram. Soc. 24, 1069 (2004).
21. Reis N., Ainsley, C., and Derby, B., J. Am. Ceram. Soc. 88, 802 (2005).
22. Reis N., Ainsley, C., and Derby, B., J. Appl. Phys. 97, 094903 (2005).
23. Wang, T. and Derby, B., J. Am. Ceram. Soc. 88, 2053 (2005).
24. Ainsley, C., Reis N., and Derby, B., J. Mater. Sci. 37, 3155 (2002).
25. Tseng, W. J., Lin, S. Y., and Wang, S. R., J. Electroceramics 16, 537 (2006).
26. Subrsmanian, V., Chang, J., Mattis, B., Molesa, S., Redinger, D., De La Fuente Vornbrock, and A., Volkman, S. K., Digital Fabrication 2006, 21 (2006).
27. Gamerith, S., Klug, A., Scheiber, H., et al., Adv. Funct. Mater. 17, 3111 (2007).
28. Beecher, P., Servati, P., Rozhin, A., et al. J. Appl. Phys. 102, 043710 (2007).
29. Ng, T. N., Lujan, R. A., Sambandan, S., et al., Appl. Phys. Lett. 91, 063505 (2007).
30. Wang, Y., Bokor, J., and Lee, A., Proceedings of SPIE 5374, 628 (2004).
31. Roy, S., J. Phys. D: Appl. Phys. 40, R413, (2007).
32. Ainsley, C., Reis N., and Derby, B., J. Mater. Sci. 37, 3155 (2002).
33. Liu, C. Z., Sachlos, E., Wahl, D. A., et al., Rapid Prototyping J. 13, 163 (2007).
34. Zaugg F. G. and Wagner P., MRS Bull. 28, 837 (2003).
35. Sumerel, J., Cytotherapy 8, 14 (2006).
36. Ringeisen, B. R., Othon, C. M., Barron, J. A., et al., Biotech. J. 1, 930 (2006).

CHAPTER 2

SHEAR-RATE AND TEMPERATURE DEPENDENT SHEAR VISCOSITY OF SURFACE-MODIFIED-CARBON-BLACK PIGMENTED WATER-BASED INKJET INKS

2.1 Introduction

The utilization of high material loading in inkjet inks would enhance the penetration of inkjet printing technology into various advanced applications. However, for most commercially available DOD inkjet nozzles, the viscosity of the inkjet ink must be below 100 cP to allow jettability, which limits the volume fraction of functional materials, such as particles and polymers.

Two approaches are being studied to allow increasing the volume fraction of functional materials in inkjet inks while maintaining jettability. One is to maintain the viscosity of inkjet ink low while increasing material loading and the other is to modify the inkjet nozzle. Inkjet inks with high volume fraction of functional materials are being developed with shear viscosity in the range suitable for commercially available inkjet printheads at elevated jetting temperature. Derby and coworkers [1-6] have prepared highly loaded particulate suspensions for freeform fabrication of 3D ceramic structures. They prepared suspensions with particle volume fraction up to 45% and delivered them using piezoelectric DOD nozzles at a jetting temperature of 120°C. Although they [3] pointed out that shear rate of up to 10^5 s^{-1} exists in the DOD drop formation process, the maximum shear rate used in their rheological measurements was lower than 500 s^{-1}. It is highly likely that suspensions with particle loading as high as 45 vol% exhibit shear-rate

dependent viscosity at a shear rate of 10^5 s^{-1}, which may affect DOD drop formation dynamics.

Recently, Dong *et al*. [7] compared the DOD drop formation characteristics of two Newtonian fluids with viscosities of 1 and 5 cP. At the same jetting conditions, the primary drop size and total liquid volume jetted were lower for the 5 cP liquid. Shear viscosity indicates the resistance of the liquid to fluid motion. Thus at a higher shear viscosity, more energy is viscously dissipated, and kinetic energy of the jetted liquid body is lower. As a result, both the volume and speed of the jetted liquid body decrease with increasing viscosity. Shear rate as inkjet ink is jetted from the nozzle can be scaled using Dong's data (see Figure 11(a) in reference 7). Calculations indicate that the maximum shear rate is between 1×10^5 and 1×10^6 s^{-1}, depending on the amplitude of the actuating signal to the piezoelectric element.

Since inkjet inks are subjected to very high shear rates in DOD inkjet printing, the characterization of high material loading inkjet inks using shear viscosity measured at low shear rates, which was done in both academy [1-7] and industry [8, 9], is questionable. No experimental data on shear viscosity at shear rate up to 10^5 s^{-1} for inkjet inks was found in the literature. One of the objectives of this thesis research was to investigate the shear rate dependency of shear viscosity of inkjet inks. A capillary rheometer was designed, constructed and used to measure shear viscosity for shear rate ranging from 10^3 to 2×10^5 s^{-1}.

The typical geometries used for measuring viscosity are concentric cylinder, parallel plate, cone/plate, capillary, and slit viscometers [10]; however, at high shear rate, it is difficult to obtain accurate measurements using these viscometers due to secondary flow. For the parallel plate and cone/plate geometry, evaporation at the edges of the gap between the two plates or cone and plate also affects the accuracy of the measurement. Decreasing the gap distance between the two plates of the parallel plate viscometer allows measurement at higher shear rates for some fluids; however, for suspension with

rigid particles, bridging of particles may lead to inaccurate measurement [11]. Typically, for shear rate higher than 10^4 s^{-1}, either a capillary viscometer or a slit viscometer is used.

Capillary viscometry was chosen in this study for measuring shear viscosity of inkjet inks at high shear rate for the following reasons: 1) the fluid motion of inkjet ink in the printhead nozzle is typical annular flow; 2) a capillary viscometer is relatively inexpensive to build and simple to operate; and 3) there is no solvent evaporation and secondary flow at high shear rate. Commercially available capillary viscometers capable of measuring shear viscosity at high shear rate are mostly designed for high-viscosity fluids such as polymer melts. As a result, the sensitivity of the instruments is not sufficient for inkjet inks with low viscosity (typically less than 100 cP). Although the commercially available instruments can be modified to have higher sensitivity, the expense of modification is much higher than the cost of setting up a capillary viscometer specifically for inkjet inks.

One existing pressure-driven ultra high shear viscometer ACAV-A2 from ACA Systems Oy was used to characterize coating color flow (with shear viscosity less than 100 cP at high shear rate) in paper coating at shear rate up to about 5×10^6 s^{-1} [12]. However, the cost of the system is no less than $100,000 and it may not be capable of characterizing inkjet inks with shear viscosity less than 15 cP.

2.2 Objective

The objective of research discussed in this chapter was to characterize the viscosity of inkjet inks over shear rates from about 1 to 2×10^5 s^{-1}. To achieve this objective, a high shear rate capillary viscometer was designed, set up and used to measure shear viscosity of surface-modified-carbon-black pigmented water-based inkjet inks. In order to justify that the rheological data measured by using the developed capillary

viscometer was independent of viscous heating effect, temperature dependent shear viscosity of inkjet inks was also investigated.

2.3 Design and Setup of Capillary Viscometer

2.3.1 Design Considerations

An instrument was designed and constructed for accurately measuring steady state shear viscosity of inkjet inks with viscosity less than 30 cP at shear rate up to 2×10^5 s^{-1}. The design requirements for this instrument are discussed in this section.

Figure 2-1 shows the basic structure of a capillary viscometer. Pressure is applied to the test fluid in a reservoir by using a piston, and the test fluid is pushed through a capillary tube of radius R and length L. The pressure drop over the capillary, Δp, and the

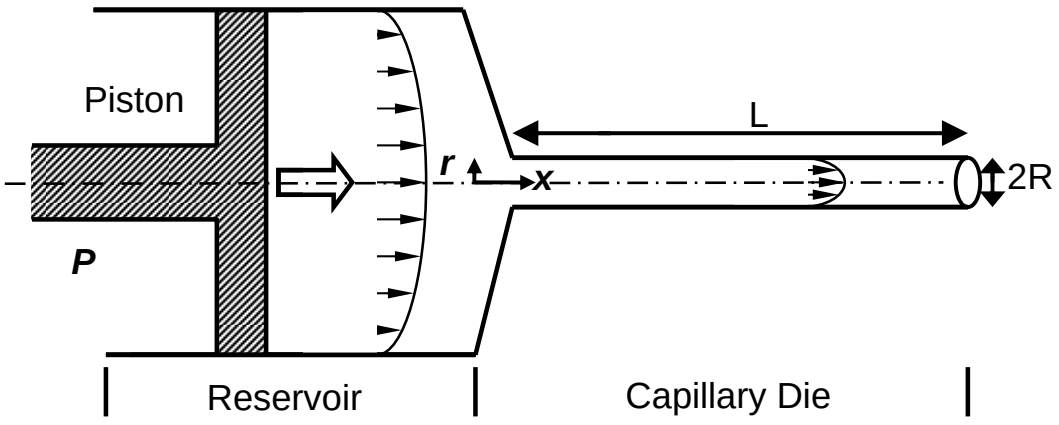

Figure 2-1: Schematic of the basic structure of a capillary viscometer.

volumetric flow rate, Q, are measured. If end effects are negligible, the fluid is Newtonian, and the flow is laminar and isothermal, the shear viscosity at the wall is

$$\eta_w = \frac{\pi R^4 \Delta p}{8QL}\left(\frac{4n}{3n+1}\right), \tag{2-1}$$

and the corresponding shear rate at the capillary wall is

$$\dot{\gamma}_w = \frac{4Q}{\pi R^3}\left(\frac{3n+1}{4n}\right). \tag{2-2}$$

Eq. (2-1) is the so-called Weissenberg-Rabinowitsch equation [10], where $\frac{1}{n} \equiv \frac{d \ln Q}{d \ln \Delta P}$ and $n = 1$ for Newtonian fluids.

In order to neglect the end effects, the ratio of capillary length to capillary radius, *L/R*, should be higher than 60 [10]. In our experiments the minimum value of *L/R* for the capillaries used was greater than 240. The Reynold's number, *Re*, was less than 300 for all test conditions, indicating that the assumption of laminar flow condition was valid. Since the shear viscosity was measured at high shear rate, it was necessary to determine if the flow could be considered isothermal. When the Nahme number, *Na*, is less than 1 [10], viscous heating effects are negligible. For capillary flow,

$$Na = \frac{\beta \eta_w \dot{\gamma}_{aw}^2 R^2}{4k} \qquad [10] \tag{2-3}$$

where β is the temperature sensitivity of viscosity and k is thermal conductivity of the fluid. For the tests conducted in this study, the values of *Na* were less than 0.1.

Among all of the specifications required for the components of the system, the diameter and length of the capillary dies are particularly important and must be optimized so that 1) the sample volume for the test is minimized, 2) the force required to obtain the desired shear rate is less than the upper limit of the system, and 3) the system is simple, easy-to-setup, and easy-to-operate. Eqs. (2-1) and (2-2) were used as guidance for the selection of the components and the determination of the operating procedure of the system, which is presented in detail in the following sections.

2.3.2 Description of Capillary Viscometer

The designed capillary viscometer is shown schematically in Figure 2-2. It was composed of five parts, which are fluid supply, sample refill line, sample testing line, easy plug-in capillary and data acquisition system.

A 100 mL stainless steel syringe (Harvard Apparatus, Part No. BS4 70-2261) and a high pressure programmable syringe pump (Harvard Apparatus, Part No. PHD 4400 Hpsi) were used as the fluid reservoir and the flow rate controller for the "fluid supply" part in Figure 2-2. The syringe had an inside diameter of 34.9 mm (1.374 inch) and a Swagelok fitting connection for high pressure applications. Stainless steel tubing with 3.2 mm (0.125 inch) outside diameter and 1.8 mm (0.069 inch) inside diameter was used as the fluid channel. The syringe pump can deliver a constant flow rate ranging from 0.0001 μL/hr to 220.82 mL/min with 0.35% accuracy and maintain an average linear force up to 890 N (220 lb). With the syringe pump and the system setup shown in Figure 2-2, the maximum operating pressure was 2.4×10^6 Pa (345 psi) at the static pressure sensor, which was sufficient for generating shear rate up to 2×10^5 s^{-1}. The syringe pump can store up to 4 sets of 9 different flow rates, which allowed achieving 9 different shear rates for one capillary die in a single test.

Two fluid lines were designed for refilling the syringe and testing the sample fluid. Quick-connect stems (Swagelok, Part No. SS-QM2-S-200) in both fluid lines were used to connect the lines to a quick-connect body (Swagelok, Part No. SS-QM2-B1-200) on the syringe. Thus, the syringe can be easily refilled by connecting the syringe pump to the refill line using this quick connection. In addition to the quick-connect stem, the sample testing line consisted of an in-line filter (Swagelok, Part No. SS-2F-05) with 0.5 μm pore size for filtering the dusts and large particles in the ink samples, a tee for connecting a static pressure sensor, and a quick-connect body (Swagelok, Part No. SS-QM2-B1-200) for easily switching the capillary dies. Totally three different static

pressure sensors (Omega, Part No. PX309-005 GV, PX309-050 GV, and PX309-500 GV) were used with testing ranges of 0 – 3.45×10^4, 0 – 3.45×10^5, and 0 – 3.45×10^6 Pa (0 – 5.00, 0 – 50.00, and 0 – 500.0 psi), respectively, and ± 0.25% accuracy including linearity, hysteresis and repeatability. The response time of the pressure sensor was less than 1 ms. In order to have sufficient high accuracy of measurement, for each pressure sensor, measured values lower than 10% of the full range were not used; instead, another pressure sensor with a full range that was 10% of the full range of the previous pressure sensor was used. The pressure sensor was also connected to the tee by a quick connect stem and body type configuration so that switching of pressure sensors was easy.

An easy plug-in capillary part consisted of a quick-connect stem (Swagelok, Part No. SS-QM2-S-200) and a Swagelok reducing union (Swagelok, Part No. SS-200-6-1ZV) which held the capillary die. Stainless steel micro-tubing purchased from Scientific Instrument Services, Inc., was used as capillary dies. Stainless steel was chosen because it is chemical resistant to aqueous based inkjet inks and most solvent based inkjet inks. Various combinations of capillary diameters and lengths allowed viscosity measurement covering different viscosity and shear rate ranges as indicated by Eqs. (2-1) and (2-2). Inside diameters of 0.12, 0.20 and 0.25 mm ± 0.025 mm (0.0050, 0.0075 and 0.0100 ± 0.0010 inch) , respectively, with the same outside diameter of 0.50 mm (0.020 inch) were used. Tubing of each size was cut to several lengths. The cutting can cause the ends to be irregular shaped. According to Eq. (2-1), pressure drop over the capillary was inversely proportional to R^4, so the end effect due to the irregular shaped ends could be significant. In order to minimize this effect, a ratio of capillary length L to capillary diameter D was kept higher than 120. Also two cutting methods were used to obtain the desired tube lengths. The first method was to cut the stainless steel micro-tubing using an abrasive cut-off wheel and to deburr the interior of the micro-tubing using a tungsten wire. The second method was to cut it using an electrical discharge machining (EDM) tool. The calibration process using Newtonian fluids showed that the difference of the inside

diameters between the two cases was less than 2.0%. Pressure drop was inversely proportional to R^4 and the inside diameter of the stainless steel tubing and Swagelok fittings was more than 5 times larger than the inside diameter of the capillaries dies. Consequently, the pressure drop caused by the stainless steel tubing and Swagelok fittings was less than 0.2% of the pressure drop induced by the capillary dies. Once the measurement is done, the system can be cleaned up either by using the syringe pump to pump water or solvent through the system or by taking it apart and cleaning it using a sonicator.

In the data acquisition system, a strain gauge meter (Omega, Part No. DP41-S-S2) was used for exciting the static pressure sensors and transferring the measured signal to a computer through RS-232 communication protocol. Windows HyperTerminal® was used to capture and store the data. The strain gauge meter can also display the value of static pressure with two significant numbers after decimal on a LED screen.

2.3.3 Calibration of the Effective Radius of the Capillary Die

Since for a given flow rate, the pressure drop across the capillary die is inversely proportional to R^4, the size of the capillary die is critical in capillary viscometry. For each selected capillary die, a calibration process to obtain the effective capillary radius was carried out using Newtonian fluids with viscosity in the range of 1.0 to 10.0 cP. Before each measurement, the static pressure reading of the strain gauge meter was set to zero. For selected viscosities, flow rate was systematically varied, and the corresponding pressure drop was measured and recorded. The effective radius of the capillary die was then calculated using Eq. (2-1) assuming that the pressure measured by the static pressure sensor was entirely induced by the capillary die. This is a reasonable assumption as the radius of the capillary die was less than one hundredth of the radius of the fluid channel and the pressure drop was inversely proportional to R^4. As an example, Figure 2-3 shows

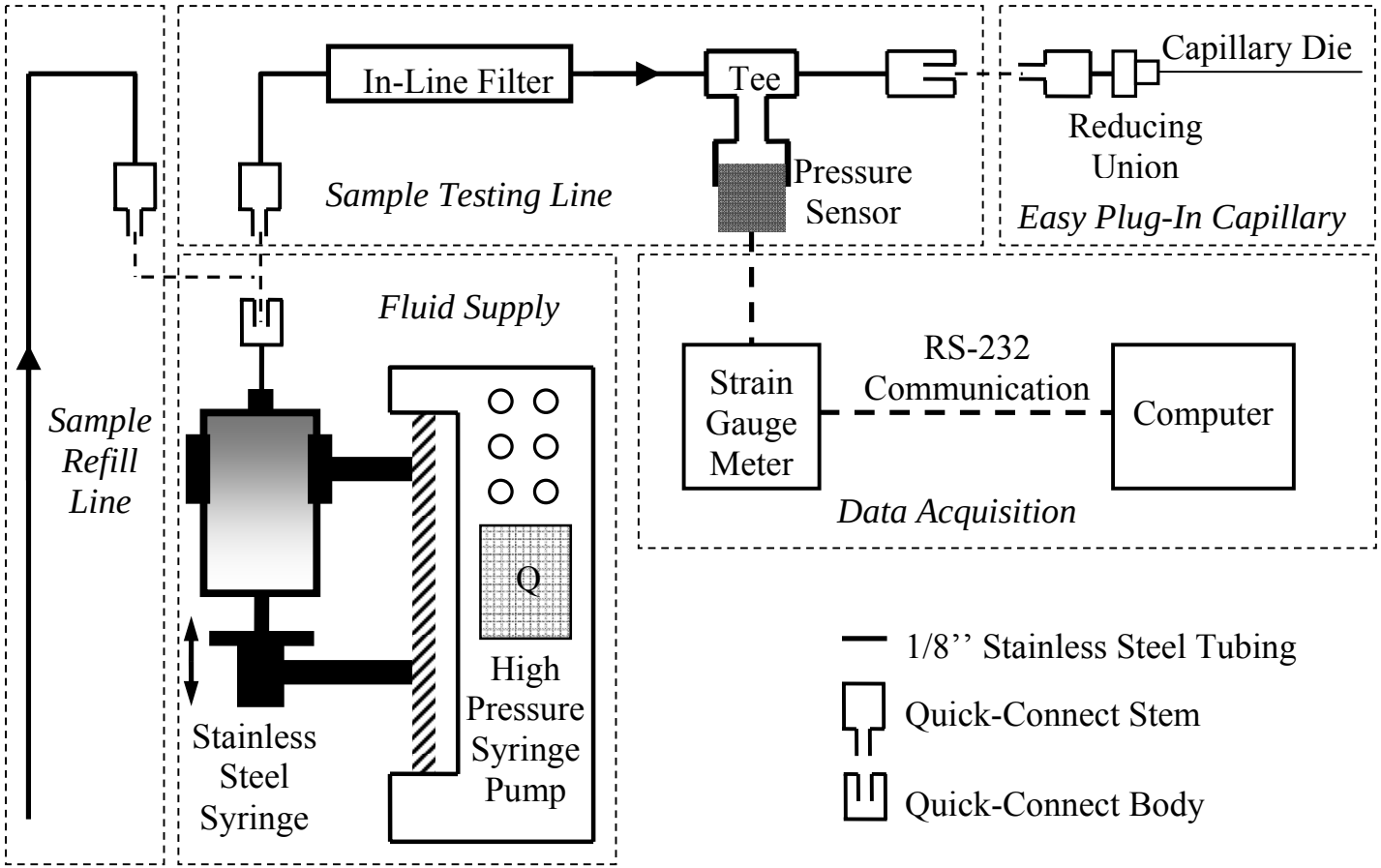

Figure 2-2: Schematic of the designed capillary viscometer.

the pressure drop across a capillary die with length of 115.0 mm was linearly proportional to flow rate for distilled water at a temperature of 22.0°C. By substituting the data illustrated in this figure into Eqs. (2-1) and (2-2), the effective inside radius of the capillary die at different shear rates was determined as illustrated in Figure 2-4. When the shear rate was higher than 1000 s^{-1}, the effective radius was determined to be 0.0775 mm with an error of less than 1.0%; yet when the shear rate was less than 1000 s^{-1}, the effective radius varies significantly with shear rate. This suggests that shear viscosity measurement at shear rate lower than 1000 s^{-1} was not accurate. Results for other capillaries with different inside diameters and lengths also indicated that shear rate should

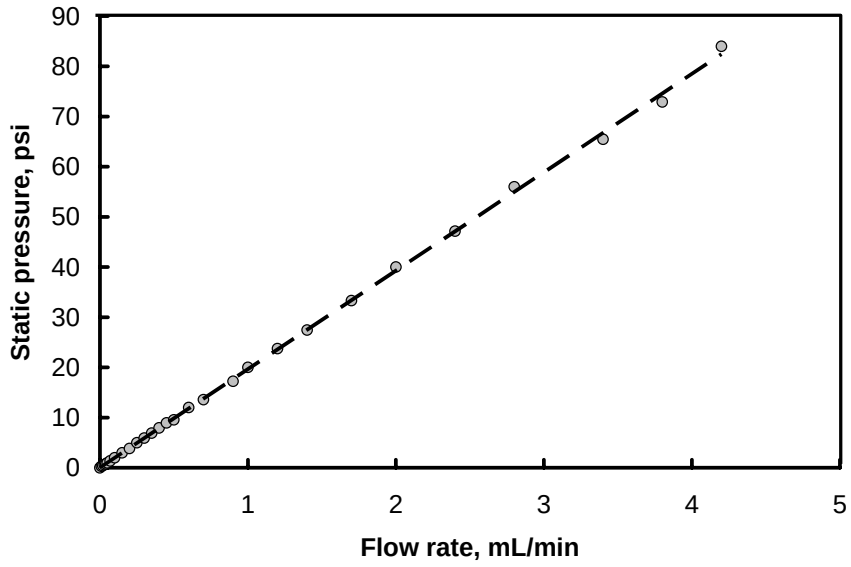

Figure 2-3: Static pressure drop across a 115.0 mm long capillary versus flow rate of distilled water at 22.0°C.

be higher than 1000 s^{-1} for accurate measurement of shear viscosity. Cho *et al*. [13] pointed out that capillary viscometry is not capable of measuring low shear rate (less than 200 s^{-1}) viscosity unless a complicated vacuum system is applied in the sample reservoir.

Since, in our case, the objective was to measure shear viscosity of inkjet inks at high shear rates, the measurement was done at shear rates higher than 2000 s^{-1}.

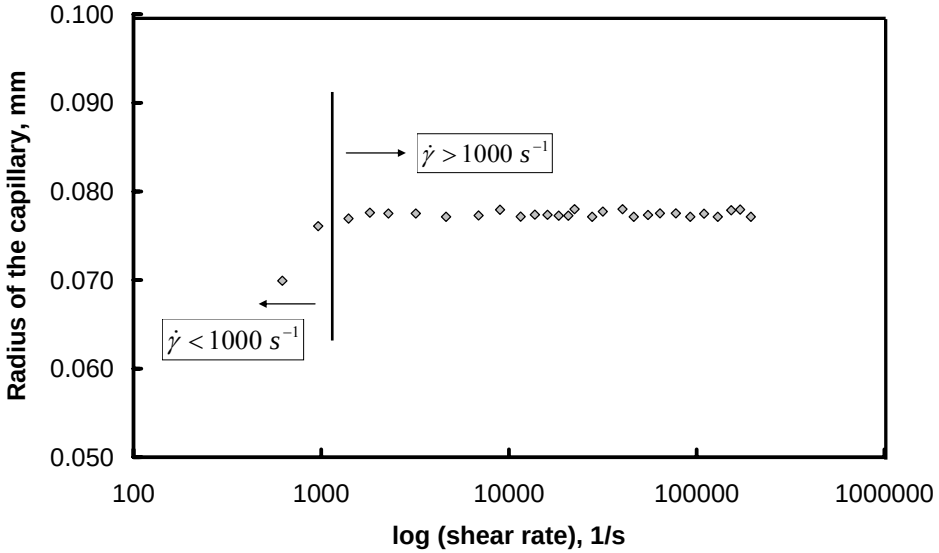

Figure 2-4: Effective radius of a capillary die with a length of 115.0 mm at different shear rates.

2.3.4 Operational Procedures of the Capillary Viscometer

Capillary die radius and length were selected for the tests and calculations were made to determine if system pressure limits were satisfied. Using Eq. (2-2), the required flow rates were calculated to obtain the desired shear rates, and using Eq. (2-1), the approximate pressure drop induced by a selected capillary die was calculated using the low-shear-rate (< 100 s^{-1}) viscosity of the ink sample. If the calculated pressure drop was higher than the maximum allowed pressure (2.4×10^6 Pa or 345 psi) of the system, another capillary die with either a bigger inside diameter or a shorter capillary length was selected for re-calculation. This was repeated until an allowable maximum pressure drop was obtained. Then the appropriate static pressure sensor was selected. A set of flow rates

was programmed in the syringe control panel, and the pressure sensor was plugged into the tee in the "sample testing line". The syringe was filled up with the ink sample using the "sample refill line", and then connected to the "sample testing line". With a zero flow rate, the readout from the strain gauge meter was set to zero. Once the syringe pump starts pumping, the operator started recording data using Windows HyperTerminal® at a sampling rate of 2.75 Hz. When the system reached steady state, pressure drop was recorded, and the syringe pump was advanced to the next flow rate. As illustrated in Figure 2-5, this was continued until data were obtained for the entire set of flow rates or the sample in the syringe was exhausted. Using Eqs. (2-1) and (2-2), the data was used to calculate the shear viscosity at eight different shear rates.

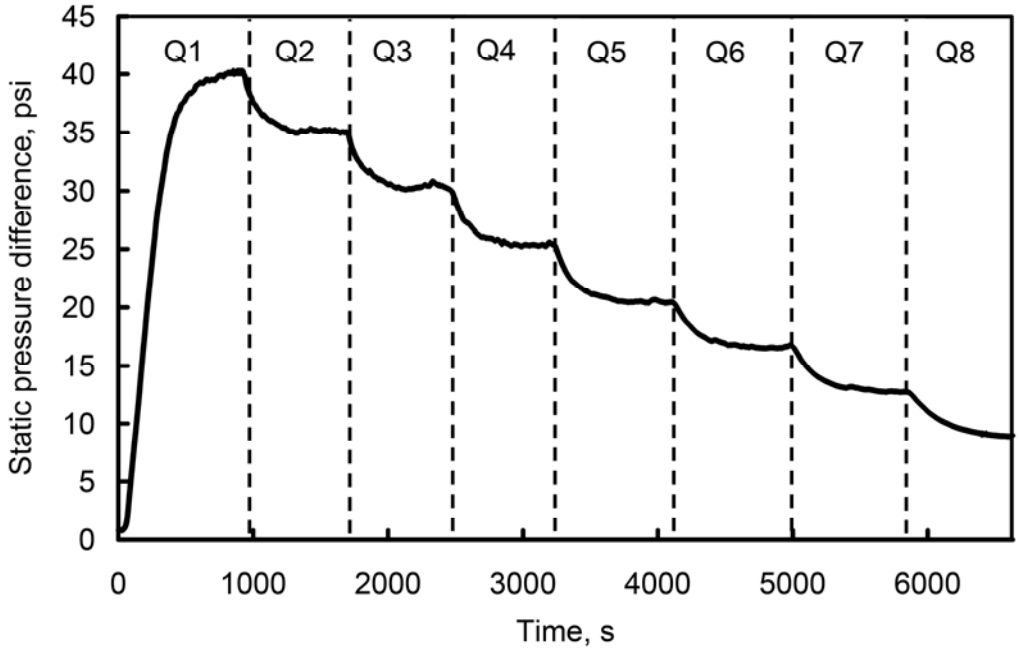

Figure 2-5: Eight static pressure differences for a set of eight flow rates.

As can be seen in Figure 2-5, when flow rate was changed, a period of time was needed before the steady state static pressure difference was reached. The required time decreased with increasing flow rate. The longest time for the experiments in this study was about 20 minutes.

The major feature of this capillary viscometer is that it can be easily set up with a few simple steps. The operational procedure and maintenance are easy to carry out. The capillary viscometer can also be further developed to measure the shear viscosity of inkjet inks at various temperatures by having the capillary die immersed in a fluid bath, which was demonstrated by Rushing and Hester [15].

2.4 Instrumentation and Testing Conditions for Measuring Temperature Dependent Shear Viscosity

A Couette viscometer (Brookfield, Part No. LVDVI+) was used as the key instrument for measuring the temperature dependent shear viscosity of inkjet ink samples. Figure 2-6 shows the schematic of the Couette viscometry used in this study. A spindle with diameter and length of 25.0 and 90.0 cm, respectively, was centered non-rigidly in a sample reservoir with a diameter of 27.5 cm. A thin layer of silicon oil floating on the top of the test sample was used to prevent evaporation of solvent, and a cap for isolating the sample from ambient environment was designed to sit on the top of the reservoir without touching the spindle bar. A heating/cooling jacket attached to the sample reservoir and a recirculation bath (Julabo, Part No. MW) were used to adjust the temperature of the inkjet ink sample.

The selected testing temperatures were 23.0 (room temperature), 25.0, 37.5, 50.0, 62.5, and 75.0°C. At testing temperature of 23.0°C, the samples were tested on one day and the testing temperature variation was less than 0.1°C. However, for the testing temperature of 25.0°C, the recirculation water bath (Julabo, Part No. MW) cannot control this temperature well because the control temperature was too close to room temperature.

At this selected testing temperature, samples were tested at temperatures in the range of 25.0 to 27.2°C, but for any individual sample, the testing temperature variation was less than 0.5°C. For test temperatures of 37.5, 50.0, 62.5, and 75.0°C, the temperature was well controlled with a less than 0.1°C variation.

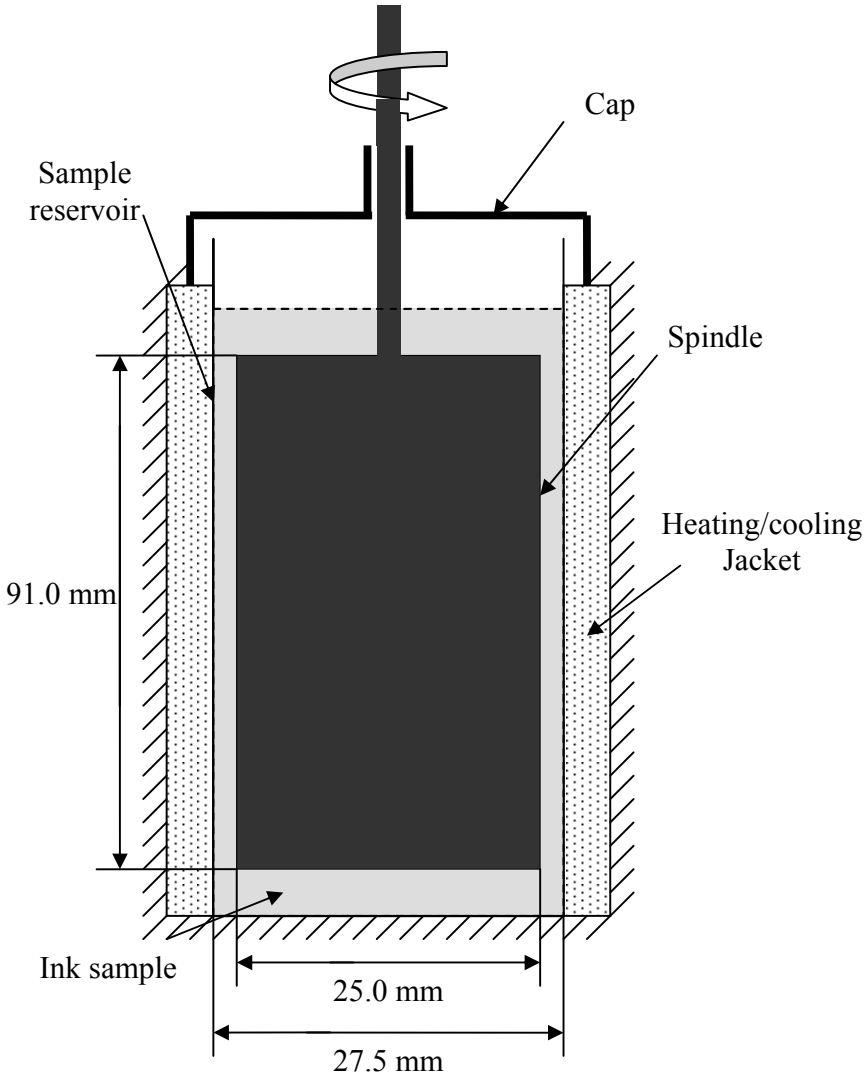

Figure 2-6: Schematic of the Couette viscometry used in this study.

2.5 Preparation of Inkjet Ink Samples for Testing

Inkjet ink preparation CAB-O-JET® 200 (Cabot Corp.), batch No.433824, was used to prepare carbon-black pigmented water-based inkjet ink samples. The pH value and surface tension of the inkjet ink preparation were 7.53 and 70.35 dynes/cm, respectively. The surface of the pigment was modified by covalently grafting $-SO_3Na^-$ group so that it was stable in water without adding any surfactants, dispersion aids or polymers. This ink preparation had about 20% w/w pigment (10.3 vol%, with pigment density of 1.95 g/ml), 0.2% w/w foaming agent, about 79.8% w/w water and a concentration of sodium of 4952 ppm/solids. The particle size distribution (PSD) of the carbon black pigment is shown in Figure 2-7, and the mean particle size was 130 nm.

Based on this ink preparation, various amounts of water and glycerin were added to adjust the shear viscosity and particle volume fraction of the inkjet ink samples. For the study discussed in this chapter, two groups of inkjet ink samples were prepared (see Table 2-1). The first group was for the study of shear-rate dependent viscosity, and the inkjet ink samples in this group were formulated by changing the contents of glycerin and water to adjust viscosity and volume fraction of pigment. The second group was for the study of temperature dependent viscosity, and the volume fraction of pigment in the inkjet ink samples was adjusted by changing the content of water. The volume fraction of pigment was calculated based on a pigment density of 1.95 g/ml. The shear viscosity was measured using a Brookfield Part No. LVDVI+ Couette viscometer at shear rate of 52.3 s^{-1}.

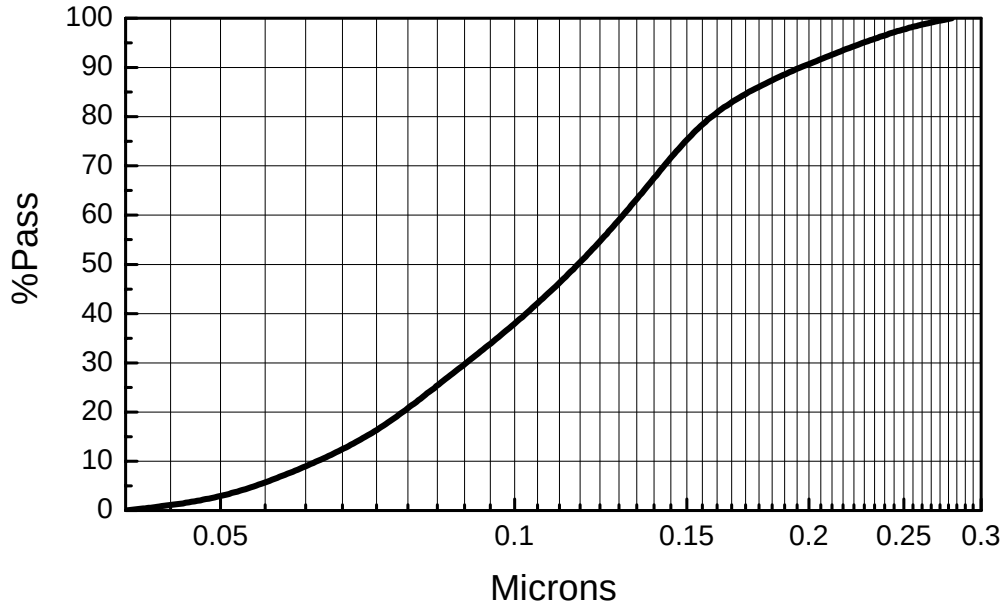

Figure 2-7: Particle size distribution (PSD) of CAB-O-JET® 200 ink preparation measured at very low concentration. Information provided by CABOT, Inc.

Table 2-1: Summary of inkjet ink samples prepared for studying the shear-rate dependent and temperature dependent shear viscosity

Group 1				
Ink	Pigment, vol%	Water, vol%	Glycerin, vol%	Shear viscosity, cP
#1	11.6	88.4	0	3.60
#2	15.0	85.0	0	6.33
#3	5.7	58.8	35.5	6.40
#4	17.2	82.8	0	10.40

Group 2: part I											
Ink	#1	#2	#3	#4	#5	#6	#7	#8	#9	#10	#11
Pigment, vol%	1.6	3.3	5.1	6.8	8.7	10.6	12.5	13.6	16.4	17.2	19.9
Water, vol%	98.4	96.7	94.9	93.2	91.3	89.4	87.5	86.4	83.6	82.8	80.1

Group 2: part II					
Ink	#12	#13	#14	#15	#16
Pigment, vol%	21.9	22.1	22.6	23.2	23.3
Water, vol%	78.1	77.9	77.4	76.8	76.7

2.6 Results and Discussion

2.6.1 Shear Rate Dependent Shear Viscosity

The measured pressure drop (ΔP) across the capillary die includes the following components [10]: pressure loss due to viscous dissipation within the capillary (P_{visc}), pressure needed to obtain the kinetic energy of the testing fluid (P_{kin}), pressure loss due to end effects including the entrance pressure loss (P_{ent}) and the exit pressure loss (P_{exit}), and pressure drop for viscoelastic fluids associated with elastic energy (P_{elast}). Overall, the measure pressure drop can be described by the following equation

$$\Delta P = P_{visc} + P_{kin} + P_{ent} + P_{exit} + P_{elast.} \quad (2\text{-}4)$$

For calculating shear viscosity, P_{visc} is the component needed. In order to determine it from ΔP, kinetic energy correction and Bagley correction were used for determining P_{kin} and $P_{ent} + P_{exit} + P_{elast}$, respectively.

The kinetic energy correction for capillary die geometry is

$$P_{kin} = \rho \bar{v}^2 . \quad (2\text{-}5)$$

where ρ is the density of the fluid, $\bar{v}$ is the averaged velocity of the flow. Our data indicated that for all of the flow rates and capillary dies used in this study, P_{kin} was less than 1.0% of ΔP. For this reason, the effects of kinetic energy were neglected.

Bagley correction [10] includes both viscous and elastic components of the end pressure drops and can be used for non-Newtonian viscoelastic fluids. The pressure loss due to end effects was determined by using Bagley correction and found to be negligible for all tests conducted. For example, four capillary dies with the same capillary diameter, but different lengths, were used to obtain the Bagley plot shown in Figure 2-8, where ΔP is plotted versus the length-to-diameter ratio. Each straight line was obtained by linearly fitting the experimental data at a fixed flow rate. The pressure loss due to end effects was

the intercept of the straight line with the *y*-axis, i.e., L/D = 0. Figure 2-8 indicates that the end pressure losses were negligible as the intercepts were all less than ±0.5 psi, which falling into the range of measurement error. Since the corrections were negligible, the measured value of ΔP can be substituted directly into in Eq. 2-1 to calculate shear viscosity.

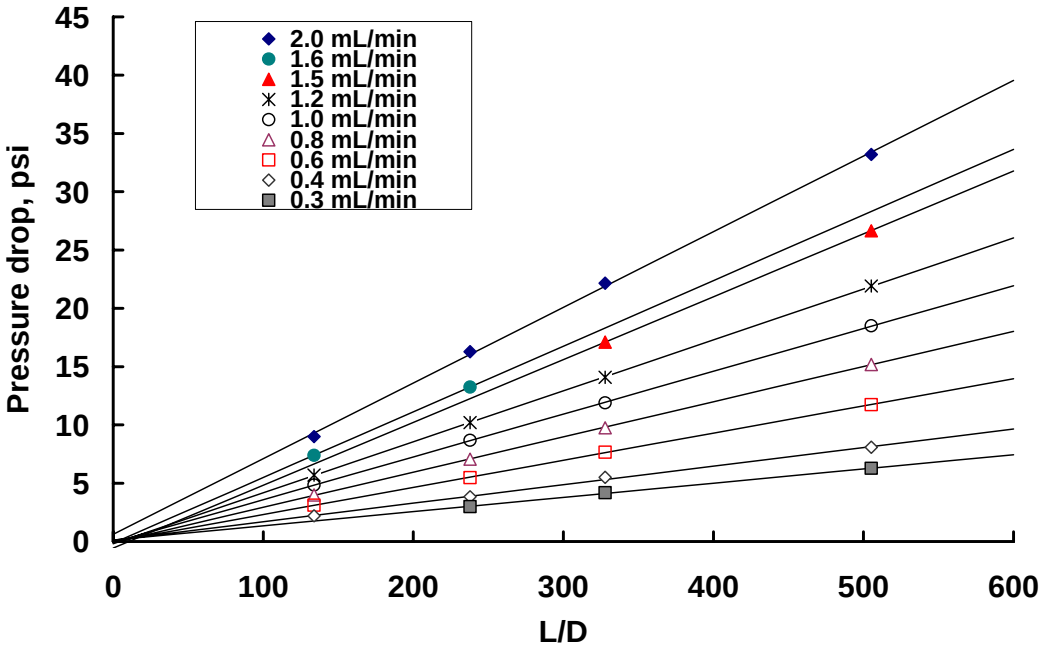

Figure 2-8: Bagley plot obtained from capillary measurements of Sample #2 in Table 2-1, Group 1, with 15.0 vol% of pigment at temperature of 22.0°C. The four capillary dies used for the measurement have a diameter of 0.229±0.001 mm and lengths of 3.08, 5.47, 7.54, and 11.52 cm.

To test the performance of the capillary viscometer, Newtonian fluids (glycerol/water mixtures) with viscosity of 3.6 and 6.3 cP were used. The viscosities of Newtonian fluids were measured by using a Couette viscometer (Brookfield, Part No. LVDVI+) which was calibrated by using standard silicon oils (Brookfield, Part No. 5, 10, and 50 cP). Figure 2-9 shows shear viscosities at a temperature of 22.0°C obtained using

the Couette viscometer and the designed capillary viscometer. Different capillary dies were used for the measurement and the inside diameters of all of them were calibrated by using distilled water at 22.0°C. The averaged values for all data points in Figure 2-9 are 3.6 ± 0.2 and 6.3 ± 0.2 cP at shear rate up to 2×10^5 s^{-1}, which indicates that the capillary viscometer was accurate.

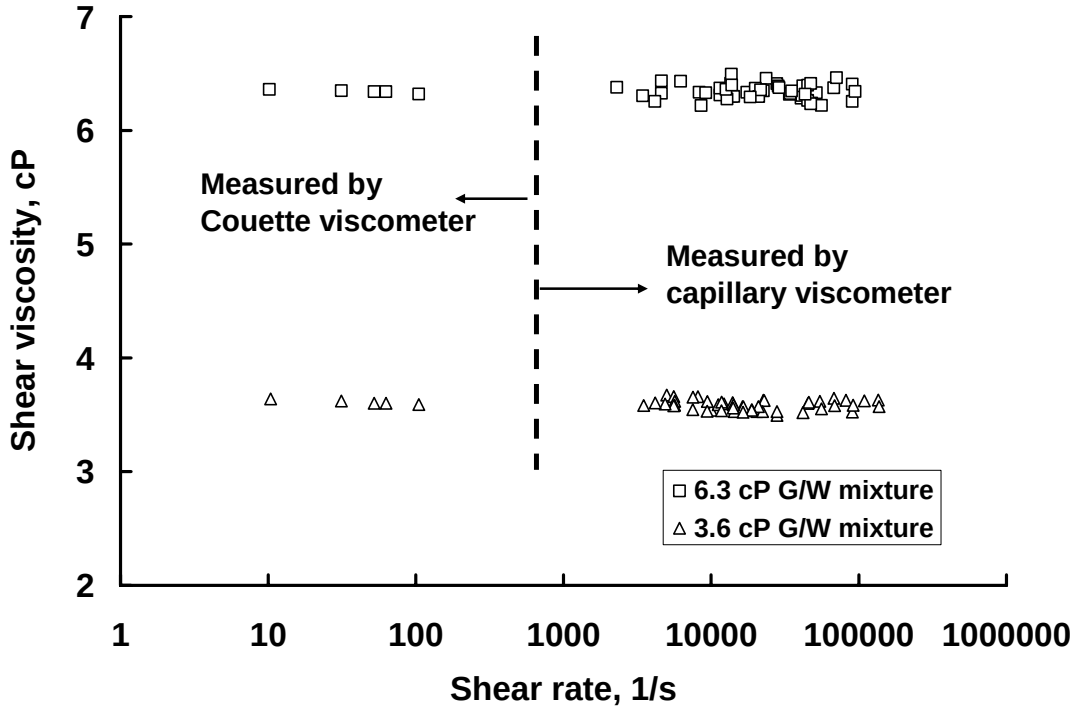

Figure 2-9: Shear viscosity of two Newtonian fluids (glycol/water mixtures) with viscosities of 3.6 and 6.3 cP, measured using a Couette viscometer and a capillary viscometer at temperature of 22.0°C.

The low-shear-rate viscosity of the inkjet ink samples in Table 2-1 (Group 1) was measured using the Couette viscometer. The capillary viscometer was then used to measure the shear viscosity at shear rates up to 2×10^5 s^{-1} by using several capillary dies. The results are shown in Figures 2-10 and 2-11. In Figure 2-10, the shear-rate dependent

viscosity of samples #1, #2 and #4 in Group 1 (see Table 2-1) are shown. In Figure 2-11, the shear-rate dependent viscosity of samples #2 and #3 in Group 1 (see Table 2-1) and a 6.3-cP G/W mixture (48.4 vol% glycerin and 51.6 vol% distilled water) is demonstrated.

Among the numerous rheological models available [10], the well-known Cross model [16] was found to be quite appropriate to fit the measured data:

$$\eta = \eta_\infty + \frac{\eta_0 - \eta_\infty}{1 + A\dot{\gamma}^m} \tag{2-6}$$

where $\dot{\gamma}$ is the shear rate, η_0 the zero-shear rate viscosity (lower Newtonian plateau), η_∞ the infinite-shear-rate viscosity (upper Newtonian plateau), *A* and *m* the fitting parameters. To give a quite reasonable estimation for the four parameters, η_0, η_∞, *A*, and *m*, a spread-sheet-type program Microsoft Excel was used to obtain the best visual fits after multiple trials, as indicated by Barnes, *et al.* [17].

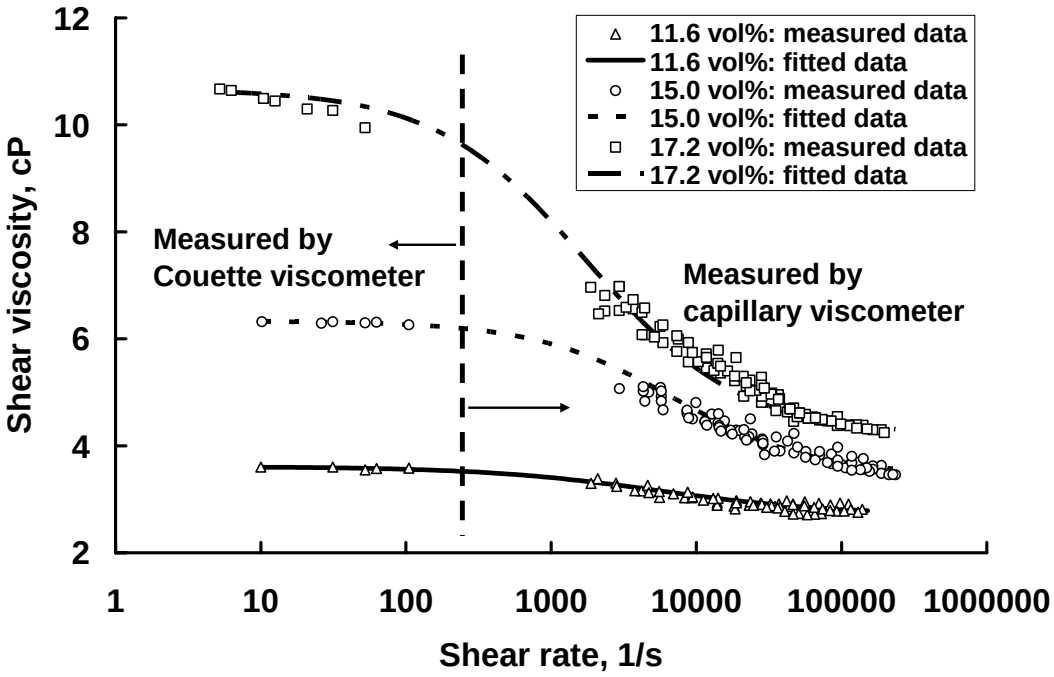

Figure 2-10: Shear viscosity of inkjet ink samples #1, #2 and #4 in Group 1 (Table 2-1) as a function of shear rate at temperature of 22.0°C. Fitting curves were obtained with a generalized Cross equation Eq. (2-6). The fitting parameters, *A* and *m*, are 0.00210 and 0.715 for the ink sample with 11.6 vol% of pigment, 0.000346 and 0.900 for the ink sample with 15.0 vol% of pigment, and 0.00201 and 0.830 for the ink sample with 17.2 vol% of pigment, respectively.

The results, shown in Figure 2-10, reveal that surface-modified-carbon-black pigmented water-based inkjet ink samples exhibited a Newtonian behavior at low shear rates, a pseudo-plastic one in the middle shear rate range, and a second Newtonian plateau at very high shear rates. The magnitude of the change in viscosity occurring over the pseudo-plastic region increased with the volume fraction of particles. At low shear rates, the shear viscosities for 11.6, 15.0, and 17.2 vol% inkjet ink samples are 3.6, 6.4, and 10.6 cP, respectively. As the shear rate approaches 2×10^5 s^{-1}, the shear viscosities drop to about 2.7, 3.5, and 4.2 cP, respectively.

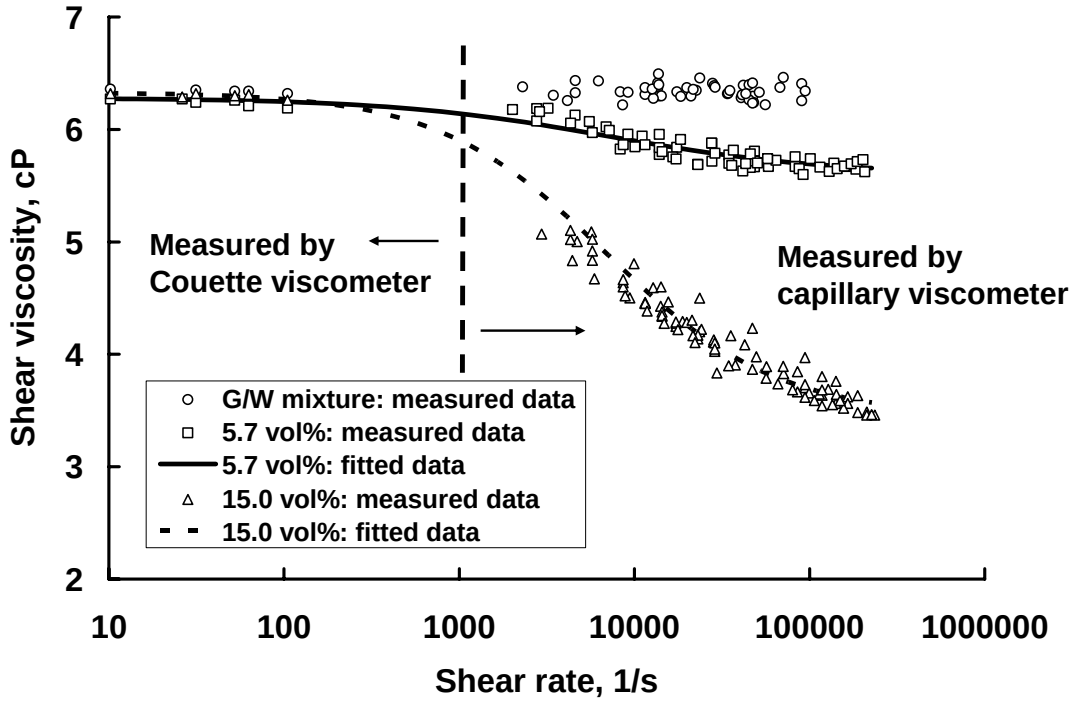

Figure 2-11: Shear viscosity of inkjet ink samples #2 and #3 in Group 1 (Table 2-1) and a 6.3-cP G/W mixture as a function of shear rate at temperature of 22°C. Fitting curves were obtained with a generalized Cross equation Eq. (2-6). The fitting parameters, *A* and *m*, are 0.00204 and 0.699 for the ink sample with 5.7 vol% of pigment and 0.000346 and 0.900 for the ink sample with 15.0 vol% of pigment, respectively.

The data in Figure 2-11 show that inkjet ink samples with similar low-shear-rate viscosity exhibited significantly different shear viscosities at high shear rates. Shear rate occurring when inkjet ink is jetted from the inkjet nozzle is in the range of $10^3 – 10^6\ s^{-1}$, depending on the amplitude of the actuating signal. Thus the shear viscosity measured at low shear rates may not sufficiently characterize inkjet ink samples with high material loading.

2.6.2 Temperature Dependent Shear Viscosity

The temperature dependent shear viscosity of inkjet ink samples in Table 2-1, Group 2 (Part I) at a shear rate of 10.5 s^{-1} is shown in Figure 2-12. The data, plotted in two figures for better clarity, show a decrease in shear viscosity as temperature increases. The Arrhenius law is often used to describe the temperature dependent shear viscosity [18-20]

$$\eta = \eta_B \exp\left(\frac{A}{T}\right), \tag{2-7}$$

where η_B is a constant and A is the activation energy. The experimental data were fitted using this equation (see Figure 2-12). The values of η_B and A are shown in Table 2-2.

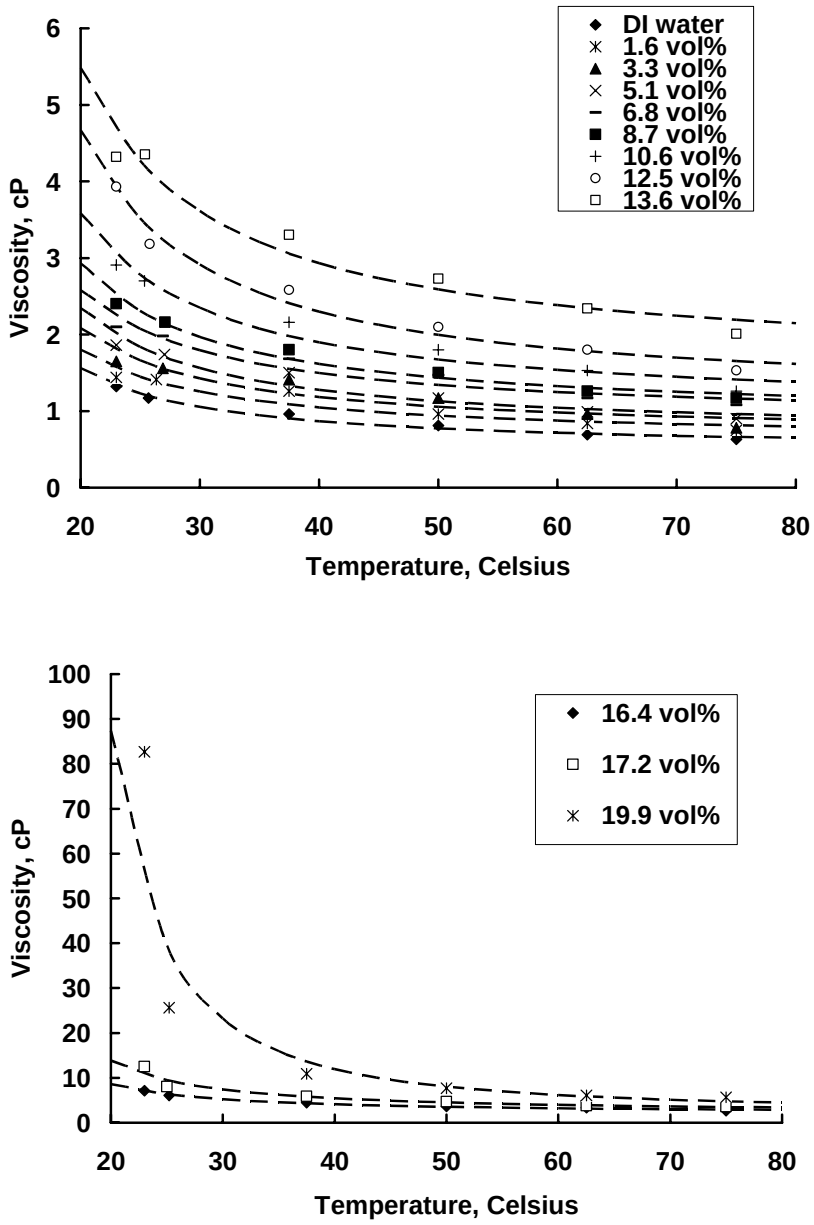

Figure 2-12: Temperature dependent shear viscosity of inkjet ink samples in Table 2-1, Group 2 (Part I) at shear rate of 10.5 s^{-1}. The measured data were fitted using Eq. (2-7) and plotted in dashed lines.

Table 2-2: Parameters in Eq. (2-7) obtained by fitting the experimental data shown in Figure 2-12

Volume fraction of pigment, %	η_B, cP	A, K	R^2
0	0.484	23.4	0.978
1.6	0.609	21.7	0.905
3.3	0.672	22.6	0.861
5.1	0.695	24.3	0.941
6.8	0.869	21.7	0.928
8.7	0.891	23.8	0.972
10.6	1.007	25.4	0.947
12.5	1.132	28.3	0.972
13.6	1.570	25.0	0.955
16.4	1.960	29.5	0.979
17.2	2.141	37.3	0.954
19.9	1.641	79.5	0.914

Figure 2-13 shows the shear viscosity of inkjet ink samples in Table 2-1 (Group 2) as a function of volume fraction of pigment. The shear rate was 1.7 s^{-1} and the two testing temperatures were 23.0 and 62.5°C. If a printhead can jet a fluid with a low-shear-rate viscosity of as high as 30.0 cP, according to Figure 2-13, the maximum material loading at a jetting temperature of 23.0°C for the particular inkjet ink formulation discussed in this study is approximately 18.0 vol%; it is approximately 23.5 vol% at a jetting temperature of 62.5°C. This demonstrates that by increasing jetting temperature to an even higher value, a higher jettable volume fraction might be achieved. Derby and his coworkers [3] showed that suspensions with particle volume fraction up to

45.0% could be delivered by using conventional printheads operating at a jetting temperature of 120°C. According to their data, the suspension with 45.0 vol% particles had a shear viscosity of about 170 cP at shear rate of 10 s^{-1} and temperature of 120°C. Thus increasing jetting temperature is a promising approach to increase throughput of high material loading inkjet inks.

For dilute hard sphere suspensions, the well-known Einstein's equation is used for predicting viscosity as a function of volume fraction,

$$\eta = \eta_0 (1 + 2.5\phi), \tag{2-8}$$

where η and η_0 are the viscosities of suspension and based fluid, respectively, and ϕ is the volume fraction of particles. For concentrated hard sphere suspensions, the Krieger and Dougherty equation [21] is often adopted,

$$\eta = \eta_0 \left(1 - \frac{\phi}{\phi_m}\right)^{-[\eta]\phi_m} \tag{2-9}$$

where ϕ_m is the maximum packing fraction and $[\eta]$ is the intrinsic viscosity of suspensions, which is 2.5 for spherical particles. Another often used equation is Mooney's equation [22],

$$\eta = \eta_0 \exp\left(\frac{a\phi}{1 - \phi/\phi_m}\right) \tag{2-10}$$

where a is a coefficient.

Both Mooney's equation and Krieger and Dougherty equation were used to fit the data shown in Figure 2-13. The determined parameters are listed in Table 2-3. To obtain the best fit using Eqs. (2-9) and (2-10), the maximum packing fractions adopted were much smaller than that of spherical particles, where theoretically ϕ_m is 0.74 for a close-packed array of same size spherical particles.

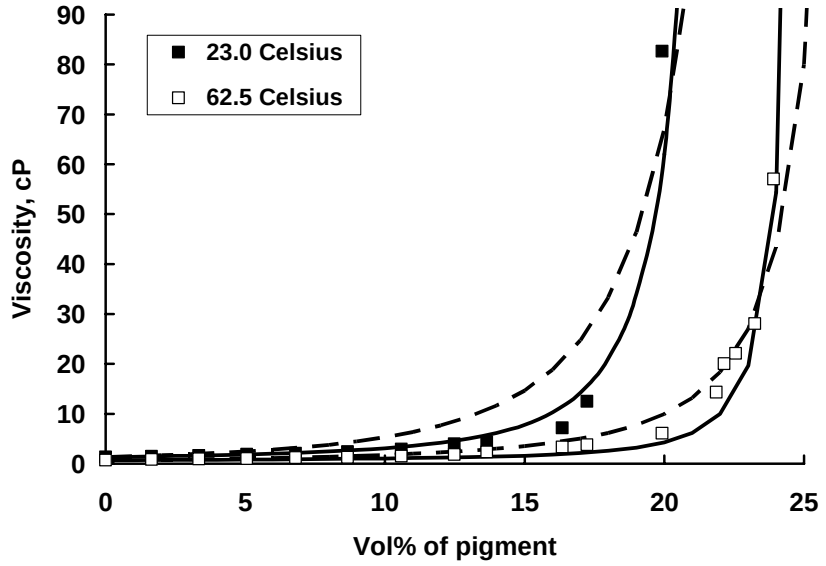

Figure 2-13: Shear viscosity of inkjet ink samples in Table 2-1 (Group 2) as a function of volume fraction of pigment. The shear rate was 10.5 s^{-1} and the two testing temperatures were 23.0 and 62.5°C. The solid and dashed lines represent predicted values using Mooney's equation (Eq. (2-10)) and Krieger and Dougherty equation (Eq. (2-9)), respectively.

Table 2-3: Parameters used in Eqs. (2-9) and (2-10) to fit the experimental data shown in Figure 2-13

	Krieger and Dougherty equation			Mooney's equation		
Temp. °C	$[\eta]$	ϕ_m	R^2	a	ϕ_m	R^2
23.0	11.2	0.28	0.90	5.5	0.28	0.98
62.5	7.6	0.28	0.95	2.6	0.28	0.98

The surface modification process for the carbon black pigment was done when the carbon black was in the form of aggregates. Consequently, the contact surface between adjacent primary particles was not grafted with the $-SO_3Na^-$ group. In the inkjet ink samples, the basic unit is thus an aggregate, where multiple pseudo-spherical primary

particles are connected to each other as shown in Figure 2-14. Geometrically, the branched aggregate structures prevent the tight packing obtainable with spherical particles. As a result, the maximum packing fraction, ϕ_m, of carbon black pigment is much lower than that of spherical particles.

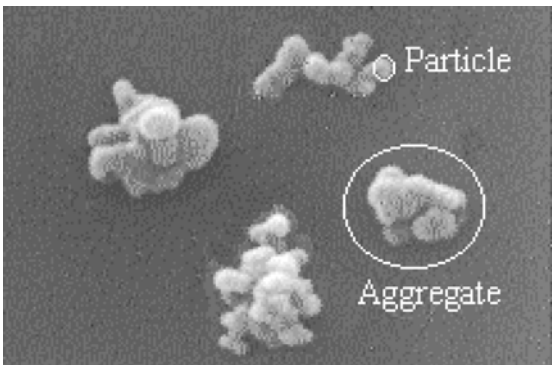

Figure 2-14: TEM picture of carbon black particle and aggregate [23].

For the inkjet ink samples used in this study, the surface of pigment was modified by covalently grafting the $-SO_3Na^-$ group so that the pigment can stabilize in water without adding any surfactants, dispersion aids or polymers. As the concentration of pigment in water is increased, the available water ions per pigment particle decrease. It is conjectured that at high volume fraction, the surface-modified carbon black pigment aggregates forming weakly jointed agglomerate. At sufficiently high concentration, the agglomerates interact forming a gel-like structure with an example shown in Figure 2-15.

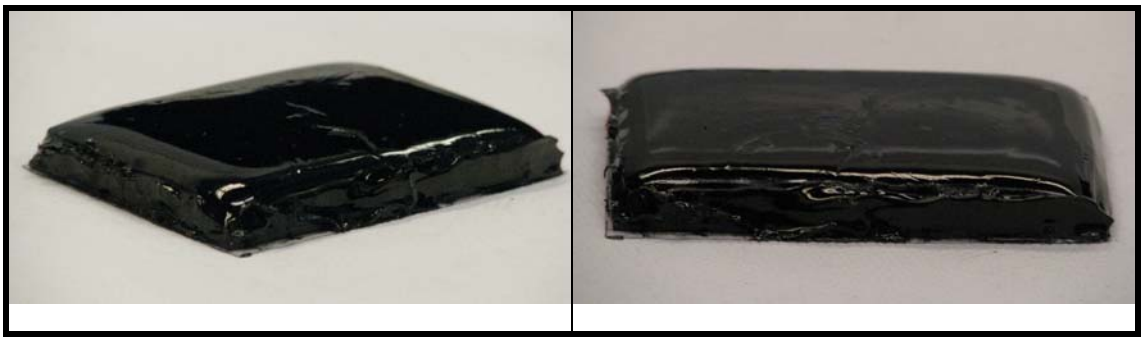

Figure 2-15: Gel-like structure of 28.0 vol% inkjet ink sample at 22.0°C on a glass slide.

One issue left in discussing the design and setup of the capillary viscometer is the determination of Nahme number, (see Eq. 2-3, $Na = \frac{\beta \eta_w \dot{\gamma}_{aw}^2 R^2}{4k}$). When the Nahme number, *Na*, is less than 1 [10], viscous heating effects are negligible. In Eq. 2-3, β is defined by the following equation

$$\beta = -\frac{1}{\eta}\frac{\partial \eta}{\partial T} \approx -\frac{\ln \eta_{T1} - \ln \eta_{T2}}{T_1 - T_2}, \tag{2-11}$$

where η_{T1} and η_{T2} are the shear viscosities measured at temperatures T_1 and T_2, respectively. The data in Figure 2-12 were used to determine the Nahme number for the inkjet ink samples with volume fraction up to 19.9%, and the results are shown in Figure 2-16. For calculating Nahme number, the values of the shear rate and the radius of the capillary die were chosen to be the maximum values used for this study, which are 200,000 s^{-1} and 0.22 mm, respectively. The shear viscosity used in Eq. 2-3 was chosen to be the low-shear-rate shear viscosity. These values of $\dot{\gamma}_w$, R, and η_w were chosen so that the values of *Na* calculated would be largest possible for the experiments conducted. This was done to ensure that the effects of viscous heating were negligible for all experiments reported. The thermal conductivity, K_{mix}, of the suspensions was calculated

using $\frac{1}{K_{mix}} = \frac{\phi}{K_{carbon}} + \frac{1-\phi}{K_{water}}$ where conductivities of water and carbon, K_{water} and K_{carbon}, are 0.58 and 1.70 W/m·K, respectively, and ϕ is the volume fraction of particles.

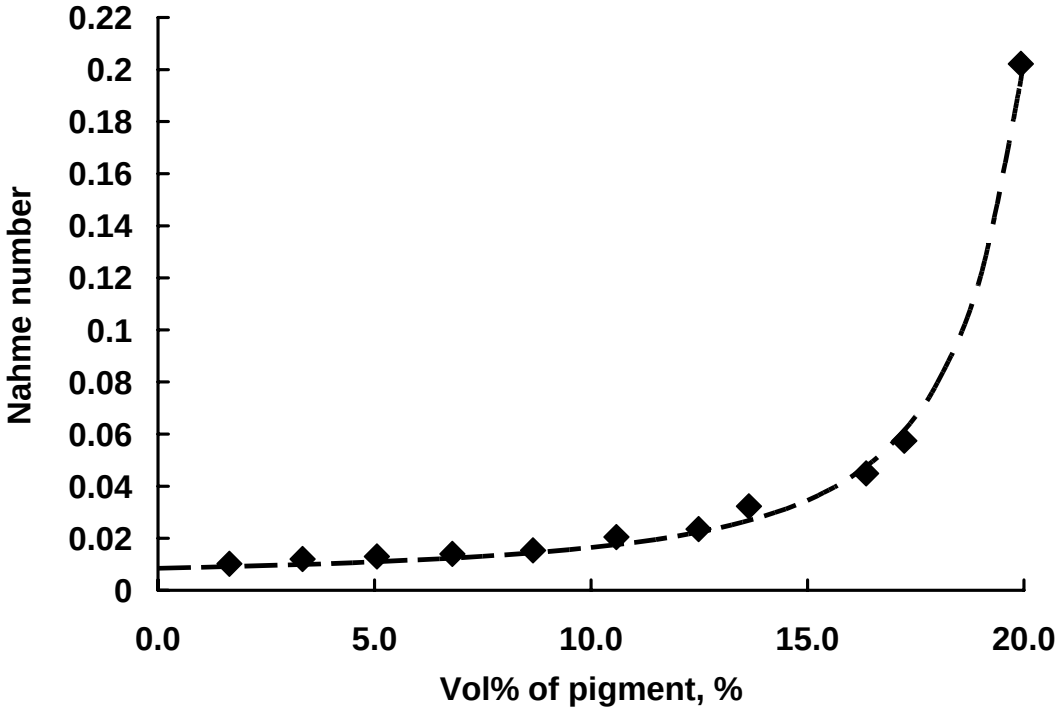

Figure 2-16: Nahme number (Eq. 2-3) for the inkjet ink samples with volume fraction up to 19.9% as a function of volume fraction of pigment. The dashed line represents predicted values using Eq. (2-12).

As shown in Figure 2-16, except for the last data point (volume fraction of 19.9%), Nahme numbers were all below 0.1, indicating that the viscous heating effect was negligible for the measurement of the inkjet ink samples at shear rate up to 200,000 s^{-1}. The trend of increasing of Nahme number as a function of volume fraction of pigment is similar to the trend of increasing of low-shear-rate shear viscosity as a function of volume

fraction of particles as shown in Figure 2-13. Thus, an equation similar to the structure of Mooney's equation (see Eq. (2-10)) was adopted to fit the data in Figure 2-16

$$Na = 0.008457 \times \exp\left(\frac{4.200\phi}{1-3.683\phi}\right). \quad (2\text{-}12)$$

Eq. (2-12) predicts that the Nahme number is 0.98 and 50 for volume fractions of 21.9 and 24.0%, respectively. Consequently, inkjet inks with high material loading may have significant viscous heating effect. A local temperature gradient may be generated, complicating DOD drop formation dynamics. Costa and Macedonio [18] studied magma flows at high Nahme number in tubes of finite lengths, and their results indicated viscous heating led to a flow profile evolution from Poiseuille flow, with a uniform temperature distribution at the inlet, to a plug flow with a hotter layer near the wall. They also mentioned local instabilities may exist due to viscous heating induced three-dimensional temperature gradients, possibly triggering secondary flow. For inkjet printing of highly material loaded suspensions, this issue may be important.

2.6.3 Mechanism of Shear-Thinning Behavior of the Inkjet Ink Samples and its Significance on DOD Drop Formation

It is important to understand the mechanism of shear-thinning behavior of inkjet ink samples in order to explore the significance of shear-thinning behavior on DOD drop formation dynamics. Three factors that may be involved in the shear thinning behavior are viscous heating [10, 18], particle migration [25-27], and change of suspension microstructure [29].

As the inkjet ink is pushed out of the capillary, it is heated due to viscous dissipation. For laminar flow conditions, local temperature may increase, particularly near the capillary wall where shear rate is highest, leading to lower local shear viscosity and shear-thinning rheological behavior. In this study, the significance of viscous heating was evaluated using Nahme number, and the results indicated that the variation of fluid

temperature from the wall to the center of the capillary was negligible. A simple analysis (see Appendix A) was also made to estimate the maximum temperature increase over the length of the capillary due to viscous dissipation. The maximum temperature rise was determined to be less than 1 K or 1 °C. For this small rise in temperature, the decrease of shear viscosity is insignificant. Thus it was concluded that the effect of viscous heating on shear viscosity was negligible.

Particle migration and alignment may also lead to lower shear viscosity for particle suspensions. Segré and Silberberg [25] in 1962 observed a single rigid sphere in pipe flow migrated to a steady state position with its center located at $r = 0.6R$, with R being the pipe radius. Such a radial migration induced by inertia is termed *tubular pinch*, and Han *et al.* [26] found that it was a very robust phenomenon existing for volume fraction of particles up to 20%. The concentration of particles in the liquid near the capillary wall is lower than the average concentration throughout the liquid, reducing the effective viscosity of the fluid near the capillary wall. As a result, the fluid appears to be shear thinning.

Recently, Matas, Morris and Guazzelli [27] developed an asymptotic theory which can be used to predict the entry length L_e after which radial migration will have developed if there is any; it is

$$L_e/D \approx 6\pi A^{-1}\,\mathrm{Re}^{-1}(D/d)^3, \tag{2-13}$$

where D is the capillary inner diameter, A is the scaled amplitude of the lateral force, Re is Reynolds number, and d is the particle size. Although the theory was developed by considering neutrally buoyant particles and used in their study for suspensions with less than 1 vol% non-colloidal spherical particles, it was used here to estimate L_e for the inkjet ink samples which were colloidal suspensions with volume fraction of as high as 15.0%. As the maximum Re when characterizing the inkjet ink samples was 300, according to Matas *et al.* [27], A is less than unity. As the capillary diameter (107 – 440 μm) was much higher than the mean particle size (130 nm), the estimated entry length L_e is higher

than 100,000 m. Considering the nano-scale size, irregular shape, and surface charge of the carbon black colloidal aggregates, the location of a single aggregate can be highly affected by the Brownian motion and inter-particle colloidal forces. Thus Eq. (2-13) may be highly inaccurate for the inkjet inks; however, the predicted entry length is extremely large (>100,000 m) and is interpreted here as indicating that particle migration is unlikely to be the cause for the shear thinning behavior of inkjet ink samples tested.

A third explanation is proposed here based on the understanding of the dispersion mechanism of the inkjet ink samples studied in this thesis research. Since the surface of carbon black pigment is modified by covalently grafting $–SO_3Na^-$ group, the dispersion mechanism is electrostatic stabilization. Charged species $–SO_3^{2-}$ are present on the surface of pigment and a concentration of oppositely charged ions (H^+) builds up around the pigment and decreases in concentration with distance from the pigment. This Stern layer stabilizes the pigment in dispersion. As the concentration of carbon black particles increases in the system, the number of water ions available for stabilizing each carbon black particle decreases. As a result, at high volume fraction of pigments, aggregates form weakly structured agglomerates, leading to a drastic increase in shear viscosity. Experiments indicated that systems containing propanol and/or glycerin are less effective than water in dispersing carbon black pigment, and the shear viscosity increases drastically starting at a lower volume fraction of pigment. These results are believed to be due to propanol and/or glycerin contributing a much smaller amount of ions (H^+) than that contributed by water.

The third explanation is based on the dispersion mechanism discussed above. It is conjectured that the shear thinning behavior is associated with change of suspension microstructure. The following assumptions are made to support this explanation: 1) not only aggregate, but also some agglomerate, is present in the inkjet inks; 2) the agglomerate is composed of aggregates that are weakly held together; 3) the agglomerate can be broken down by hydrodynamic forces and thermal agitation at fixed ion strength

and the process is reversible; and 4) the amount of agglomerate is associated with the ion strength of the suspension, and the lower the ion strength the higher the amount of agglomerate.

Based on these assumptions, the shear rate dependent viscosity at high shear rates, illustrated in Figure 2-10, may be due to the agglomerates in the suspension breaking down at high shear rate, and as a result viscosity decreases. At lower shear rates, the agglomerates remain intact as shear rate is increased. Over this region (lower Newtonian plateau) of shear rate, viscosity remains nearly constant. However, as shear rate is increased further, some of the agglomerates break down, resulting in reduction in viscosity. With increasing shear rate, more of the agglomerates break down and viscosity continues to fall. This trend increases with increasing shear rate until most of the agglomerates are broken down. After the shear rate is increased to a level where most of the agglomerates are broken down, further increase in shear rate has little effect on viscosity since there are few remaining agglomerates to decompose. Consequently, viscosity levels off with increasing shear rate, and the upper Newtonian plateau is reached.

An experiment was conducted to determine if the structure of the ink remains permanently changed after experiencing the high shear rate, and as a result, viscosity also remains lower. The experiment was conducted using inkjet ink with 18.2 vol% pigment content. The low shear rate viscosity of the sample was measured using a Couette viscometer. Then a 21-mL sample was ejected from the capillary viscometer at a shear rate higher than 1×10^{5} s^{-1}, collected, and immediately tested again using the Couette viscometer at lower shear rates. The data, shown in Figure 2-17, show the low shear rate viscosity before and after the sample experienced the high shear was the same. It is believed that the agglomerates in the suspension broke down under the high shear rate, but quickly re-formed after the shearing field was removed.

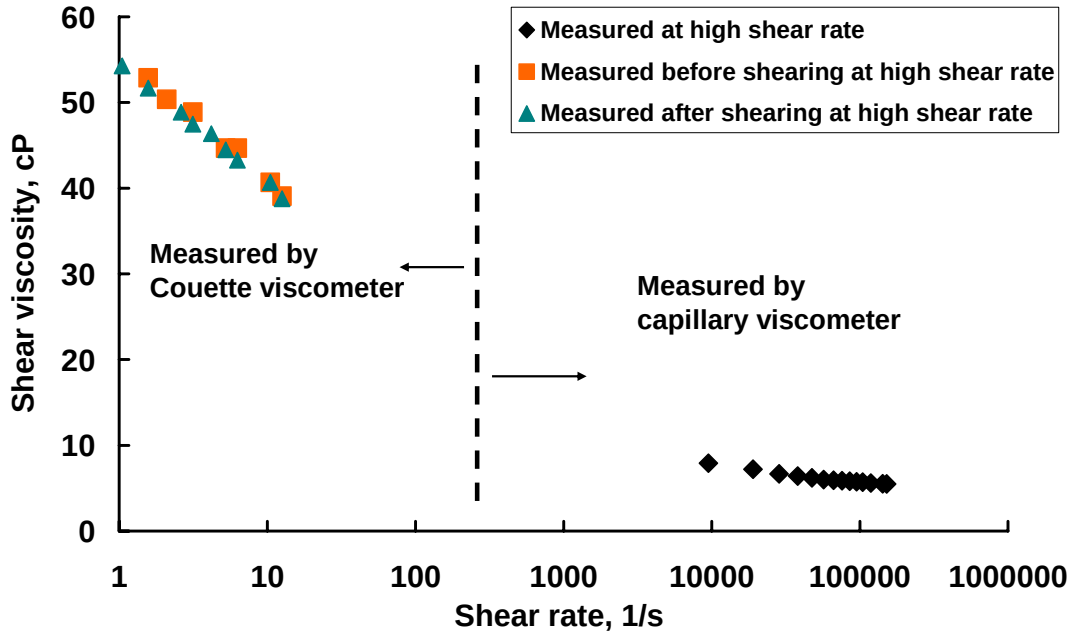

Figure 2-17: Shear viscosity of inkjet ink sample with 18.2 vol% at temperature of 22.5°C. For the data measured by the capillary viscometer, the radius and length of the capillary die were 0.0775 mm and 11.5 cm, respectively.

The low shear rate viscosity at shear rate of 10.5 s^{-1} and the high shear rate viscosity at shear rate higher than 1×10^5 s^{-1} for inkjet ink samples with 11.6, 15.0, 17.2 and 18.2 vol% pigment content can be seen in Figures 2-10 and 2-17. The effect of pigment content on shear viscosity at low and high shear rates is summarized in Figure 2-18. When the pigment volume fraction increases to a certain point, the shear viscosity increases drastically (see Figure 2-13) is attributed to the formation of agglomerates. These agglomerates existing at low shear rate are broken down at high shear rate. As a result, the effect of pigment volume fraction on shear viscosity is much lower at high shear rate and a nearly linear relationship between η_w and ϕ exists.

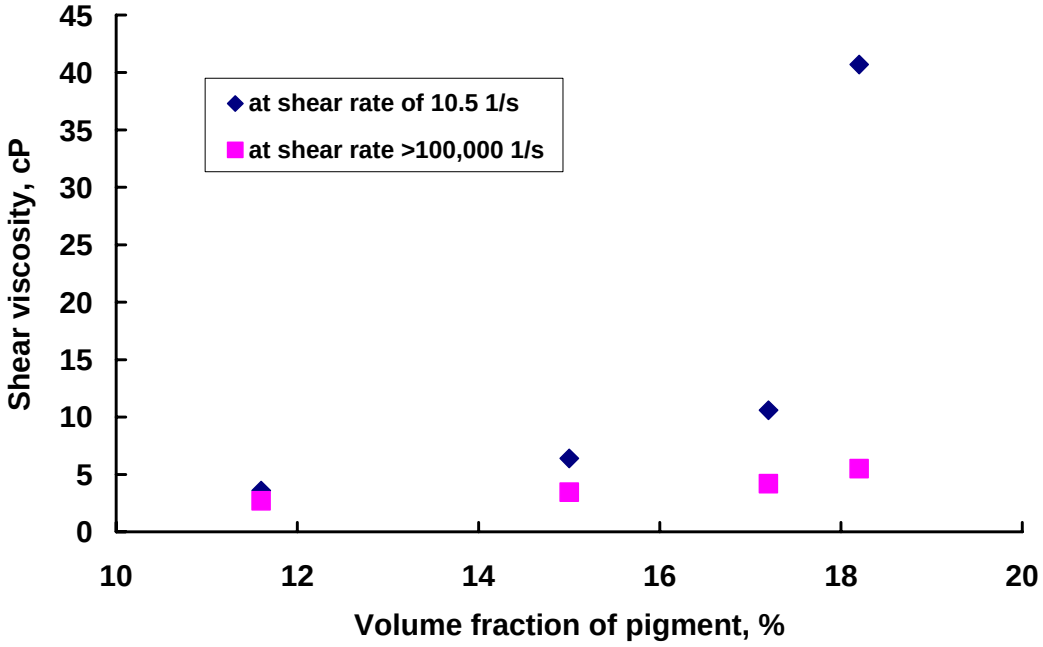

Figure 2-18: Shear viscosity at shear rate of 10.5 s^{-1} and higher than 1×10^5 s^{-1} for inkjet inks with volume fraction of 11.6, 15.0, 17.2 and 18.2%. Data are taken from Figures 2-10 and 2-17.

It was found shear viscosity of the inkjet inks with high pigment content was time dependent and a reversible viscosity change can be induced by an external shearing field at low shear rates, which is discussed in detail in Chapter 3. It is believed that agglomeration and deglomeration processes exist even at low shear rates (< 10 s^{-1}) provided pigment content is sufficiently high.

A critical question is whether or not the inkjet inks will exhibit shear thinning behavior in the inkjet printing process. There are two major differences between inkjet ink jetting from an inkjet nozzle and flowing through a capillary die:

1) One process is transient while the other is steady state. In inkjet printing, ink is jetted out of a short nozzle by a pressure pulse while, in capillary viscometry, ink is forced out from a long capillary die by a constant back pressure. Due to the short nozzle

length and varying chamber pressure, no steady state velocity field exists for inkjet printing; instead, a transient velocity field persists through the whole DOD drop formation process with velocity gradients in both *r* and *z* directions [14, 24] and with reverse flow as the pressure in the ink chamber falls and becomes negative. However, when inkjet ink flows through a capillary viscometry, a fully developed laminar flow is developed.

2) The time scales of the two processes are different. An inkjet nozzle typically has a diameter and length of less than 100 μm, and a typical DOD drop formation process lasts less than 100 μs (the period of time when high shear rate exists is less than 30 μs); in contrast, for the capillary dies used in this study, the diameter ranges from 107 to 440 μm and the length ranges from 3.1 cm to 16.0 cm. Thus the time that the suspension microstructure experiences high shear rate in a capillary die is much longer than that through inkjet nozzle. Depending on the flow rate and capillary geometry, the time taken for the flow to pass through the capillary die ranges from 5 ms to a few seconds.

An important issue is how fast does the suspension microstructure respond to a transient velocity field, i.e., how long do the agglomerates have to be sheared for deglomeration to occur. If ~ O(30 μs) is not long enough for the microstructural changes to occur, then the shear-thinning viscosity observed in capillary viscometry may not exist in the inkjet printing process. This issue will be discussed further in Chapter 4 where experimental data on DOD drop formation process will be presented.

2.7 Conclusions

The data shown in Figures 2-9, 2-10, 2-11 and 2-17 indicate that the designed and constructed capillary viscometer can be used to measure the shear rate dependent viscosity of inkjet inks with shear rate up to $2\times10^5\ s^{-1}$. The Cross model [16] was found to closely fit the experimental data. Inkjet ink samples with similar low-shear-rate viscosity exhibited significantly different shear viscosities at high shear rates depending on particle loading. It is conjectured that microstructure breakdown of agglomerates at high shear rate is the mechanism of the shear thinning behavior. Since the shear rate occurring when inkjet ink is jetted from the inkjet nozzle is in the range of $10^3 - 10^6\ s^{-1}$, the shear viscosity measured at low shear rates may not sufficiently characterize inkjet inks with high material loading; however, due to two major differences between inkjet ink jetting from an inkjet nozzle and flowing through a capillary die, the shear thinning in the capillary viscometer may not occur in the inkjet printing process.

By measuring the temperature dependent shear viscosity of the inkjet ink samples, it was shown that the viscous heating effect is insignificant for the samples tested in the viscometer. Extrapolation of the data to higher volume fractions of particles indicates that the viscous effect increases rapidly as volume fraction is increased.

2.8 References

1. Derby, B. and Reis N., MRS Bull. 28, 815 (2003).
2. Lee, D. H. and Derby, B., J. Eur. Ceram. Soc. 24, 1069 (2004).
3. Reis N., Ainsley, C., and Derby, B., J. Am. Ceram. Soc. 88, 802 (2005).
4. Reis N., Ainsley, C., and Derby, B., J. Appl. Phys. 97, 094903 (2005).
5. Wang, T. and Derby, B., J. Am. Ceram. Soc. 88, 2053 (2005).
6. Ainsley, C., Reis N., and Derby, B., J. Mater. Sci. 37, 3155 (2002).
7. Dong, H., Carr, W. W., and Morris, J. F., Phys. Fluids 18, 072102 (2006).
8. Xu, M., Private communication.
9. Creigh, L., Private communication.
10. Macosko, C. W., Rheology: principles, measurements, and applications, New York: VCH, (1994).
11. Colo, S. M., Private communication.
12. Egorova, N., Using Slit Rheometry in Characterizing Coating Colour Flow in the Blade Coating Process, Doctorial dissertation, Helsinki University of Technology, (2006).
13. Cho, Y. I., Kim, W. T., and Kensey, K. R., Rev. Sci. Instrum. 70, 2421 (1999).
14. Shield T. W., Bogy, D. B., and Talke F. E., IBM J. Res. Develop. 31, 96 (1987).
15. Rushing, T. S. and Hester, R. D., Rev. Sci. Instrum. 74, 176 (2003).
16. Cross, M. M., J. Colloid. Sci. 20, 417 (1965).
17. Roberts, G. P., Barnes, H. A., and Carew, P., Chem. Eng. Sci. 56, 5617 (2001).
18. Costa, A. and Macedonio, G., Nonlin. Processes Geophys. 10, 545 (2003).
19. Marcotte, M., Taherian, A. R., Trigui, M., and Ramaswamy, H. S., J. Food Eng. 48, 157 (2001).
20. Herceg, Z. and Lelas, V., J. Food Eng. 66, 433 (2005).
21. Krieger, I. M. and Dougherty, T. J., Trans. Soc. Rheol. 3, 137 (1959).

22. Mooney, M., J. Colloid Sci. 6, 162 (1951).

23. http://nanoparticles.org/pdf/Palumbo.pdf, (05/2008)

24. Xu, Q. and Basaran, O. A., Phys. Fluids 19, 102111 (2007).

25. Segré, G. and Silberberg, A., J. Fluid Mech. 14, 136 (1962).

26. Han, M., Kim, C., Kim, M., and Lee, S., J. Rheol. 43, 1157 (1999).

27. Matas, J.-P., Morris, J. F., and Guazzelli, E., J. Fluid Mech. 515, 171 (2004).

28. Furbank, R. J., Drop Formation from Particulate Suspensions, Doctorial dissertation, Georgia Institute of Technology, Atlanta, (2004).

29. Barnes, H. A., J. Non-Newtonian Fluid Mech.70, 1 (1997).

CHAPTER 3

TIME DEPENDENT SHEAR VISCOSITY OF SURFACE-MODIFIED -CARBON-BLACK PIGMENTED WATER-BASED INKJET INKS

3.1 Introduction

Surface-modified carbon-black pigmented water-based inkjet inks with sufficiently high pigment content was found to exhibit temporal viscosity variation at constant shear rate including thixotropy, viscoelasticity, viscosity oscillation, and ageing.

Barnes [2] gave a thorough review of thixotropy and pointed out that there are numerous definitions of thixotropy. The definition that will be used in this chapter was defined by Barnes, *et al.* [1] as follows: "decrease (in time) of … viscosity under constant shear stress or shear rate, followed by a gradual recovery when the stress or shear rate is removed". However, Barnes [2] also stated that "a better and extended definition of thixotropy … should contain the idea of both considerable shear thinning (i.e., gel-fluid transition) and also time changes over and above those encountered when in its structured state the thixotropic material might be viscoelastic with its attendant time effects". For thixotropic phenomenon, the time scale for the fluids to reach to the final viscosity can be dramatically different; some fluids may take a few seconds, while others may take days.

Generally shear thinning is used to mean viscosity decreases with increasing shear rate. In some cases the viscosity appears to change immediately with shear rate with no time dependency. Thixotropic materials are sometimes considered to be shear thinning materials with viscosities that are time dependent, i.e., if the shear rate is changed, the change in viscosity does not occur instantaneously, but over time. In both cases, the variation in viscosity is due to microstructural changes. The structural recovery when shearing is decreased is essentially applicable to all shear thinning materials in such a

way that a finite time rearrangement of microstructural elements takes place. The difference is that for thixotropic materials, the time taken for the microstructure to change is longer than the response time of the instrument; however, for shear thinning materials with no time dependency, the microstructural response time is shorter than the response time of the instrument. To be even more general, thixotropy exists for all liquids containing microstructure if we relate thixotropy to a finite time shifting of microstructure among different microstructural states [2].

The shifting of microstructure in flow of a suspension is a result of particle-particle interaction. In weak agglomerations, a competition exists between structural breakdown due to shearing and buildup due to in-flow collisions and Brownian motion or diffusion. If breakdown exceeds buildup at a constant shear rate over a sufficiently long time scale, thixotropy occurs; if weakly attached microstructural elements induced by in-flow collision are destroyed by Brownian motion at rest, anti-thixotropy occurs where "flow structures and rest destructures the material [2]". This suggests that both thixotropy and anti-thixotropy could coexist for one material depending on the intensity of breakdown induced by shearing.

Another important time dependent phenomenon different from thixotropy is caused by viscoelasticity [2]. The time-dependence shear viscosity due to viscoelasticity exhibits both short time elastic responses, where the microstructural elements responds yet retains its structure, and long time viscous effect, where the microstructural elements break down. According to Barnes [2], it is highly possible that viscoelastic effects coexist with thixotropic effects for situations with a full structure recovery. Typically, a startup experiment, where the material has reached a fully rested state, can reveal such a viscoelastic effect.

Bagusat *et al*. [4-8] conducted a series of studies on time dependent viscosity of kaolin [4, 6], alumina [5, 8], and technical China clay powder [7]. They found that the shear viscosity for a constant shear rate oscillates with an oscillation period ranging from

a few minutes to 2 hours. They assumed that such an oscillation was caused by shear induced self-organized structural changes where a periodic organization of agglomeration and deglomeration processes exists. Both kinetic modeling [4] by using Lotka-Volterra scheme [3] and optical detection techniques [7, 8] were adopted to elucidate these structure changes. The viscosity oscillations they observed depended on shear rates at which the energy of the mechanic shear field approximately equals the stabilization energy of the agglomerates. At higher or lower shear rates, such a balance may be destroyed. For the rheological experiment, a preshear [7] was conducted for a period of over several 1000 s before starting the measurement in order to establish a consistent initial condition of the suspension structure. They argued that sedimentation and stick-slip effect were not the causes for the oscillations as it existed for more than 50,000 s and could be found using a wide gap measurement geometry. The viscometry they used was Couette geometry and both rigidly and non-rigidly linked inner cylinder [6] were utilized.

3.2 Objective

Temporal instability of rheological properties was found for the surface-modified-carbon-black pigmented water-based inkjet ink samples prepared in this study and believed to be associated with suspension structure. The phenomena were originally discovered by a serendipitous series of events; later experiments found them to be reproducible. The objective of this chapter is to investigate time dependent shear viscosity for understanding the long term stability of dispersion structure and providing information for microstructural changes of highly loaded inkjet inks. Qualitative study was conducted and a few representative data are presented in this chapter.

3.3 Experimental

3.3.1 Instrumentation for Measuring Time Dependent Viscosity Profiles

A Couette viscometer (Brookfield, Part No. LVDVI+) was used as the key instrument for measuring the time dependent shear viscosity properties of inkjet ink samples. The geometry and structure of the viscometer is shown in Figure 2-6 in Chapter 2. Silicon oil was used to float on the top of the tested sample to prevent evaporation of solvent and a cap was designed to sit on the top of the reservoir yet without touching the spindle bar for isolating the sample from ambient environment.

The Couette viscometer measures the torque required to rotate the spindle at a certain rotational speed (RPM) in the sample and converts the torque into shear viscosity of the sample. The shear viscosity is calculated by

$$\eta_a \cong \frac{15T\left(R_r - R_s\right)}{\pi^2 R_s^3 L_s \omega}, \tag{3-1}$$

where T is torque, R_r is the radius of the reservoir, R_s is the radius of the spindle, L_s is the length of the spindle, ω is the rotational speed of the spindle (RPM). The Couette viscometer transmits 0 – 1 V signal with 0 and 1 V representing 0 and 100% torque of the full range value, respectively. Distilled water with viscosity of 1.0 cP was used to determine the full range torque. A strain gauge meter (Omega, Part No. DP41-S-S2) was used for receiving, conditioning, and transferring the signal to a computer through RS-232 communication protocol. Windows HyperTerminal® was used to record the data (percentage of the full range torque) at a sampling rate of 2.75 data per second. Time dependent shear viscosity at a known rotational speed of the spindle is determined using the recorded data, the full range torque, and Eq. (3-1).

3.3.2 Sample Preparation

Two inkjet ink samples were prepared from the inkjet ink preparation CAB-O-JET® 200 (Cabot Corp.) which had a pigment volume fraction of 10.3%. The properties of the inkjet ink preparation are given in Chapter 2. Samples #1 and #2 had volume fractions of 19.9% and 17.7%, respectively. Water was removed from the preparation via evaporation at 100°C. The volume fraction of pigment was calculated using pigment density of 1.95 g/ml. During the evaporation process, magnetic stirring was applied and the sample was contained in a conical flask. Once the process was completed, the conical flask was placed in water and sealed for cooling with magnetic stirring applied. Once the temperature of the sample dropped to room temperature, the magnetic stirring was stopped and measurement of the resting time of the sample was started so that the history of the sample would be known. After the preparation process, the samples were stored in conical flasks at rest and the conical flask was sealed and placed in an environment at a temperature of 21.5±1.5°C and relative humidity of 60±3%.

3.3.3 Transient Experimental Methods and Test Conditions

As indicated by Barnes [2], varied transient experimental methods can be used to reveal time dependence of shear viscosity of suspensions. Here is a list of the major ones:

(1) a step function in shear rate or shear stress;

(2) a sudden change in shear rate or shear stress after a preshearing for sufficient time until no further structural changes occur;

(3) a sudden change in shear rate or shear stress after a sufficient preshearing of fixed time followed by a rest with varied resting time (for investigating the extent of recovery by measure the overshoot stress/viscosity);

(4) a consecutive linear increase and decrease in shear rate for multiple loops until steady state (for fast screening or comparison of thixotropic materials); and

(5) a start-up experiment for suspensions at rest.

Results for methods (2), (3), and (5) are presented in this chapter. According to Barnes [2], for experimental study of thixotropic material, "... the level for the original value will not necessarily be the same, because that will depend on how carefully or vigorously the material was initially loaded into the viscometer and how long it was left to rest before shearing". For each transient experimental test conducted, the history of the sample was recorded. Tests were conducted with great care so that the history of the sample before the tests would be preserved.

The sample with a volume of 21±2 ml was slowly poured into the sample reservoir of the viscometer, eliminating the need for either syringe or pipette so that the effects of loading on the suspension microstructure would be minimized. Then the sample was at rest in the reservoir for 300 s for equilibrating before the transient experiment. A shearing test consisting of a sequence of steps where both shear rate and shear time were changed in each step was conducted.

Since the gap between the spindle and the sample reservoir of the viscometer is 1.25 mm in the Couette viscometry, a constant shear rate throughout the whole sample was achieved. The maximum shear rate of the Couette viscometer was 105 s^{-1} and it was used as the preshearing rate. For all the data collected, instrument inertia was neglected because the time for the spindle to change speeds was much shorter than the time over which changes in shear viscosity occurred.

3.4 Results and Discussion

3.4.1 Preliminary Study and General Observations

Time dependent shear viscosity was observed by a serendipitous series of events during the sample preparation process; later experiments show that it was reproducible. Initially, the random observations were not recorded with a few exceptions. One group of data recorded manually is shown in Figure 3-1. The history of the sample (pigment of 7.0 vol%, 1-propanol of 13.4 vol%, and water of 79.6 vol%) before the test is unknown. Two periods of shearing at shear rate and temperature of 20.9 s^{-1} and 21.0°C, respectively was applied, between which a 60-s rest was imposed. As shown in Figure 3-1, when the sample was at rest, the shear viscosity decreased and when the sample was again under external shearing, the shear viscosity increased. For both shearing periods, the steady state value of shear viscosity was approximately 28.0 cP. Thus the material appeared to be anti-thixotropic, where it was structured by shearing and de-structured by rest.

As illustrated in Figure 2-13 for suspensions containing water and surface-modified carbon black pigment, the shear viscosity monotonically increases as the volume fraction of pigment increases. Once the pigment loading reaches a critical value, the viscosity increases drastically and time-dependent behavior occurs. With even higher pigment content, the suspension becomes a gel-like structure as shown in Figure 2-15. For suspensions with glycerin and/or propanol, similar behavior is observed; however, since glycerin and propanol are much less effective in dispersing carbon black pigment, time dependent shear viscosity is exhibited at an even lower volume fraction of pigment.

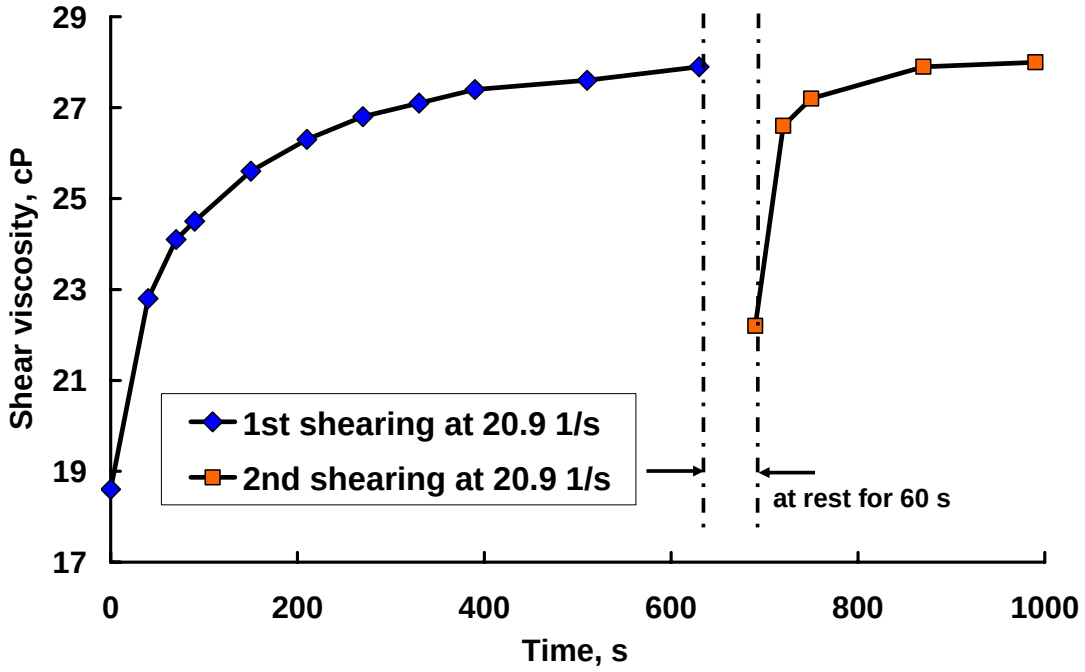

Figure 3-1: Manually recorded data for suspension (pigment of 7.0 vol%, 1-propanol of 13.4 vol%, and water of 79.6 vol%) exhibiting anti-thixotropic behavior at a testing temperature of 21.0°C.

3.4.2 Structure Build Up After Sample Preparation

During the preparation of the ink sample with volume fraction of 17.7%, a high shear rate was imposed by the magnetic stirring bar at temperature of 100°C. It is believed that this de-structured the material (reduce the number of agglomerates), and once the magnetic stirring was removed and the temperature of the sample dropped to room temperature, structure rebuilt over time. This is consistent with the variation of shear viscosity vs. time at shear rate of 10.5 s^{-1} directly after the sample preparation was completed. As described above, the sample was magnetically stirred at high shear rate

during and after the cooling process for 3.5 hr. Then a small volume of the sample was slowly poured into the sample reservoir of the viscometer and immediately (< 1 min), a shear rate of 10.5 s^{-1} was applied at a temperature of 23.1±0.1°C until the shear viscosity reached the steady state value. The temporal variation of shear viscosity is shown in Figure 3-2.

The temporal variation of shear rate shown in Figure 3-2 is interpreted to indicate that the sample was thixotropic. Prior to the test, the sample was heated to a temperature sufficient to greatly de-structure (reduce the number of agglomerates) the material. Although the material was cooled, magnetic stirring was applied for 3.5 hr which is believed to bring the material to a steady state with low structure. During the test at shear rate of 10.5 s^{-1} which is a lower shear rate than that produced by the magnetic stirring, the structure began building up, and correspondingly, viscosity increased with time. With continued shearing, the structure built up until it reached steady state after about 3200 s. Once the steady state structure was reached, viscosity remained constant throughout the rest of the test.

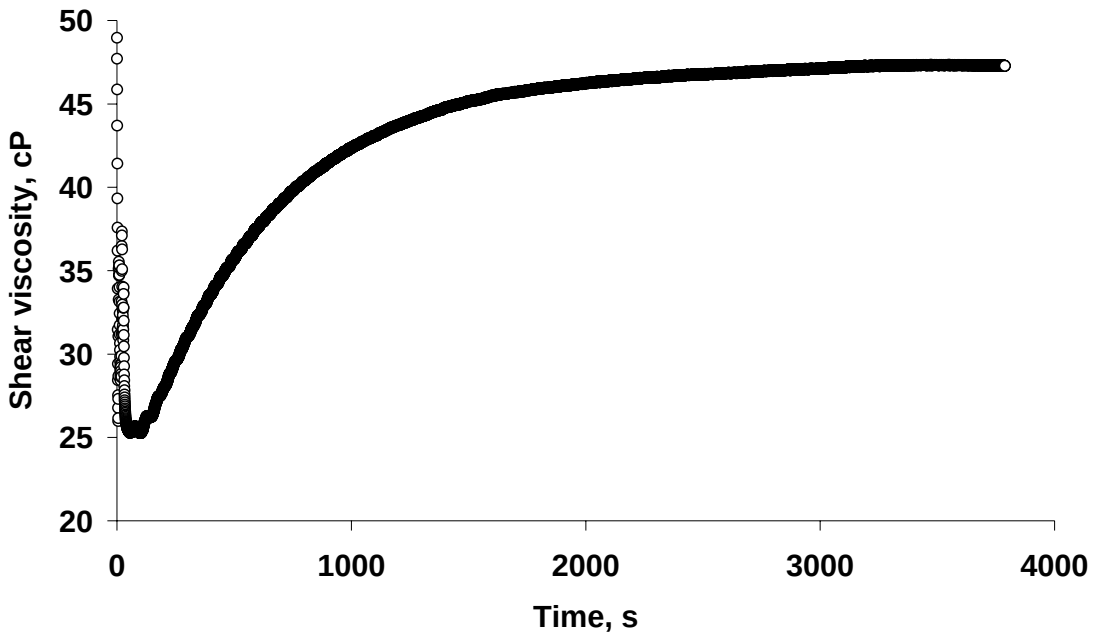

Figure 3-2: Temporal variation of shear viscosity for sample with pigment content of 17.7 vol% directly after the sample preparation process. The test was done at shear rat of 10.5 s^{-1} and temperature of 23.1±0.1°C.

3.4.3 Effect of Shelf Time on Structure Build-Up

The data discussed above indicate that the structure of the ink sample with 17.7 vol% pigment content was shear rate and time dependent. It was conjectured that this sample would have a slow structure build up over the shelf time. In order to investigate this, the sample was stored in different bottles at a temperature of 22.0±1.0°C after the preparation process. The shelf time was counted starting from the moment when the magnetic stirring was stopped. The sample was tested at five shelf times of 44, 102, 236, 500 and 572 hr using a so-called start-up test (a shear rate is applied and shear viscosity is recorded after the sample rests for a certain period of time) at shear rate of 3.1 s^{-1}. The variation of shear viscosity was recorded temporally and the results are summarized and shown in Figure 3-3. For each test, the initial value of shear viscosity was higher

(overshoot viscosity) than the steady state value and viscosity decreased over time until a steady state value was reached. The decrease of shearing viscosity over time is interpreted to be due to a destruction of the suspension microstructure. Another observation is that an ageing process occurred where as the shelf time increased, the steady state value of shear viscosity also increased

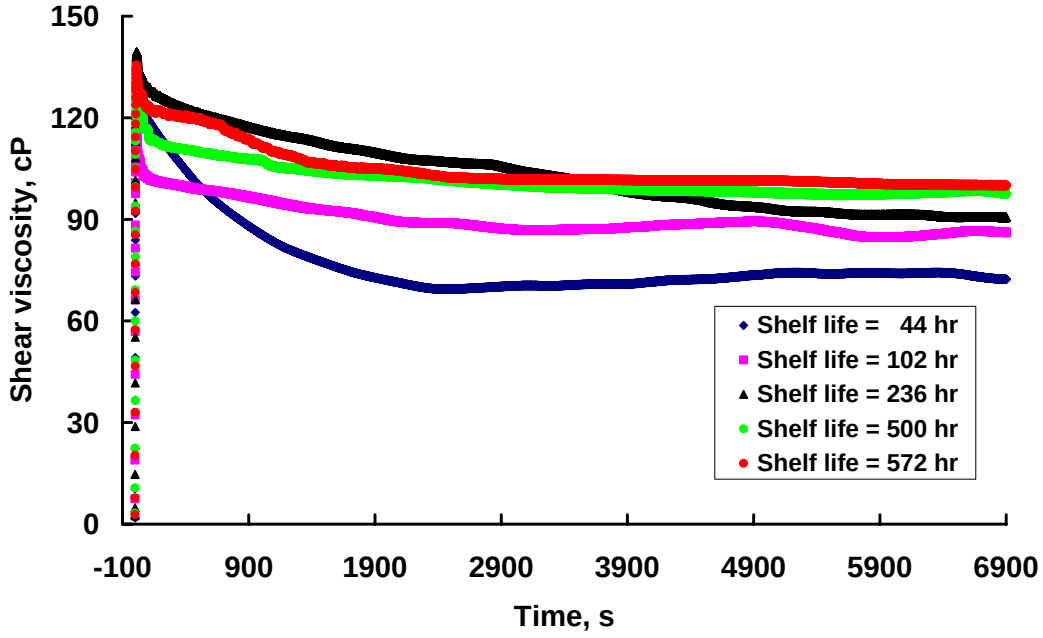

Figure 3-3: Effect of shelf time on start-up (a shear rate is applied and shear viscosity is recorded after the sample rests for a certain period of time) behavior of inkjet ink sample with 17.7 vol% pigment content at shear rate of 3.1 s^{-1} and temperature of 22.0±1.0°C.

3.4.4 Build-Up Test: Effect of Preshearing Time at Shear Rate of 105 s^{-1} on Structure Recovery at Lower Shear Rates

In transient experiments, a preshearing at high shear rate for a certain period of time followed by a low-shear-rate test is used to indicate the characterization recovery time of the microstructure. The time taken until steady state viscosity is reached at low-shear-rate test is defined as the structure recovery time. The preshearing time at high shear rate is adjusted to establish a varied initial condition of the suspension microstructure. It is believed that the varied initial condition of the suspension microstructure will lead to different temporal variation of viscosity at the low-shear-rate test.

Two test results are presented here. Before each test, a start-up experiment was conducted at low shear rate for sufficient period of time to clean up the history of the suspension microstructure. The high shear rate used for preshearing was 105 s^{-1}. During preshearing, no shear viscosity data was taken because the torque was too high and out of the instrument range. The change of shear rates was done instantaneously.

Test 1 was done using the sample with pigment content of 17.7 vol% at temperature of 22.1±0.1°C. Before the test, the sample was stored for 14 hr and presheared at shear rate of 20.9 s^{-1} for 4 hr to establish an initial condition of the suspension microstructure. And then the following sequence of shear rate was applied: Step 1: 105 s^{-1} for 1200 s → Step 2: 10.5 s^{-1} until viscosity equilibrated → Step 3: 105 s^{-1} for 608 s → Step 4: 10.5 s^{-1} until viscosity equilibrated → Step 5: 105 s^{-1} for 100 s → Step 6: 10.5 s^{-1} until viscosity equilibrated → Step 7: 105 s^{-1} for 20 s → Step 8: 10.5 s^{-1} until viscosity equilibrated. Four different preshearing times (1200, 608, 100, and 20 s) at shear rate of 105 s^{-1} were used. The results are shown in Figure 3-4.

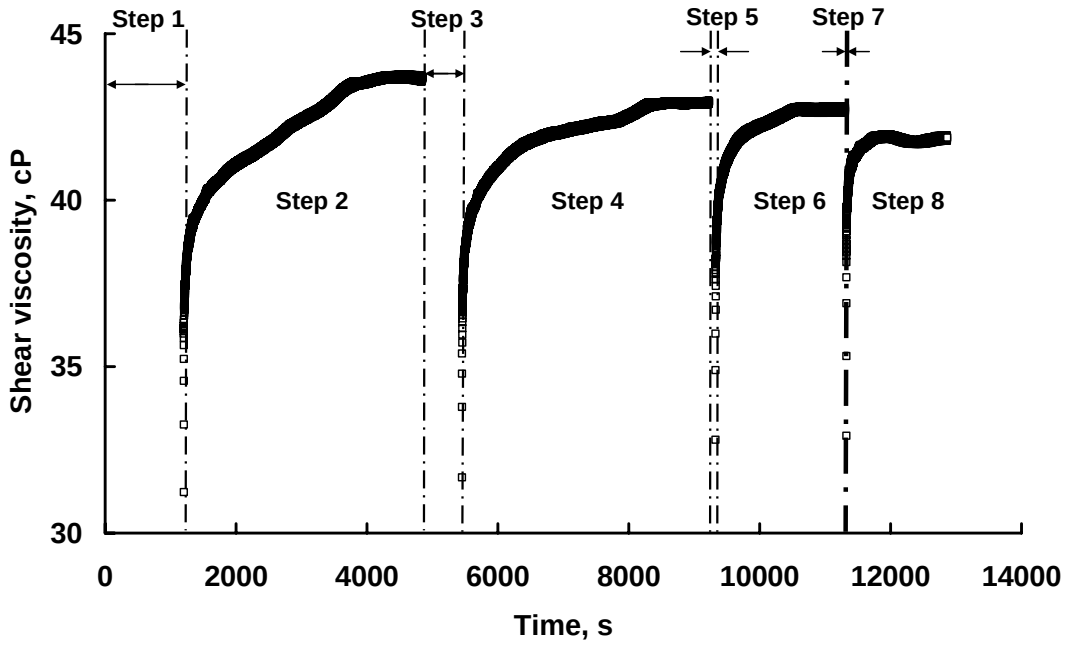

Figure 3-4: Temporal variation of shear viscosity for sample with pigment content of 17.7 vol% at temperature of 22.1±0.1°C. The shear rates for Step 1, 3, 5, and 7 and Step 2, 4, 6 and 8 were 105 s^{-1} and 10.5 s^{-1}, respectively. In steps 1, 3, 5 and 7, no data were obtained because torque was out of range.

As shown in Figure 3-4, after preshearing at shear rate of 105 s^{-1} where no shear viscosity data was taken, the shear rate was reduced to 10.5 s^{-1}, and as a result, torque fell to a value that could be measured. At low-shear-rate tests (steps 2, 4, 6 and 8), the viscosity all climbed until it reached 42.7±1.0 cP with different structure recovery time. As the preshearing time was increased, the structure recovery time also increased. At a shear rate of 10.5 s^{-1}, the structure recovery time corresponding to the four preshearing times of 1200, 608, 100 and 20 s, were approximately 3000, 2900, 1200 and 450 s, respectively. This result is interpreted to indicate that the sample was thixotropic. At steps 1, 3, 5 and 7, the sample was de-structured (reduce the number of agglomerates) and the longer preshearing time brought the sample to a lower structure. Then at steps 2, 4, 6 and 8, as shear rate was reduced, the structure began building up and correspondingly

viscosity increased with time until steady state. As longer preshearing time brought the sample to a lower structure, longer period of time was needed for the structure to rebuild at low-shear-rate test until steady-state value of viscosity was reached.

Test 2 was done using the sample with pigment content of 19.9% at temperature of 22.7±0.1°C. Before the test, the sample was stored for more than 240 hr and presheared at shear rate of 20.9 s^{-1} for 4 hr to establish an initial condition of the suspension microstructure. And then the following sequence of shear rate was applied: Step 1: 105 s^{-1} for 600 s → Step 2: 5.2 s^{-1} until viscosity equilibrated → Step 3: 105 s^{-1} for 60 s → Step 4: 5.2 s^{-1} until viscosity equilibrated → Step 5: 105 s^{-1} for 10 s → Step 6: 5.2 s^{-1} until viscosity equilibrated. Three different preshearing times (600, 60, and 10 s) at shear rate of 105 s^{-1} were used. The results are shown in Figure 3-5.

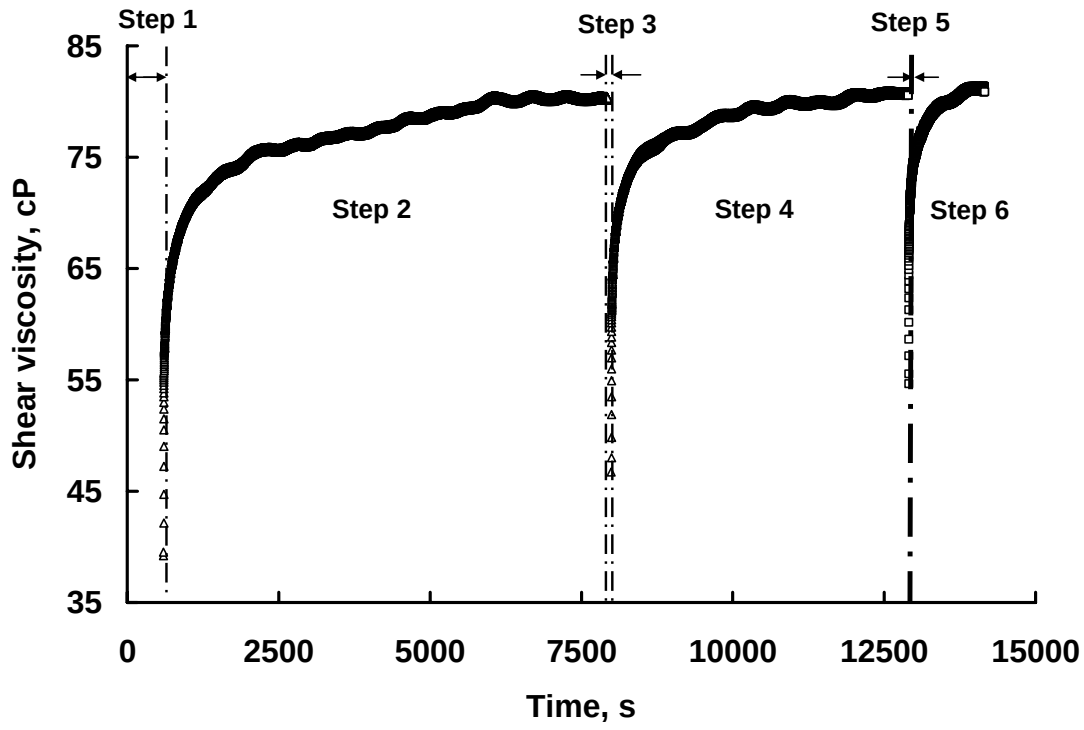

Figure 3-5: Temporal variation of shear viscosity for sample with pigment content of 19.9 vol% at temperature of 22.7±0.1°C. The shear rates for Step 1, 3 and 5 and Step 2, 4 and 6 were 105 s^{-1} and 5.2 s^{-1}, respectively. In steps 1, 3 and 5, no data were obtained because torque was out of range.

As shown in Figure 3-5, after preshearing at shear rate of 105 s^{-1} where no shear viscosity data was taken, the shear rate was reduced to 5.2 s^{-1}, and as a result, torque fell to a value that could be measured. During the low-shear-rate tests (steps 2, 4 and 6), the viscosity for all three cases climbed until it reached 80.9±0.4 cP, but structure recovery time was different for the three cases. Structure recovery time increased with increasing preshearing time. Corresponding to the three preshearing times of 600, 60 and 10 s, the structure recovery time at shear rate of 5.2 s^{-1} were approximately 5500, 3300 and 1100 s, respectively. These results are interpreted to indicate that the sample was thixotropic. At steps 1, 3 and 5, the sample was de-structured (reduce the number of agglomerates) and the longer preshearing time brought the sample to a lower structure. Then at steps 2, 4

and 6, as shear rate was reduced, the structure began building up and correspondingly viscosity increased with time until steady state was reached. As longer preshearing time brought the sample to a lower structure, longer period of time was needed for the structure to rebuild at low-shear-rate test until steady-state value of viscosity was reached.

In Figure 3-6, structure recovery time at low-shear-rate test is plotted against preshearing time at shear rate of 105 s^{-1} for both Tests 1 and 2. The structure recovery time increases with the preshearing time, but levels off at higher values of preshearing time.

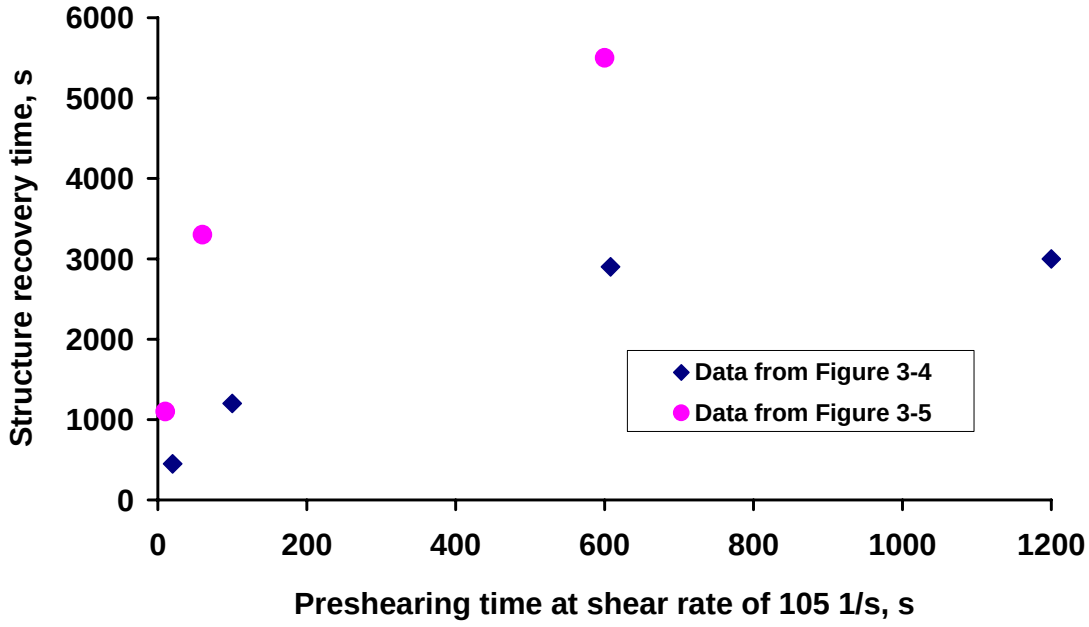

Figure 3-6: Structure recovery time at low-shear-rate test as a function of preshearing time at shear rate of 105 s^{-1} for both tests. The data are taken from Figures 3-4 and 3-5.

3.4.5 Effect of Resting Time on Structure Recovery at Low Shear Rate

If the sample is kept at rest for a certain period of time, and low shear rate is applied to the sample, an overshoot viscosity followed by an exponential decay of viscosity exists for thixotropic material. By changing the amount of resting time before applying the low shear rate, the degree of structure recovery is changed. For thixotropic material, the longer the resting time, the more the suspension is structured.

The inkjet ink sample with pigment content of 17.7 vol% was stored for about 24 hr and presheared at shear rate of 20.9 s^{-1} for 4 hr to establish an initial condition of the suspension microstructure. Then the following sequence of shear rates was applied at temperature of 21.4±0.2°C and the change of shear rates was done instantaneously: Step 1: 0 s^{-1} for 16200 s → Step 2: 10.5 s^{-1} for about 4900 s → Step 3: 0 s^{-1} for 2400 s → Step 4: 10.5 s^{-1} for about 4900 s. The results are shown in Figure 3-7. The data of Step 2 and 4 are plotted starting from t = 0 for better clarification.

As shown in Figure 3-7, the overshoot viscosity (the difference between the starting value and the steady state value of shear viscosity) is higher when the sample was at rest for longer period of time. Before Step 2 and 4, the sample was at rest for 16200 and 2400 s, respectively. For Step 2 and 4, the steady state values are similar, which are 50.4 and 49.3 cP, respectively. However, the overshoot viscosity and time taken to reach steady state value for Step 2 and 4 are 16.1 and 2.8 cP, and 4100 and ~ 300 s. It is reasoned here that the longer resting time brings the sample to a higher structured state; as a result, the starting value of shear viscosity is higher and it takes longer time to reach steady state value at a low-shear-rate test.

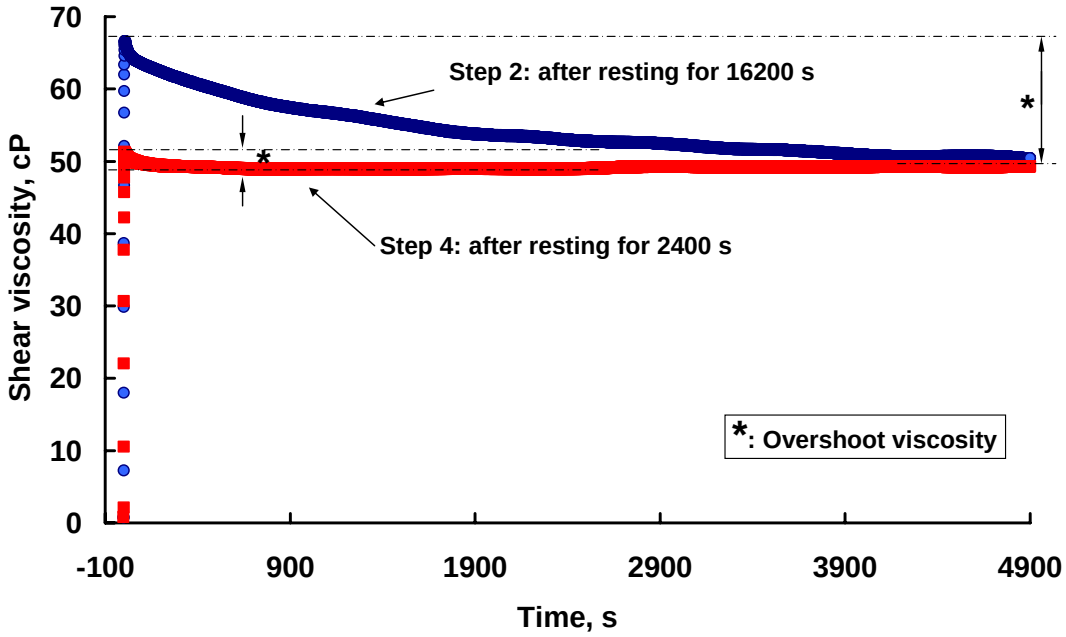

Figure 3-7: Temporal variation of shear viscosity for sample with pigment content of 17.7 vol% at temperature of 21.4±0.2°C. The shear rates for Step 2 and 4 were 10.5 s^{-1}. Before Step 2 and 4, the sample were at rest for 16200 and 2400 s, respectively. The data of Step 2 and 4 are plotted starting from t = 0 for better clarification.

3.4.6 Vibration of Time Dependent Shear Viscosity

Vibration of shear viscosity vs. time at a constant shear rate was observed for both samples with pigment contents of 19.9 and 17.7 vol% after the samples were stored for a sufficiently long period of time. In Figure 3-5, shear viscosity at shear rate of 5.2 s^{-1} approached the steady state value with periodical oscillations. This phenomenon was observed for both samples with varied amplitude and period of the oscillation.

One example of viscosity oscillation is presented here as shown in Figure 3-8 with three random chosen viscosity vs. time curves at shear rate of 5.2 s^{-1} and temperature of 23.0±0.4°C for inkjet ink sample with pigment content of 19.9 vol%. Before the test, the sample was stored for about 264 hr. Brookfield viscosity standard (50

cP at 25.0°C) was tested at shear rate of 6.3 s^{-1} and temperature of 22.1±0.1°C for more than 10 hr and no vibration of viscosity was observed. The vibration of viscosity at constant shear rate may be due to shear induced self-organized structure changes where a periodic organization of agglomeration and deglomeration processes exists as pointed out by Bagusat and his co-workers [4-8]. However, when the sample was presheared at shear rate of 105 s^{-1} for sufficient long period of time, no viscosity vibration occurred.

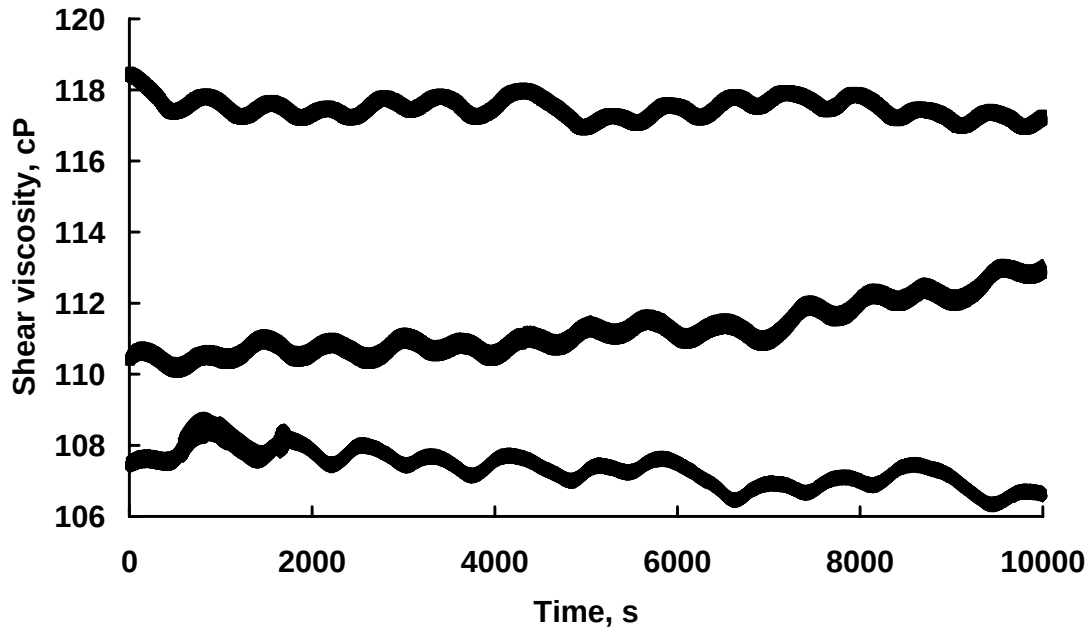

Figure 3-8: Temporal shear viscosity vibration for inkjet ink sample with pigment content of 19.9 vol% pigment content at shear rate of 5.2 s^{-1} and temperature of 23.0±0.4°C.

3.4.7 Start-Up Experiment with the Sample Exhibiting Viscoelasticity

As indicated by Barnes [2], viscoelastic effects are highly possible to coexist with thixotropic effects for situations with a full structure recovery. A start-up experiment (a shear rate is applied and shear viscosity is recorded after the sample rests for a certain

period of time) may be used to test whether or not the sample is viscoelastic. If the sample is viscoelastic, the data would be similar to the left hand side plot in Figure 3-9; if the sample is inelastic, the data would be close to the right hand side plot in Figure 3-9. Figures 3-3 and 3-7 belongs to the latter case indicating the sample is inelastic.

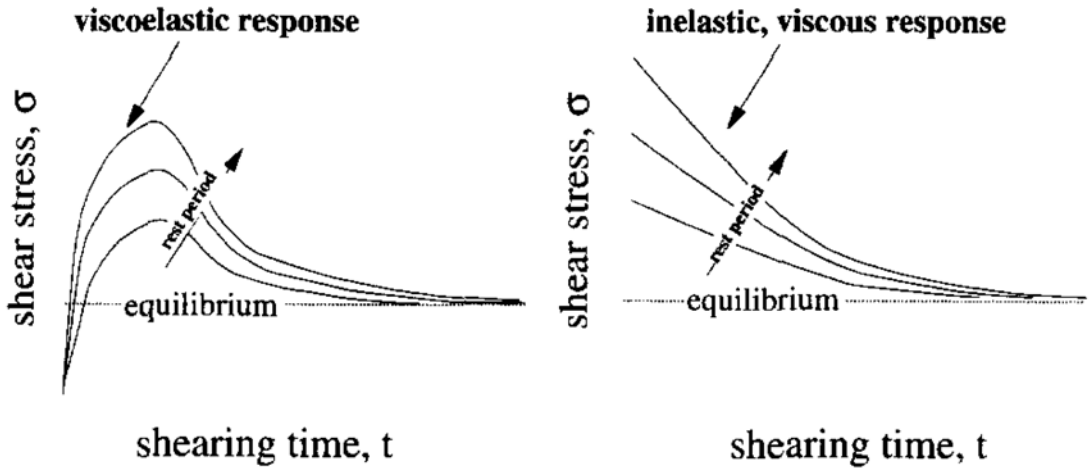

Figure 3-9: Different kinds of thixotropic behavior on start-up of shear after various degrees of rest (neglecting instrument inertia, from Figure 5 in reference 2).

For the inkjet ink sample with pigment content of 19.9 vol%, when it was stored for more than 240 hr, start-up experiment indicated that it was viscoelastic. One group of data is presented here as shown in Figure 3-10. Before the test, the sample was stored for more than 240 hr and then the sample was gently loaded to the sample reservoir with minimum disturbance to the suspension microstructure. The sample was at rest in the sample reservoir for 2 min before a shear rate of 5.2 s^{-1} was applied at temperature of 22.5±0.3°C.

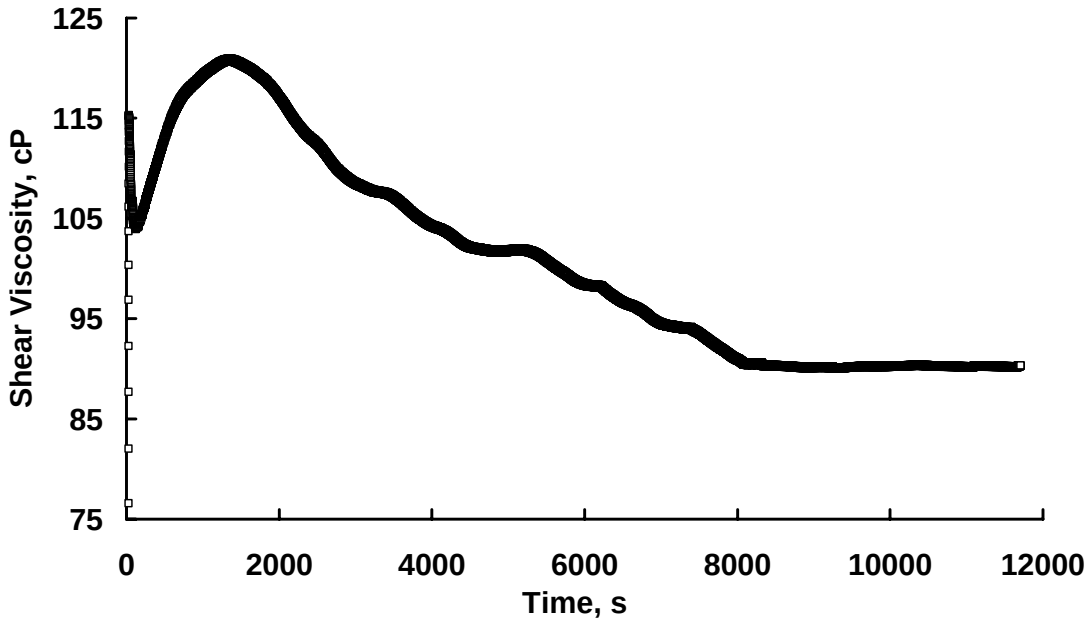

Figure 3-10: Temporal variation of viscosity vibration for inkjet ink sample with pigment content of 19.9 vol% pigment content at shear rate of 5.2 s^{-1} and temperature of 22.5±0.3°C.

The data shown in Figure 3-10 is a typical start-up experiment data for thixotropic material with viscoelastic properties, which are similar to the left hand side plot in Figure 3-9. Initially, the curve started with viscosity decreasing with time from about 115.2 cP to about 104.4 cP. Then the viscosity increased until it reached about 120.8 cP and decreased until it reached the steady state value of 90.2 cP. This phenomenon is interpreted to indicate that the sample had viscoelasticity [2] after being stored for sufficient long period of time. According to Barnes [2], the time-dependence shear viscosity due to viscoelasticity exhibits both short time elastic responses, where the microstructural elements responds yet retains its structure, and long time viscous effect, where the microstructural elements break down.

Similar phenomenon was not observed for inkjet ink sample with pigment content of 17.7 vol% even after shelf time of more than 600 hr. However, when the sample with

viscoelasticity was presheared at shear rate of 105 s^{-1} for sufficient long period of time, the suspension became inelastic.

3.5 Conclusions

The surface-modified carbon-black pigmented water-based inkjet ink samples with sufficiently high pigment loading were found to show time-dependent shear viscosity. Qualitative study was conducted using two samples with pigment loading of 17.7 and 19.9 vol%, respectively, under transient experimental procedures. The results indicate that both samples were thixotropic materials and the sample with pigment loading of 19.9 vol% exhibited viscoelasticity after being stored for sufficiently long period of time. The observations are believed to be associated with the change of suspension microstructure. At high pigment content, the ionic strength increases to an extent that double-layer repulsion is not sufficient anymore to stabilize the system, as a result, weakly structured agglomerates are formed. External shearing de-structures the material (reduce the number of agglomerates) corresponding to a temporal decrease of viscosity, and structure rebuild over time at rest or at comparably lower shear rates corresponding to a temporal increase of viscosity.

3.6 References

1. Barnes, H. A., Hutton, J. F., and Walters, K., An Introduction to Rheology, Elsevier, (1989).
2. Barnes, H. A., J. Non-Newtonian Fluid Mech.70, 1 (1997).
3. Lotka, A. J., J. Am. Chem. Soc. 42, 1595 (1920).
4. Bagusat, F., Seidel, O., and Mogel, H. J., Progr. Colloid Polym. Sci. 111, 82 (1998).
5. Lemke, T., Bagusat, F., Kohnke, K., Husemann, K., and Mogel, H. J., Colloid Surf. A: Physicochem. Eng. Asp. 150, 283 (1999).
6. Seidel, O., Bagusat, F., and Mogel, H. J., Rheol. Acta. 38, 305 (1999).
7. Bagusat, F., Schiller P., Seidel, O., Zehl, T., and Mogel, H. J., Colloid Surf. A: Physicochem. Eng. Asp. 215, 131 (2003).
8. Bagusat, F., Bohme, B., Schiller P., and Mogel, H. J., Rheol. Acta. 44, 313 (2005).

CHAPTER 4

DOD DROP FORMATION OF COLLOIDAL SUSPENSIONS CONTAINING SURFACE-MODIFIED CARBON BLACK PIGMENT

4.1 Introduction

The fundamental aspects of various drop formation processes including liquid ejection, capillary breakup, thread retraction, satellite formation, etc., have been studied over the last two decades [1-5]. A review of these studies and the major experimental investigations on DOD drop formation where various kinds of high-speed photography techniques have been utilized can be found in references 1 and 6. In this section, after reviewing Dong's Ph.D. dissertation research on DOD drop formation [6], some newer developments and related topics on DOD drop formation dynamics of complex fluids containing particles are presented.

Dong *et al.* [7] developed a high speed flash photography imaging system with spatial and temporal resolutions of 0.81 μm/pixel and 200 ns, respectively. Using this system, they studied DOD drop formation of pure Newtonian fluids in great detail. It was found that DOD drop formation of pure fluids is highly reproducible with a positional variation of 1 μm. The whole DOD drop formation process starting from the emergence of liquid body from the inkjet nozzle to the stage where the primary and satellite drops reach equilibrium drop speeds was recorded. The DOD drop formation process including liquid ejection, breakups of liquid ligament, thread contraction, formation of primary and satellite drops, and recombination of primary and satellite drops were discussed. A function for evaluating the breakup time of liquid threads and a criterion for the existence of recombination of primary drop and satellite were proposed. Their work indicates that primary drop size is scaled with the size of the inkjet nozzle.

For the jetting parameters in their study, primary drop size increased slightly with increasing surface tension and/or decreasing viscosity. The effects of driving signal amplitude and waveform shape on DOD drop formation were also investigated. When the signal amplitude is increased, the variation of primary drop size is insignificant; however, both the number and sizes of satellite drops change significantly and the higher the signal amplitude, the larger the total volume of the satellites. Waveform shape of the actuating signal can greatly affect DOD drop formation dynamics.

Chen and Basaran [8] also investigated the effect of signal waveform. By manipulating the signal waveform for driving the piezoelectric element, they significantly reduced drop radius without reducing nozzle radius. As a result, a reduction in the liquid volume greater than a factor of 10 was achieved.

Investigations were also conducted on understanding the flow pattern inside the ejected liquid thread during DOD drop formation process. Meinhart and Zhang [9] successfully visualized flow field within an inkjet nozzle by using micro-particle imaging velocimetry (μ-PIV). A 60-μm-wide and 45-μm-deep triangle-shaped nozzle was used. The spatial and temporal resolutions of the instantaneous velocity vector fields were 5-10 μm and 2-5 μs, respectively. They found that the flow in the nozzle is highly unsteady with a maximum velocity of 8 m/s, Reynolds numbers of Re = 500, and accelerations of up to 70,000 g. The flow field and meniscus shapes in the nozzle were found to be periodic for each ejection cycle. Four critical stages of shape deformations of meniscus were identified: infusion, inversion, ejection and relaxation. They also found that the center of the meniscus shape becomes inverted for a short period of time. Xu and Basaran *et al.* [10] carried out a computational analysis to simulate the formation of liquid drops of incompressible Newtonian fluids from a simple capillary tube by imposing a transient flow rate upstream of the nozzle exit. They thoroughly reviewed both experimental and computational investigations on DOD drop formation. Three different scenarios were discussed based on the value of Weber number (We): 1) breakup

does not occur, and drops remain pendant from the nozzle and undergo time periodic oscillations; 2) DOD drops form but have negative velocities, i.e., they move toward the nozzle upon breakup; and 3) DOD drops are formed with positive velocities, i.e., they move away from the nozzle.

Compared to the study of DOD drop formation of pure fluids, detailed experimental study on DOD drop formation dynamics of particle-laden suspension has not received much attention. De Jong *et al.* [11, 12] found that small particles may lead to a distorted droplet formation and a film formed by accumulated particles on the nozzle plate favors void formation once the meniscus is pulled back, which causes air entrapments in the printheads. More recently, they [13] observed a characteristic ink flow pattern occurs on the nozzle plate. An air flow induced by droplet jetting process drives the particles toward the jetting nozzle, causing air entrapment into the ink channel and nozzle failure. Even without droplet jetting process, they found [14] Marangoni flow induced ink flow on the nozzle plate.

Although no refereed literature was found on experimental study of DOD drop formation dynamics of particle laden suspension, Furbank and Morris [15, 16] investigated millimeter-size drop formation dynamics of particle-laden suspensions. The particles utilized in their study were on the order of 100 μm and the orifice from which the drops were formed was on the order of 1 mm. The particles were neutrally buoyant and colloidal forces were negligible. They found that "*during necking, particles in the thread resist its further thinning and, depending on the number of particles present, this resistance can have either a destabilizing or a stabilizing effect on the thread relative to the case of the pure liquid* [15]". However, in DOD drop formation process, the nozzle size and particle size are typically smaller than 100 μm and 1 μm, respectively, and colloidal forces are important. Effect of individual colloidal particle or a group of colloidal particles on the evolution of ejected liquid thread is difficult to experimentally

investigate, particularly considering the short duration of DOD drop formation process (~ O(100 μs)).

4.2 Objective

The objective of the research discussed in this chapter is to investigate DOD drop formation dynamics of colloidal suspension containing surface-modified carbon black pigment with various pigment loading and to compare it with that of pure fluid. Part of the effort is directed at elucidating whether or not steady state rheological data measured at high shear rate typical of those experienced in DOD drop formation can be correlated with DOD drop formation dynamics of highly loaded inkjet inks. Since the work presented in this chapter is a follow-up of Dong's DOD drop formation studies of pure liquids, the analysis of the experimental data is similar.

4.3 Experimental

4.3.1 Imaging Strategy

The high-speed flash photography imaging system was originally developed by Dong *et al.* [6, 7]. Detailed information related to the imaging system including synchronization strategy, apparatus, image properties etc. is available in references 6 and 7. The temporal and spatial resolutions for this study were 1 μs and 0.87 μm/pixel, respectively. The calibration of the image system was done using a standard micron ruler (Nikon Stage Micrometer, 1 mm).

In order to successfully conduct the experimental work, the imaging system was modified by using a jetting frequency of 10 kHz. The jetting frequency used in Dong's study was 20 Hz. At a jetting frequency of 20 Hz, it was found that the DOD drop

formation dynamics of the ink sample with highly pigment loading has poor reproducibility. In order to study the effect of particle loading on DOD drop formation, the formulation of the ink sample was simple with no chemical added for controlling the wetting behavior of the nozzle plate. It is conjectured that at a jetting frequency of 20 Hz, the nozzle continually experienced clogging due to evaporation of solvent, leading to accumulation of particles around and inside the nozzle [11, 12]. As a result, the jetting was highly unstable and easily stopped. To successfully use the imaging system developed by Dong to obtain a full set of data for representing DOD drop formation process of one inkjet ink sample, no less than 30 minutes of jetting is needed. During this period of time, the jetting behavior must be highly reproducible. Due to the poor jetting performance mentioned above, no data was found to be significantly consistent through a period of 30 minutes. It was found empirically that the jetting behavior for the ink sample with high pigment loading is improved by increasing the jetting frequency. It is conjectured that at higher jetting frequency, the time window for solvent evaporation between drop ejections is shorter and the mass flux of solvent from the nozzle is increased, leading to a balance between solvent loss and solvent supply. As a result, the wetting around the nozzle meniscus is well maintained and a stable jetting behavior is obtained.

A jetting frequency of 10 kHz was chosen for the following reasons: 1) at this frequency, the imaging system can be set up to allow continuous jetting of the nozzle and to obtain high reproducibility; 2) for the copper vapor laser used in this study, the optimum lasing frequency is 10 kHz, which means that at this frequency the energy per pulse is maximized. Operating the nozzle at 10 kHz required modifying the synchronization strategy for the CCD camera, copper vapor laser, and the inkjet nozzle. Correspondingly, the operating procedure for the imaging system originally developed by Dong *et al.* [6, 7] was changed.

4.3.2 Inkjet Nozzle

The printhead (Trident) used in this study is based on a push-mode design (Trident User's Manual, 1997). The diameter and length of the inkjet nozzle are 53 and 75 μm, respectively, as shown in Figure 4-1. The waveform used for actuating the piezoelectric inkjet nozzle is shown in Figure 4-2. Detailed information related to the functionality and actuating mechanism of the double-peak waveform signal is available in reference 6.

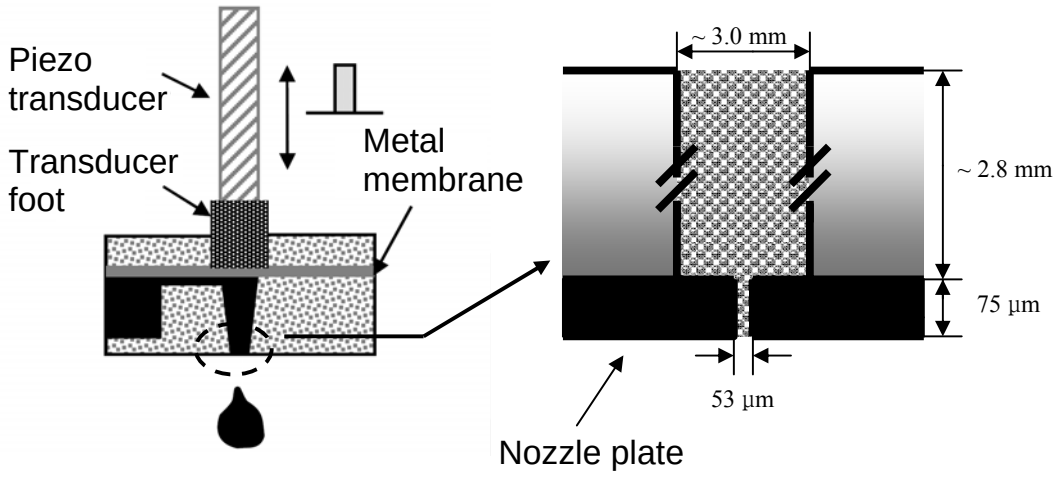

Figure 4-1: Geometry of the inkjet nozzle used in this study.

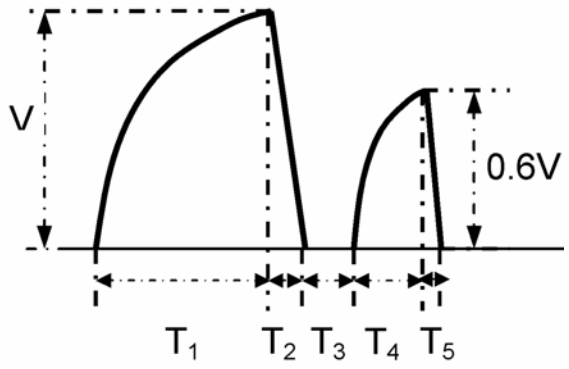

Figure 4-2: Double-peak waveform for actuating the piezoelectric nozzle used in this study: rising time of the first pulse T_1 = 10.6 μs, falling time of the first pulse T_2 = 2.6 μs, dead time T_3 = 5.3 μs, rising time of the second pulse T_4 = 4.4 μs, falling time of the second pulse T_5 = 3.0 μs.

4.3.3 Sample Preparation and Characterization

Properties of three inkjet ink samples used for investigating the effects of particle loading on DOD drop formation dynamics are given in Table 4-1. Inkjet ink Samples #2 and #3 were prepared from the inkjet ink preparation CAB-O-JET® 200 (Cabot Corp.) which had a pigment volume fraction of 10.3%. The properties of the inkjet ink preparation are given in Chapter 2. A Newtonian fluid with no pigment added (Sample #1) was used as a reference. The low-shear-rate shear viscosity was measured using a Brookfield Part No. LVDVI+ Couette viscometer at shear rate of 52.3 s^{-1} and temperature of 22°C. The static surface tension was measured using a KRUSS Bubble Pressure Tensiometer BP2 with capillarity of 1.110 mm at temperature of 23°C. As can be seen in Table 4-1, the three samples have similar values of low-shear-rate shear viscosity, surface tension and density. Yet the volume fraction of pigment varies significantly.

Table 4-1: Inkjet ink samples used for studying DOD drop formation of particle suspension

Sample	Pigment, vol%	Base fluid			Shear viscosity at shear rate of 52.3 s^{-1}, cP	Surface tension, mN/m	Density, g/ml
		Glycerin, vol%	DI water, vol%	Viscosity, cP			
#1	0	48.4	51.6	6.4	6.4	67.8	1.14
#2	5.7	35.5	58.8	3.7	6.4	69.5	1.19
#3	15.0	0	85.0	1.0	6.3	71.0	1.24

By using the capillary viscometer discussed in Chapter 2, the shear viscosity at shear rates up to 2×10^5 s^{-1} was characterized. The data in Figure 4-3 show that inkjet ink samples with similar low-shear-rate viscosity exhibited significantly different shear viscosities at high shear rates. At shear rate of 2×10^5 s^{-1}, the shear viscosities of Sample #2 and #3 drop from 6.4 to 5.7 cP and from 6.3 to 3.5 cP, respectively. This shear-thinning behavior is attributed to breakdown of weakly structured agglomerates in the suspension at high shearing field as discussed in Chapter 2.

Since no polymeric dispersant or surfactant was present in the three samples, dynamic surface tension was found to be the same as the static surface tension by using KRUSS Bubble Pressure Tensiometer BP2 at bubble frequency up to 10 Hz. Since Sample #1 contains no pigment, it is reasonable to expect that the dynamic surface tension is constant even at very high surface deformation. Yet, it is unclear for Samples #2 and #3. If at very high surface deformation, pigment particles adsorb to the air-suspension interface, the interfacial tension would be decreased [17]. Considering the highly unsteady flow during DOD drop formation process as indicated by Meinhart and Zhang [9], the time duration and spatial location for the appearance of particles on the interface are thus extremely hard to predict. No commercially available instrument is

capable of measuring dynamic surface tension at surface dilatational rate encountered in DOD drop formation process. As a result, dynamic surface tension of inkjet ink during DOD drop formation process is unknown.

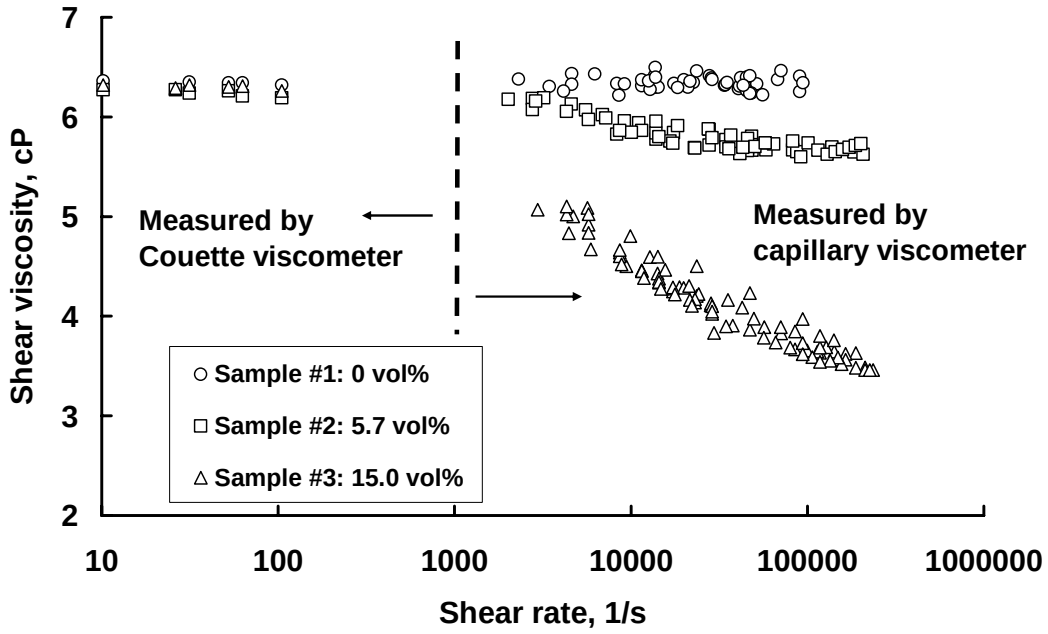

Figure 4-3: Shear viscosity of inkjet ink samples in Table 4-1 as a function of shear rate at temperature of 22°C.

DOD drop formation is triggered by periodic movement of the piezoelectric transducer (see Figure 4-1) at frequency typically between 1 kHz and 50 kHz. The induced propagating pressure waves in the fluid makes the jetting process an acoustic phenomenon. As a result, the acoustic wave speed of the inkjet ink becomes an important parameter. The influence of jetting frequency on the speed and volume of ejected liquid body is shown in Chapter 5.

According to Derby *et al.* [18], when the viscous boundary layer thickness is much larger than the particle size, acoustic wave propagation occurs in the viscous

regime and the acoustic wave speed of suspension, *c*, can be calculated using effective medium concepts [19]

$$c(\phi) = \sqrt{\frac{K_{eff}(\phi)}{\rho_{eff}(\phi)}}, \tag{4-1}$$

where $K_{eff}(\phi)$ and $\rho_{eff}(\phi)$ are the effective bulk modulus and density, respectively, of a suspension containing a volume fraction ϕ of particles and they can be determined by the rule of mixtures approach:

$$\rho_{eff}(\phi) = \phi_1\rho_1 + \phi_2\rho_2 + \phi_3\rho_3 + \cdots \tag{4-2a}$$

$$\frac{1}{K_{eff}(\phi)} = \frac{\phi_1}{K_1} + \frac{\phi_2}{K_2} + \frac{\phi_3}{K_3} + \cdots \tag{4-2b}$$

The viscous boundary layer thickness $\delta_V = \sqrt{\frac{2\eta_m}{\rho_m\varpi}}$, where η_m and ρ_m are the suspending medium viscosity and density, respectively, and ϖ is the angular frequency of the acoustic excitation, is used to determine the dominant effects on particle drag. For the suspensions and a jetting frequency of 10 kHz used in this study, the viscous boundary layer thickness is determined to be more than 100 times larger than the particle size (mean particle size of 130 nm). Eq. (4-1) was used to predict the acoustic wave speed of the inkjet ink samples in Table 4-1 plus three additional particle suspensions. In Table 4-2, the predicted acoustic wave speeds are compared with acoustic wave speeds measured using an acoustic speed measurement device developed by FUJIFILM Dimatix, Inc. Eq. (4-1) predicted the acoustic wave speed of particle suspension with an error no more than 5%. The measured acoustic wave speeds of three inkjet ink samples with pigment loading of 0, 5.7, and 15.0 vol% are 1628, 1671, and 1494 m/s, respectively.

Table 4-2: Acoustic wave speed calculated using Eq. (4-1) and measured acoustic wave speeds of the three samples listed in Table 4-1 and three additional particle suspensions

Sample	Pigment, vol%	Water, vol%	Glycerin, vol%	*c*, m/s (predicted)	*c*, m/s (measured)	Error, %
#1	0	51.6	48.4	1612	1628	1.0
#2	5.7	58.8	35.5	1587	1671	5.0
#3	15.0	85.0	0	1504	1494	0.7
#4	3.2	96.8	0	1485	1427	4.1
#5	6.5	93.5	0	1488	1494	0.4
#6	10.1	89.9	0	1494	1494	0.0

4.3.4 Experimental Protocol and Image Analysis

Investigation conducted by De Jong *et al.* [11-14] implies that inkjet printing of particle-laden suspensions may involve dried particles accumulating on the nozzle plate, which can lead to nozzle failure. During the experimental study of the samples with 5.7 vol% and 15.0 vol% pigment loading, the inkjet nozzle often jetted a ligament with non-straight flying trajectory and/or highly non-axisymmetric ligament formation, as shown in Figure 4-4. Usually, when those phenomena occurred, the temporal duration of the continuous firing process of an individual inkjet nozzle was very short, ranging from several seconds to a few minutes. However, in some cases, the nozzle was capable of continuously firing for a sufficient long period of time for collecting data, but the flying trajectory varied periodically or randomly. The opportunity to obtain excellent jetting behavior was rare and in most cases the jetting behavior was non-ideal in terms of: 1) non-straight flying trajectory, 2) non-axisymmetric ligament formation, 3) insufficient long period of duration of excellent jetting behavior, and 4) long duration of non-

consistent jetting behavior. It is suspected that the non-ideal jetting behavior is attributed to the accumulated particles and non-ideal wetting condition on the nozzle plate as discussed by De Jong *et al.* [11-14]. None of the data taken when the jetting problems occurred are included in the discussion below.

Non-straight flying trajectory		→ later on	
Non-axisymmetric ligament shape		→ later on	

Figure 4-4: Examples of non-ideal jetting conditions frequently encountered in studying DOD drop formation of highly pigmented inkjet inks used in this study.

The same nozzle was used for testing all three inkjet ink samples at a testing temperature of 21±1°C. The data used in this chapter were obtained at a jetting condition where the inkjet nozzle continued firing for a period of more than 5 hrs at a frequency of 10 kHz with consistent jetting behavior. The reproducibility was well maintained. The straightness of flying trajectory and axisymmetry of the jetted liquid ligament were superior. The data used for discussion were collected through a trail-and-error approach until optimum jetting conditions were reached. So the repeatability is defined here as

how much the jetting behavior can be reproduced at the optimum jetting condition, namely, consistent jetting with straight, axisymmetric ligament.

Totally four signal amplitudes (24.7, 27.8, 30.9, and 36.5 V) were used for all three samples. The sequence of adjusting signal amplitude was as following: 36.5→30.9→27.8→24.7→36.5 V. The last step was used to compare with the first step in order to ensure the jetting consistency during the test. Experimental procedures [6] were carried out to ensure the liquid jetted from the nozzle had the same material composition of the liquid in the ink reservoir.

During the experiment where data were collected, the nozzle continuously fired. Thus, the so-called "first drop problem" [1, 6] did not appear. Time was counted starting from the moment when the liquid thread started to appear on the nozzle. More than 20 images were taken at each time in increments of one microsecond. Figure 4-5 shows a group of ten pictures, indicating DOD drop formation of the particle suspension used in this study was highly reproducible. It was found that at an exposure time of 1 μs, the spatial variation is less than 2.0 μm.

Similar to Dong's approach [6], Microsoft paint was used for quantitatively analyzing the recorded images and Matlab program was only used to crop the images for the discussion. A typical image representing an ejected liquid thread is shown in Figure 4-6. Five representative positions are selected and the temporal evolutions of their positions are determined to form a series of curves for quantitatively discussing DOD drop formation dynamics. $x_1(t) - x_5(t)$ are used to determine the axial distances from the five representative positions to the nozzle exit.

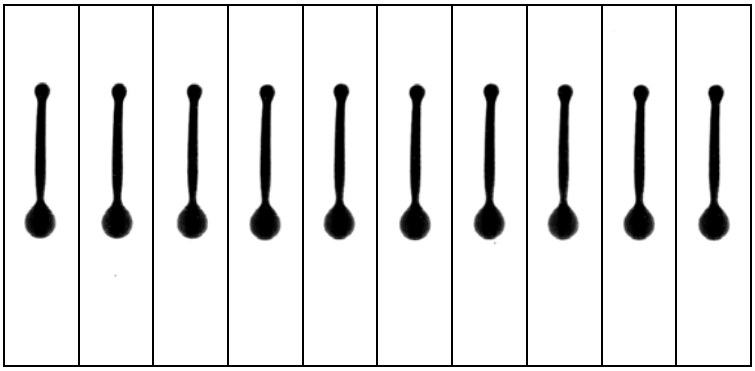

Figure 4-5: Reproducibility of drop generation of 15.0 vol% sample using the double-peak waveform shown in Figure 4-2 with signal amplitude of 30.9 V and frequency of 10 kHz.

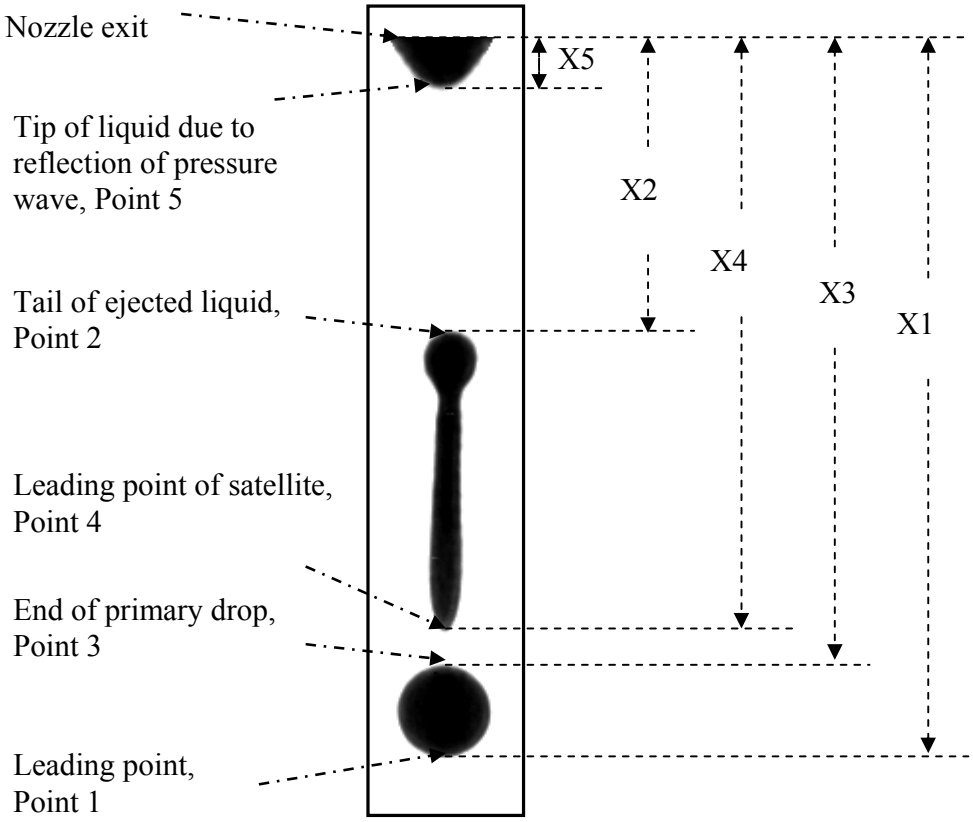

Figure 4-6: Five representative points used for quantitatively discussing DOD drop formation dynamics.

4.4 Results and Discussion

In this section, the results are presented in a format developed originally by Dong [6]. The discussion is focused on comparing DOD drop formation behavior of particle suspension with that of Newtonian fluid with the same low-shear-rate shear viscosity.

4.4.1 General Description of DOD Drop Formation

A typical DOD drop formation process of pigmented inkjet ink where formation of satellite drops is involved is illustrated in Figure 4-7. DOD drop formation typically involves the following stages: 1) ejection and stretching of liquid thread (images 1-4), 2) necking and pinch-off of liquid thread from nozzle (images 5-10), 3) recoil of free liquid thread (images 11-13), 4) breakup of the free liquid thread (images 14-16), and 5) formation of primary drop and satellite(s) (images 17-22).

In Figure 4-8, the evolution of ejected liquid ligament versus time is shown for the five representative points in Figure 4-6. Figure 4-8 can be used [6] to calculate parameters related to the drop formation including speed of the representative points at various positions, speeds of primary drop and satellites, pinch-off length and time of the liquid thread from the nozzle exit, time of breakup of liquid thread into satellites and primary drop, sizes of primary drop and satellite. Detailed discussion of each stage illustrated in Figure 4-7 and for usage of Figure 4-8 can be found in references 1 and 6.

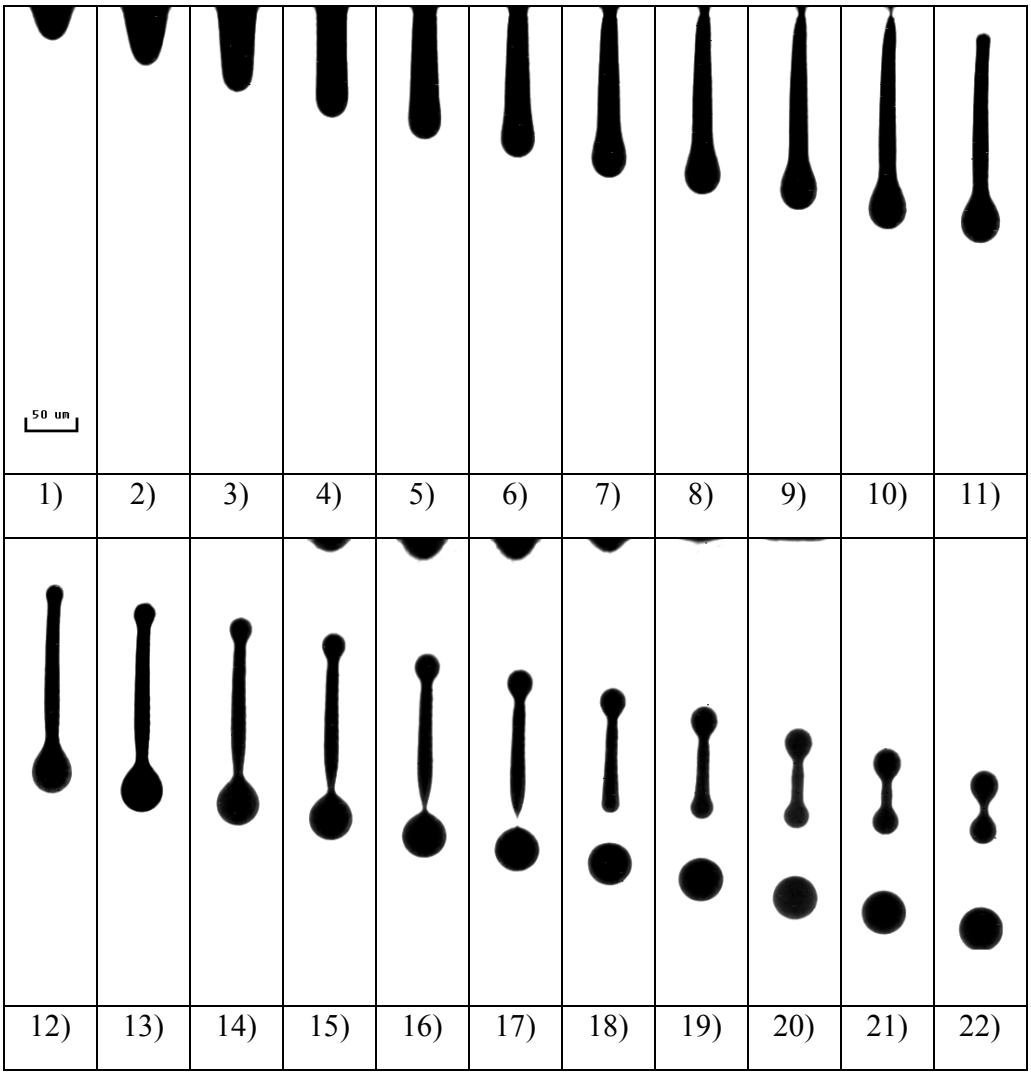

Figure 4-7: Sequence of images of DOD drop formation for Sample #3 in Table 4-1 using the double-peak waveform shown in Figure 4-2 with signal amplitude = 30.9 V and jetting frequency = 10 kHz. Interframe time = 3 μs and image size = 87 μm × 418 μm. The inkjet ink sample contains carbon black pigment of 15.0 vol% and water of 85.0 vol%.

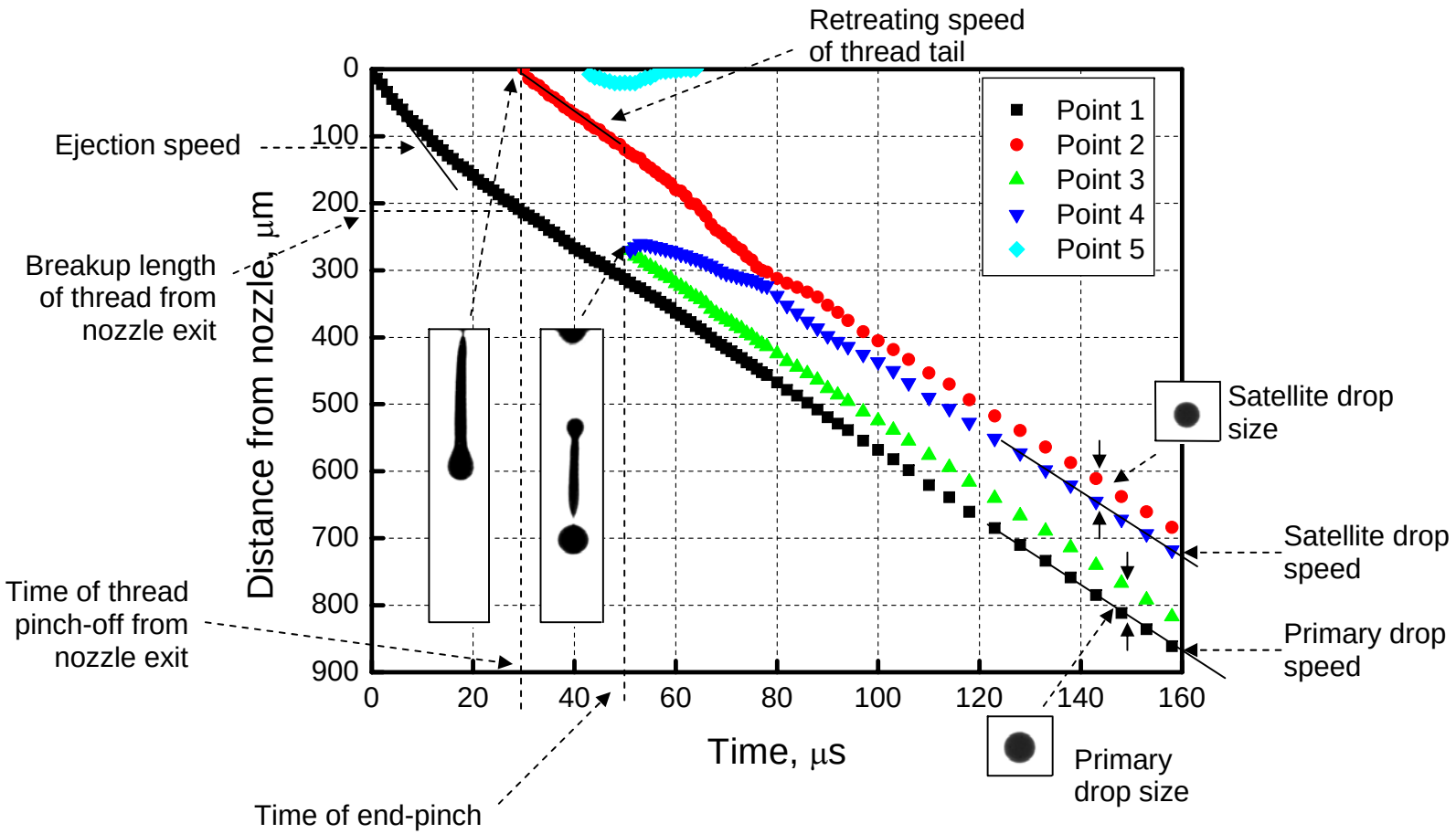

Figure 4-8: Curves of DOD drop formation corresponding to the images shown in Figure 4-7.

4.4.2 Ejection and Stretching of Liquid Thread

In Figure 4-9, sequential images of the ejection and stretching of three inkjet inks at two signal amplitudes of V = 24.7 and 30.9 V are shown. Although pigment loading varies from 0 vol% to 15.0 vol%, there is no significant difference in this stage for the three inks. The first breakup time, t_{b1}, of these three samples (static surface tension of 69±2 mN/m and low-shear-rate shear viscosity of 6.3±0.1 cP) at four different signal amplitudes is 30±2 μs. In Dong's study [6], the first breakup time of the glycerin/water mixture (surface tension of 68 mN/m and viscosity of 5.0 cP) was 28 μs at different signal amplitudes. Such a similar result indicates a strong reliance of breakup time on surface tension. The existence of a slightly longer first breakup time in this study is attributed to the higher shear viscosity of the inkjet ink samples and the resulting stronger resistance to the fluid motion.

In Figure 4-10, a detailed comparison for the three inkjet inks is made by plotting the position of the leading edge measured from the nozzle exit versus the radial position measured from the left wall of the nozzle at time of 4 μs and signal amplitude of 30.9 V. The similar parabola profiles indicate that no significant difference existed among these three inkjet inks.

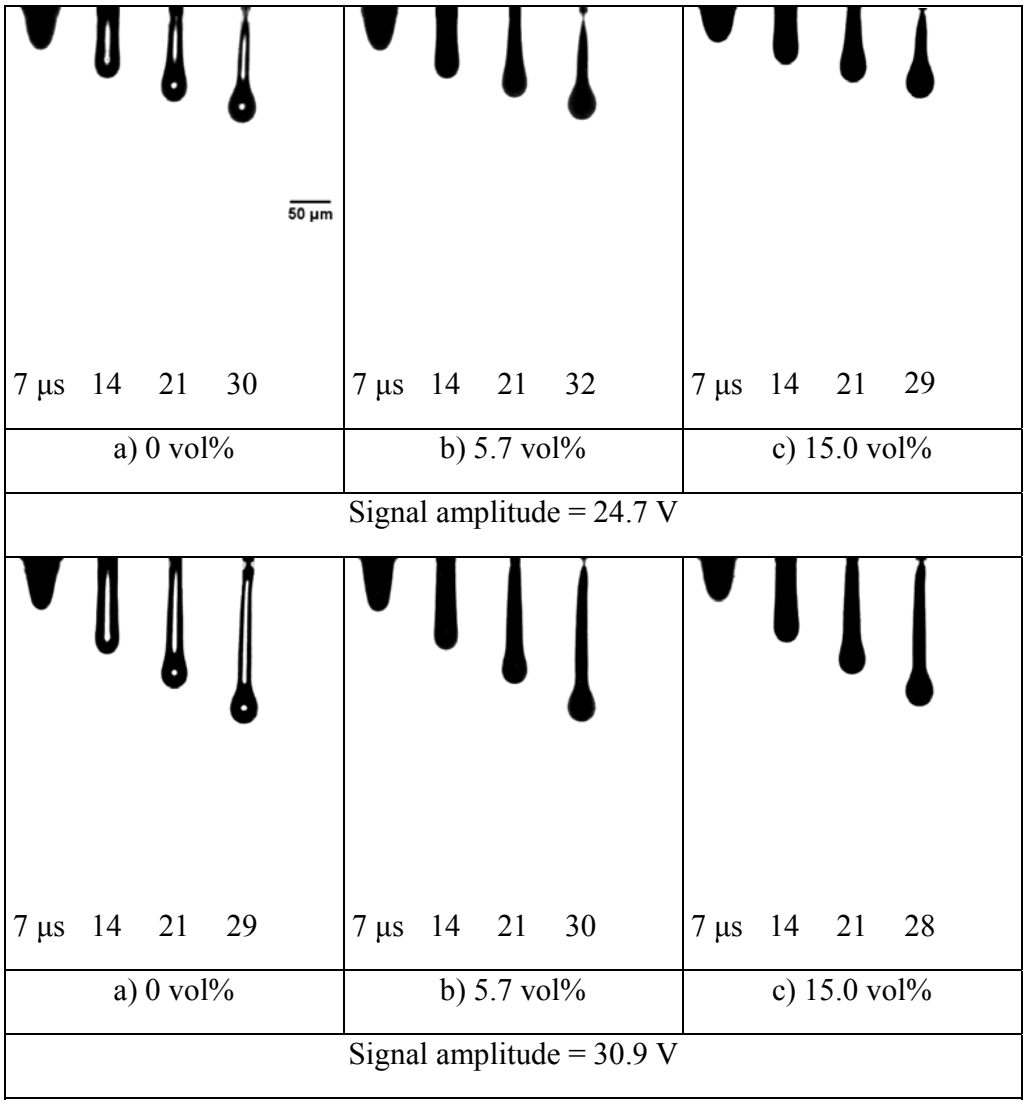

Figure 4-9: Sequential images of ejection and stretching of three inkjet ink samples tested (see Table 4-1) using the double-peak waveform in Figure 4-2 with signal amplitude = 24.7 and 30.9 V and frequency = 10 kHz. Image size = 87 µm × 418 µm.

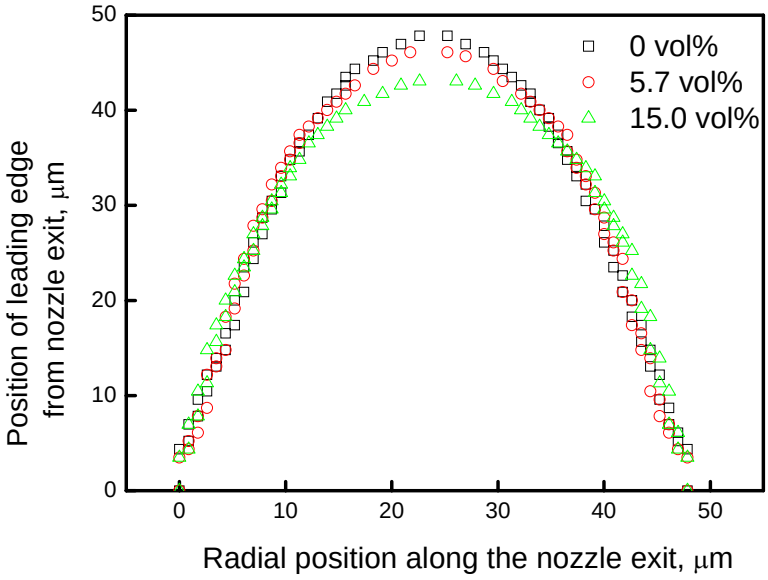

Figure 4-10: Position of leading edge of Sample #1, #2, #3 in Table 4-1 at time = 4 μs, signal amplitude = 30.9 V and frequency = 10 kHz. X-axis is the radial position along the nozzle exit and Y-axis is the distance of the leading edge from the nozzle exit.

In Figure 4-11, the temporal variations of x_1 are shown for the three samples at signal amplitudes of 24.7 and 30.9 V. Pinch-off occurs at the last time shown in each of the plots. The liquid pinch-off length, $l_b = x_1$ at t_{b1}, increases with the driving signal amplitude. The speed of Point 1 (dx_1/dt) decreases as it moves away from the nozzle, and is faster for a higher driving voltage. The first breakup time, t_{b1}, is slightly faster for ink sample with pigment loading of 15 vol% than those of ink samples with pigment loadings of 0 and 5.7 vol%. This may be due to a lower apparent shear viscosity of the 15 vol% pigment loading ink sample during the ejection process.

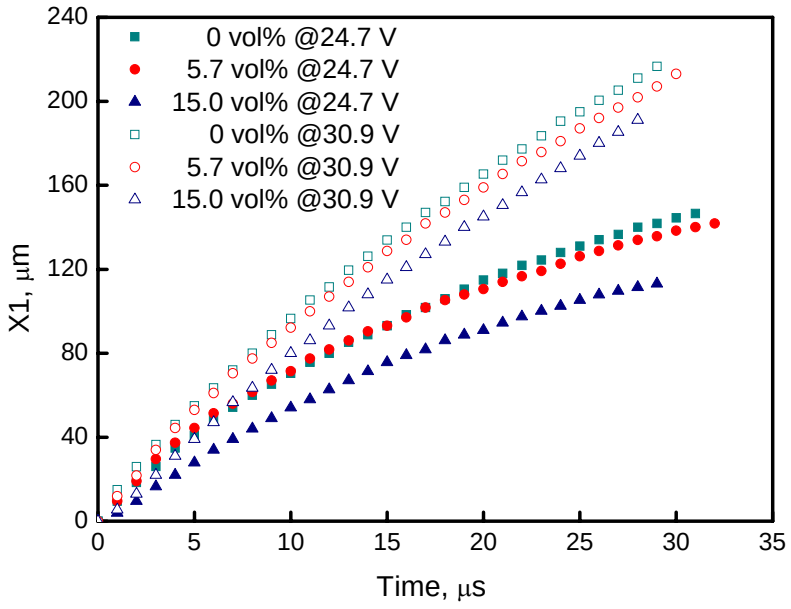

Figure 4-11: Temporal variation of Point 1 in Figure 4-6 before pinch-off from the nozzle exit for three samples tested using the double-peak waveform in Figure 4-2 with signal amplitudes = 24.7 and 30.9 V and frequency = 10 kHz. Highest time shown for each plot corresponds to the time of pinch-off from nozzle exit, t_{b1}.

The speed of Point 1 (dx_1/dt) was found to be constant for the first few seconds during the ejection process and it is defined as ejection speed, v_e. The shortest traveling time taken for the ejected liquid to go through the 75-µm length inkjet nozzle (see Figure 4-1), t_e, is calculated based on v_e. Since v_e is the maximum value of the speed of Point 1 (dx_1/dt) during DOD drop formation process, t_e is the time scale where the strongest hydrodynamic motion is applied to the ink. The speed of Point 1 at pinch-off from nozzle exit is defined as v_{b1}. These parameters are summarized in Table 4-3.

Table 4-3: Ejection speed, speed of Point 1 at pinch-off from nozzle exit, and traveling time of ink through the nozzle at ejection speed

Liquid	Voltage, V	Ejection speed, v_e, m/s	Speed of Point 1 at pinch-off from nozzle exit, v_{b1}, m/s	Traveling time of ink through the nozzle, at ejection speed, t_e, μs
0 vol%	24.7	8.0	2.5	9.4
	27.8	9.1	4.4	8.2
	30.9	10.4	5.2	7.2
	36.5	12.9	8.8	5.8
5.7 vol%	24.7	8.1	2.1	9.3
	27.8	9.2	3.6	8.2
	30.9	10.3	5.1	7.3
	36.5	12.4	7.8	6.0
15.0 vol%	24.7	5.8	2.1	12.9
	27.8	7.8	3.9	9.6
	30.9	8.1	5.7	9.3
	36.5	10.0	6.7	7.5

When compared to ink samples with pigment loadings of 0 and 5.7 vol%, the 15 vol% sample exhibited a lower ejection speed and consequently a longer t_e; however, v_{b1} is similar for all three samples. For the three inks, t_e ranged from 6 to 13 μs. Thus the time over which shear stress is applied to the ink in the nozzle is extremely short.

The volume and surface area of liquid ejected as a function of time were determined for Sample #3 (15.0 vol%, see Table 4-1) at signal amplitudes of 24.7, 27.8, 30.9 and 36.5 V and a jetting frequency of 10 kHz, see Figure 4-12. The results indicate

that the higher the signal amplitude, the higher the volume, and correspondingly, a larger surface area of the ejected liquid thread. Before the first breakup, the liquid volume first increases and then decreases since part of the liquid body is sucked back into the nozzle until pinch-off at the nozzle exit occurs, after which the liquid volume maintains constant.

The data in Figure 4-12(a) are used for calculating the magnitude of shear rates during the emergence of liquid thread out from the inkjet nozzle before the liquid volume reaches the maximum value. The scale of shear rate, $\bar{\dot{r}}$, is given by

$$\bar{\dot{r}} \sim O\left(\frac{\bar{V}}{R_{noz}}\right) \sim O\left(\frac{\frac{S}{A_{noz}}}{R_{noz}}\right), \tag{4-3}$$

where $\bar{V}$ is the averaged speed of liquid ligament being jetted out from the inkjet nozzle, S is the volumetric flow rate, A_{noz} and R_{noz} are the cross-section area and the radius of the inkjet nozzle, respectively. $\bar{\dot{r}}$ vs. time during the ejection process is given in Figure 4-13. It indicates that higher signal amplitude leads to higher shear rates. Although the shear rate is ~ 1×10^5 s^{-1} for the first few microseconds depending on the signal amplitude, it drops immediately to 1×10^4 s^{-1} at about 15 μs.

The data in Figure 4-12(b) are used to estimate the average rate of surface dilatational deformation [20], $\dot{\lambda}_{\exp}$, as following

$$\dot{\lambda}_{\exp} \sim O\left(\frac{\Delta A}{A_{\max}}\frac{1}{\Delta t}\right), \tag{4-4}$$

where $A_{\max}$ is the maximum surface area the liquid ligament reached during the ejection process and is determined using the maximum value in each plot shown in Figure 4-12(b), ΔA is the difference between the maximum surface area and the minimum surface area $A_{\min}$, and Δt is the time taken for the surface area to reach to the maximum value.

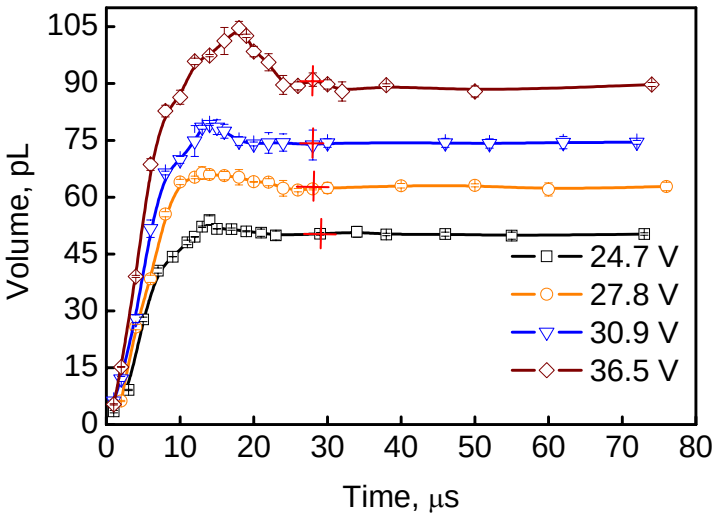

(a)

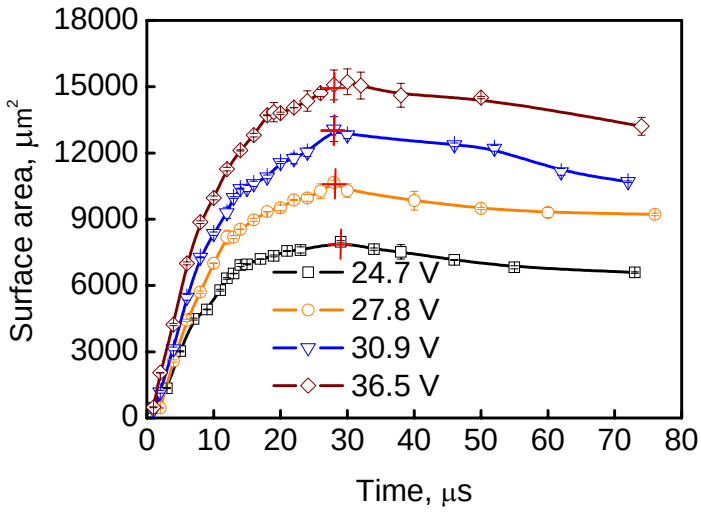

(b)

Figure 4-12: Volume (a) and surface area (b) of ejected liquid vs. time for Sample #3 (15.0 vol%) in Table 4-1 with signal amplitudes = 24.7, 27.8, 30.9 and 36.5 V and frequency = 10 kHz. Marker "+" indicates the time of liquid separation from the nozzle exit. The error bar stands for one standard deviation.

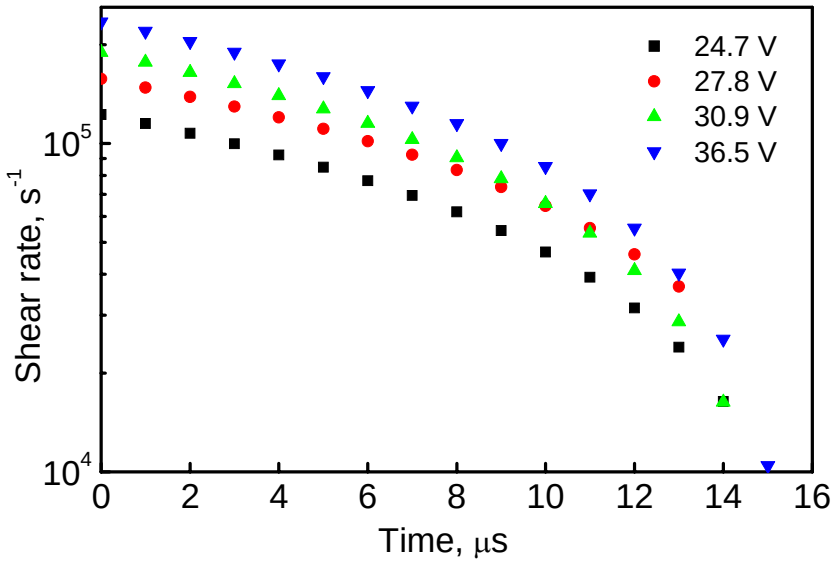

Figure 4-13: Magnitude of shear rate vs. time using the data in Figure 4-12(a) and Eq. (4-3) for Sample #1 (15.0 vol%) in Table 4-1 with signal amplitudes = 24.7, 27.8, 30.9, and 36.5 V and frequency = 10 kHz.

In the case of DOD drop formation, the value of A_{min} may be defined as the cross-section area of the inkjet nozzle. Based on this definition, the values of $\dot{\lambda}_{exp}$ with signal amplitudes of 24.7, 27.8, 30.9 and 36.5 V are approximately 25000, 28300, 28500 and 29700 s^{-1}, respectively. This indicates that the time of surface aging is no more than ~ O(100 μs). As a result, if surfactant is used for adjusting the surface tension of the inkjet ink, with such a short period of surface aging, dynamic surface tension (DST) may become a very important parameter. However, no commercially available instrument is available for measuring DST at surface aging time of less than 100 μs. In order to understand the effect of the rapid surface deformation in the ejection process on the interfacial tension of inkjet ink, it is necessary to compare DOD drop formation dynamics of a fluid with surfactant with that of a fluid with no dynamic surface tension. It is unclear yet extremely difficult to determine whether or not the pigment particle is

adsorbed to the air-suspension interface. However, if it does appear, a decrease of interfacial tension would take place [17]. It is noticed that after the surface area of the ejected liquid thread reaches to the maximum value, the change of surface area vs. time becomes much slower as shown in Figure 4-13(b).

As shown in Figure 4-14, the volume and surface area of liquid ejected as a function of time are also determined for all three samples in Table 4-1 at signal amplitude of 30.9 V and frequency of 10 kHz. Using the data in Figure 4-14(a) and Eq. (4-3), the magnitude of shear rate as a function of time during the ejection process is determined and shown in Figure 4-15. The data shown in Figures 4-14 and 4-15 indicate that the ejection process of all three samples is very similar except that the total volume ejected for the inkjet ink with pigment loading of 15.0 vol% is slightly higher than that for the other two samples.

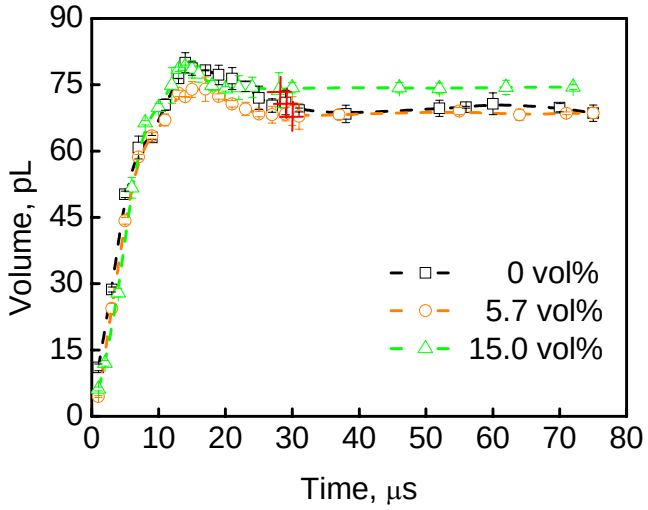

(a)

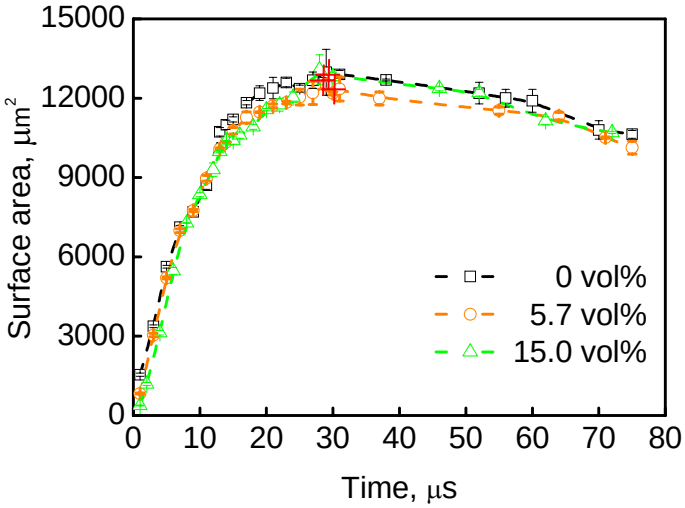

(b)

Figure 4-14: Volume (a) and surface area (b) of ejected liquid vs. time for all three samples in Table 4-1 with signal amplitude = 30.9 V and frequency = 10 kHz. Marker "+" indicates the time of liquid separation from the nozzle exit. The error bar stands for one standard deviation.

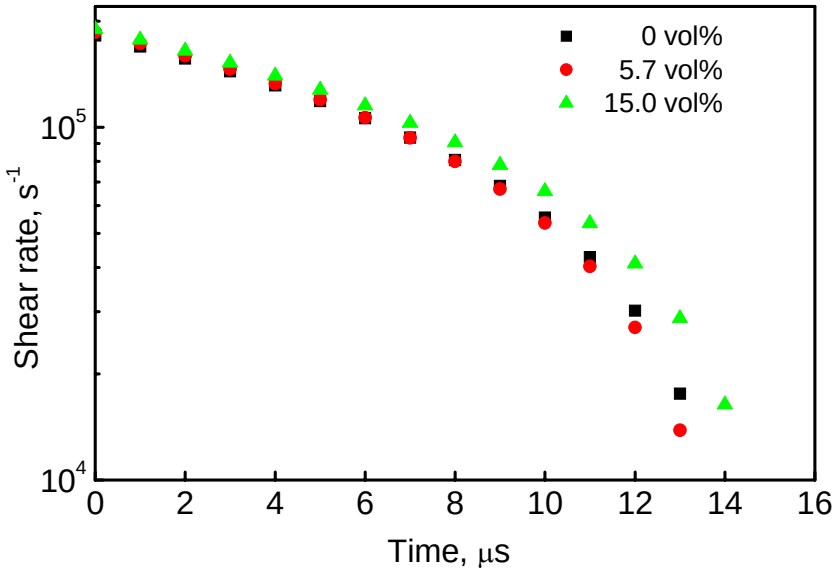

Figure 4-15: Magnitude of shear rate vs. time using the data in Figure 4-14(a) and Eq. (4-3) for all three samples in Table 4-1 with signal amplitude = 30.9 V and frequency = 10 kHz.

4.4.3 Breakup and Contraction of Liquid Thread

Dong *et al.* [1] observed two different kinds of liquid thread breakups in DOD drop formation, which are end-pinching and multiple breakup due to the wave-like instability. Under the signal amplitudes used in this study, no multiple breakup of ejected liquid thread was observed. Only end-pinching was observed, which is attributed to the comparable higher shear viscosity of the samples.

Figure 4-16 shows the enlarged images focusing on the location of the secondary breakup for all three ink samples in Table 4-1 at signal amplitudes of 30.9 and 36.5 V and frequency of 10 kHz. Each image in Figure 4-16 is chopped from the image similar to No.16 image in Figure 4-7. After the secondary breakup, a primary drop is formed and a secondary liquid thread contracts, leading to the formation of various numbers of satellites, primarily depending on the length and diameter of the secondary liquid thread

and the fluid properties of the ink fluid such as surface tension and viscosity. In Figure 4-16, the shapes at the breakup point for all three samples are similar and the shapes at the breakup point at different voltages are also similar.

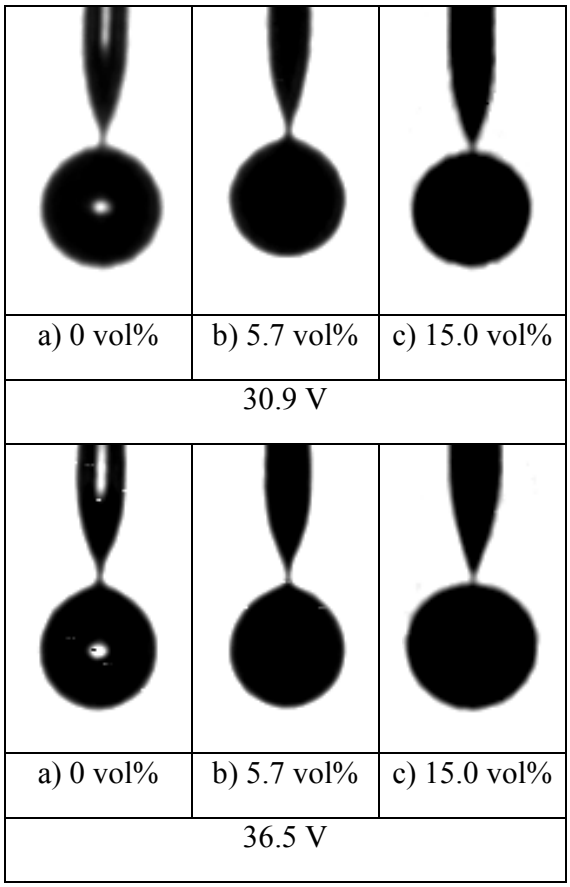

Figure 4-16: Chopped images at the instant when the liquid thread broke up into primary drop and secondary thread for three ink samples at signal amplitudes of 30.9 and 36.5 V and frequency of 10 kHz.

The secondary liquid thread formed after the secondary breakup has a cone-shaped leading point where the high local surface curvature and resulted high local capillary pressure leads to fast liquid thread contraction/recoiling toward the center of the thread (see No.17th to 22nd images in Figure 4-7 as an example). The length of the contracting/recoiling secondary liquid thread as a function of time for all three samples in

Table 4-1 at signal amplitude of 30.9 V and frequency of 10 kHz is shown in Figure 4-17. For all three samples, the secondary liquid thread contracts and oscillates into a single satellite with a similar dynamical process.

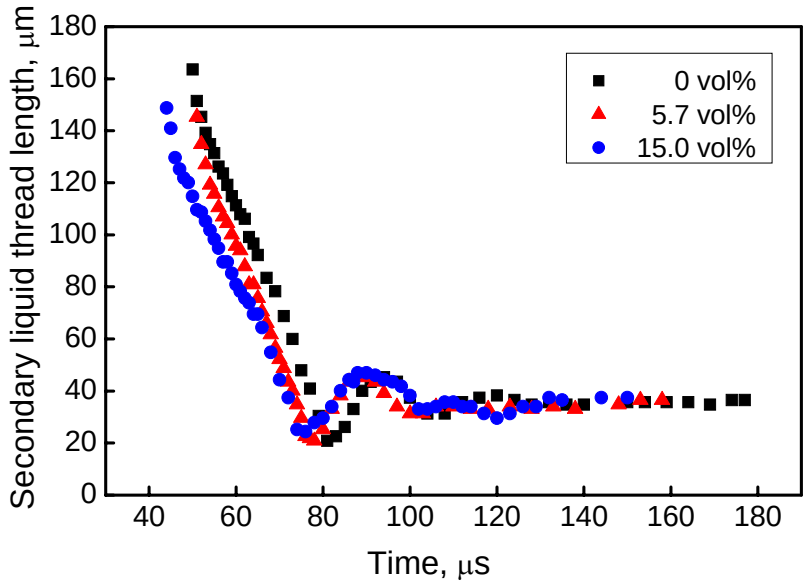

Figure 4-17: Length of the contracting/recoiling secondary liquid thread vs. time for all three samples in Table 4-1 at signal amplitude = 30.9 V and frequency = 10 kHz.

Dong *et al.* [1, 6] pointed out that the breakup time of a liquid thread depends only on the capillary time of the liquid, t_{ca}, and the fastest growth rate of disturbances along the liquid thread, $\alpha_{\max}^{*}$, and gave the following relationship

$$t_b = C\frac{t_{ca}}{\alpha_{\max}^{*}}. \qquad (4\text{-}5)$$

Here, t_b is calculated by subtracting the time taken for the ejected liquid thread to reach to its maximum volume from experimental breakup times, t_{b1} and t_{b2}, the first and second breakup time, respectively.

Table 4-4 lists the time of the pinch-off from nozzle, t_{b1}, and end-pinch, t_{b2}, of three liquid threads ejected under different signal amplitudes. In this study, C_1 and C_2 are in the ranges of 0.2 – 0.3 and 0.5 – 0.7, respectively. As pointed out by Dong *et al.* [1, 6], the comparably lower value of C_1 is attributed to the different mechanisms between the two breakups. The first breakup takes place when the liquid thread is ejected out from the nozzle, while the second breakup occurs when the ejected liquid thread is under contraction. As a result, C_1 is related to the actuating waveform since the second peak in the double-peak waveform shown in Figure 4-2 sucks part of the liquid back to the nozzle (see Figures 4-12(a) and 4-14(a)) until pinch-off at the nozzle exit occurs. Similarly, C_1 may also be related to the actuating waveform since the fluid motion inside the ejected liquid thread starts during the ejection process. Both t_{b1} and t_{b2} of the inkjet ink with pigment loading of 15.0 vol% are shorter compared to those of the other two samples; however, the reason for this observation is unknown.

Table 4-4: Breakup times of three liquid threads and related parameters

Pigment loading	Voltage, V	t_{b1}, μs	t_{b2}, μs	$\frac{t_{ca}}{\alpha^*_{\max}}$ ¤, μs	C_1	C_2
0 vol%	24.7	31	47	65.1	0.26	0.51
	27.8	29	49		0.23	0.54
	30.9	29	50		0.23	0.55
	36.5	30	54		0.25	0.61
5.7 vol%	24.7	32	48	65.2	0.28	0.53
	27.8	30	49		0.25	0.55
	30.9	30	51		0.25	0.58
	36.5	30	54		0.25	0.63
15.0 vol%	24.7	29	N/A*	65.2	0.25	N/A*
	27.8	28	45		0.24	0.53
	30.9	28	44		0.24	0.51
	36.5	28	48		0.24	0.58

*: No secondary breakup
¤: Calculated using shear viscosity measured at low shear rate

4.4.4 Speeds and Sizes of Primary and Satellite Drops

Table 4-5 summarizes the speeds of sizes of primary and satellite drops of all three samples in Table 4-1 at four different signal amplitudes and jetting frequency of 10 kHz. Again, no significant difference was found among the inkjet ink samples. Both primary and satellite drop sizes are found to be scalable to the diameter of the inkjet nozzle (53 μm).

Table 4-5: Sizes and speeds of primary and satellite drops for all three samples in Table 4-1 at signal amplitudes of 24.7, 27.8, 30.9, and 36.5 V and jetting frequency = 10 kHz

Liquid	Voltage, V	Primary drop size, d_p, μm	Primary drop speed, v_p, m/s	Satellite drop size, d_s, μm	Satellite drop speed, v_s, m/s
0 vol%	24.7*	44.3±1.0	~ 2.6	26.1±1.0	~ 4.6
	27.8*		4.1	32.6±1.0	4.5
	30.9		5.4	36.5±1.0	5.0
	36.5		7.5	43.9±1.0	6.1
5.7 vol%	24.7*	43.8±1.0	~ 2.2	25.7±1.0	~ 4.6
	27.8*		3.7	31.3±1.0	4.5
	30.9		5.0	36.5±1.0	4.8
	36.5		7.1	43.9±1.0	5.9
15.0 vol%	24.7*	45.7±1.0	N/A¤	N/A¤	N/A¤
	27.8*		3.5	29.1±1.0	4.4
	30.9		7.0	37.4±1.0	5.1
	36.5		8.1	41.3±1.0	6.5

*: Recombination of primary and satellite drop occurs
¤: No satellite formation

At signal amplitudes of 24.7 and 27.8 V, primary drops and satellites recombined for all three samples. As also observed by Dong *et al.* [1, 6], in cases where signal amplitude is low, corresponding to a low primary drop speed, only one satellite or even no satellite is formed and recombination of primary drop and satellite occurs. However,

in a typical industrial inkjet printing process, primary drop speed needs to be sufficiently high (~ 6 m/s) to obtain satisfactory impaction accuracy of the DOD drops. Elimination of satellite drop through recombination of primary drop and satellite limits the primary drop speed; thus, it is not desirable.

4.4.5 Curves of DOD Drop Formation of 15.0 vol% Pigment Loading Sample

Figure 4-18 shows the curves of DOD drop formation for Sample #3 in Table 4-1 at four signal amplitudes and jetting frequency of 10 kHz.

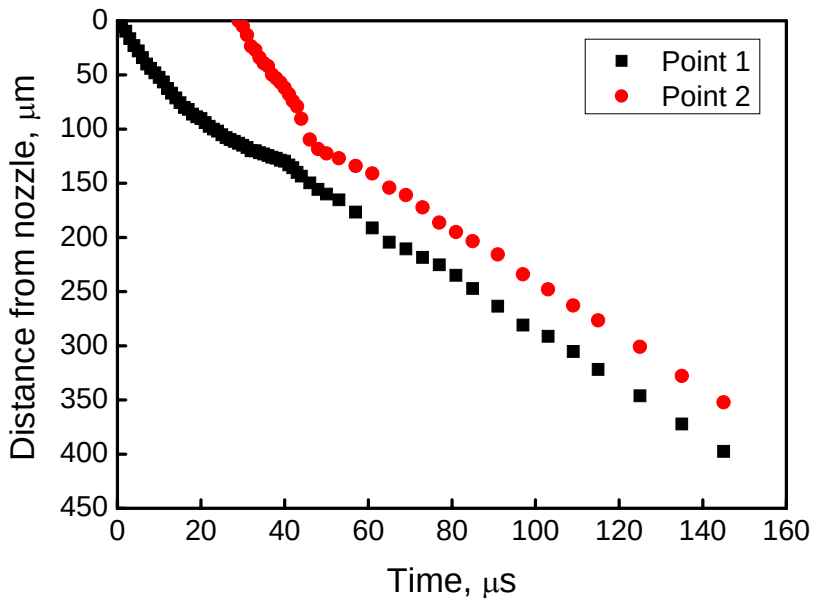

(a) Signal amplitude = 24.7 V

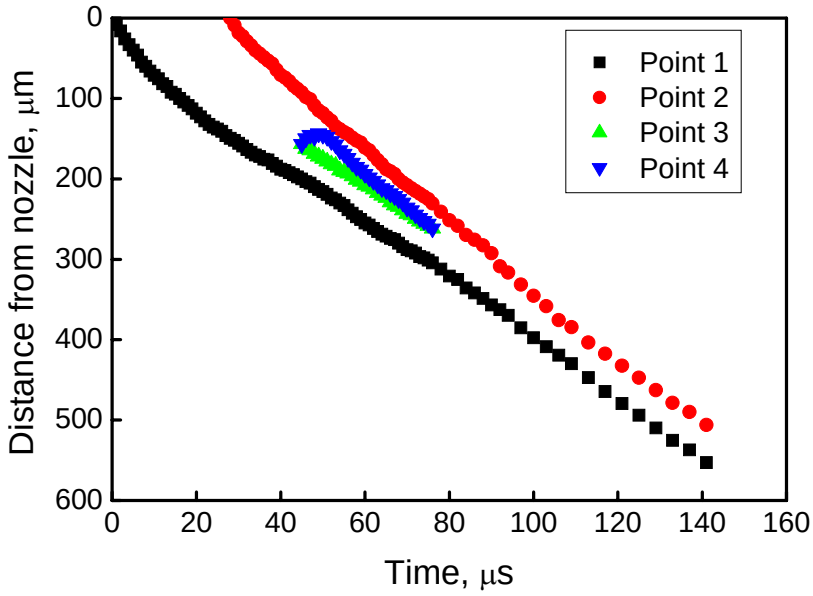

(b) Signal amplitude = 27.8 V

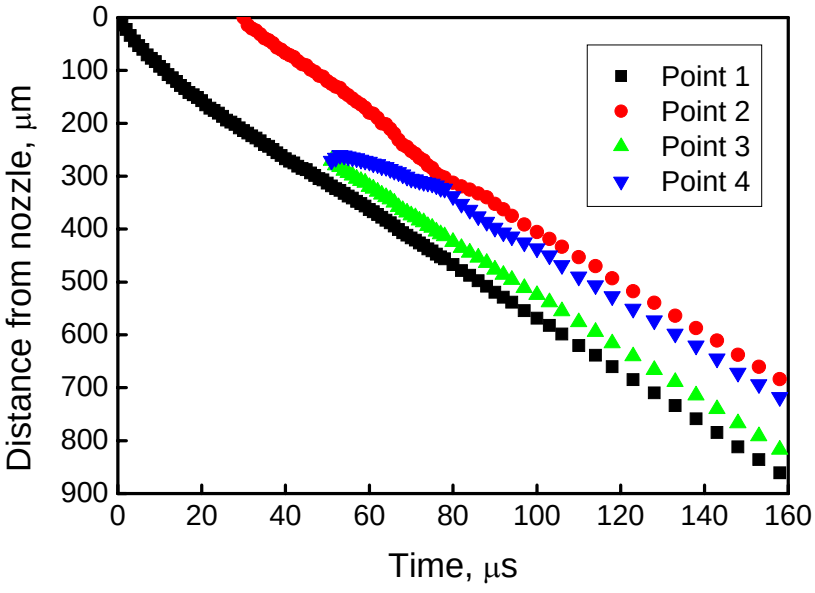

(c) Signal amplitude = 30.9 V

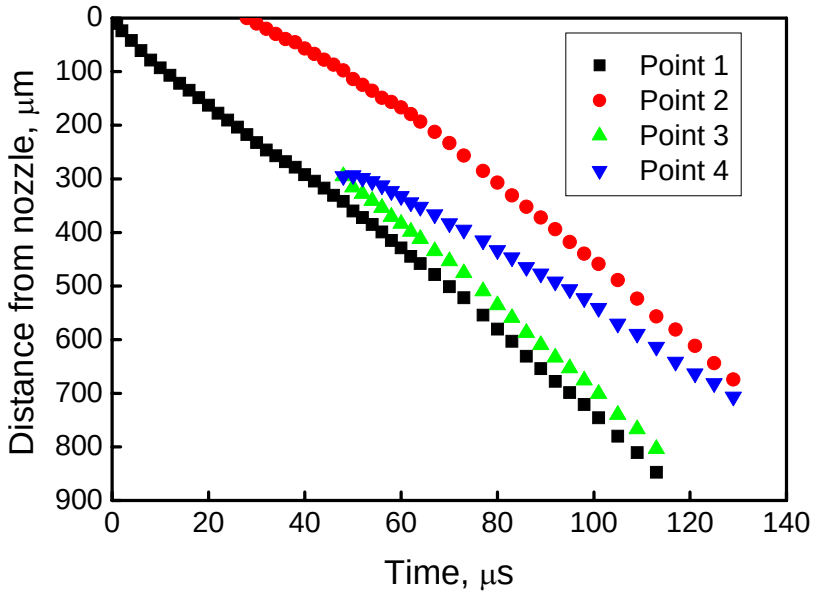

(d) Signal amplitude = 36.5 V

Figure 4-18: Curves of DOD drop formation for Sample #3 in Table 4-1 using the double-peak waveform shown in Figure 4-2 with signal amplitude = (a) 24.7 V, (b) 27.8, (c) 30.9, and (d) 36.5 V and jetting frequency = 10 kHz.

Again, the plots shown in Figure 4-18, originally developed by Dong *et al.* [1, 6], give a convenient summary of DOD drop formation dynamics. Note that the signal amplitude increases from Figure 4-18(a) to (d). As a result, the existence of satellite changed from no satellite formation (see Figure 4-18(a)), satellite formation and recombination with primary drop (see Figure 4-18(b)), to satellite formation and no recombination with primary drop (see Figures 4-18(c) and (d)). It appears that DOD drop formation of colloidal suspension with pigment loading of 15.0 vol% does not show significant difference compared to that of Newtonian fluids as discussed by Dong *et al.* [1, 6].

4.4.6 High-Shear-Rate Rheological Data, Suspension Microstructure, and DOD Drop Formation Dynamics

The rheological data at high shear rate obtained using the designed and constructed capillary viscometer indicate that inkjet ink samples with similar low-shear-rate viscosity exhibited significantly different shear viscosities at high shear rates depending on particle loading. In Figures 4-13 and 4-15, the magnitude of maximum shear rate occurring during DOD drop formation process is determined to be identical to the maximum shear rate used for characterizing the inkjet ink samples (see Figure 4-3). It was conjectured that the existence of significant difference in high-shear-rate viscosity among the three samples would affect DOD drop formation dynamics even with similar low-shear-rate viscosity. However, no significant difference is found at the same jetting conditions. Particularly, no significant difference occurred during the evolution of ejected liquid thread; in the other word, colloidal particles did not affect the appearance of ejected liquid thread as non-colloidal particles do [15]. The following reasoning is proposed to explain above observations.

In Chapter 2, it is conjectured that microstructure breakdown of agglomerates at high shear rate is the mechanism of the shear thinning behavior. To obtain a microstructure breakdown, a period of time is needed under sufficiently high hydrodynamic forces. As shown in Table 4-3, the traveling time, t_e, of ink through the nozzle at the maximum speed, i.e., ejection speed, v_e, is estimated to range from 6 to 13 μs, depending on signal amplitudes. During this period of time, the shear rate applied to the inkjet ink being ejected from nozzle is at its maximum value (~ 2×10^5 s^{-1}). Compared to the period of time (> 1000 μs) when the inkjet ink sample goes though a capillary viscometer, t_e = 6 – 13 μs is extremely short. The structure breakdown taken place under the capillary viscometer condition may not occur. Even if structure breakdown does occur during the ejection process, as shown in Figures 4-13 and 4-15, the shear rate

drops an order of magnitude at ejection time of ~ 15 μs. The intermediate structure of the pigmented ink resulting from strong hydrodynamic forces may relax soon after the shear rate drops. According to Dhont [17], for not too concentrated suspensions, typical relaxation time of the colloidal structure is in the order of a few microseconds. Figure 2-17 indicates that the microstructure of the suspension recovers after the capillary viscometer test. If this is true, then the shear viscosity may return to the low shear rate value after ejection.

To test all of the above conjectures, observation of the transient microstructure of the suspension during DOD drop formation process is needed. However, it is extremely hard [21, 22] to achieve this with available instrumentation. In the absence of such instruments, the inkjet nozzle may be a useful tool to probe if the microstructure of a defined colloidal or non-colloidal suspension responses in a time scale of 10 μs and if bulk flow is affected.

4.5 Conclusions

In the study conducted in this chapter, three inkjet ink samples were formulated and used to elucidate the effect of particles on DOD drop formation. The formulation of the samples was done in such a fashion that the fluid properties including low-shear-rate viscosity, static surface tension and density were similar or the same. Dynamic surface tension was found to be the same as the static surface tension by using KRUSS Bubble Pressure Tensiometer BP2 at bubble frequency up to 10 Hz and the acoustic wave speeds among the samples had a mean variation of less than 5%. The rheological data at high shear rate obtained using the designed and constructed capillary viscometer indicate that the samples exhibited significantly different shear viscosities at high shear rates depending on particle loading.

DOD drop formation dynamics of these three fluids was obtained at the same testing conditions. Although the jettability of pigmented inkjet inks was found to be much lower than that of the pure fluid, once they were jetted successfully, the reproducibility of DOD drop formation was very high. By comparing the various stages of DOD drop formation including liquid ejection, thread breakup, ligament contraction, speeds and sizes of primary and satellite drops, etc. of the three samples, no significant difference was found except that both t_{b1} and t_{b2} of the inkjet ink with pigment loading of 15.0 vol% are shorter than those of the other two samples. As a result, it appears that shear viscosity measured at high shear rates in a capillary viscometer are not relevant in the DOD drop formation process. This is believed to be due to the insufficient shearing time for changing and stabilizing the microstructure of the suspension during DOD drop formation process.

4.6 References

1. Dong, H., Carr, W. W., and Morris, J. F., Phys. Fluids 18, 072102 (2006).
2. Eggers, J., Rev. Modern Phys. 69, 865 (1997).
3. Burton, J. C., Rutledge, J. E., and Taborek, P., Phys, Rev. Lett. 92, 244505 (2004).
4. Kowalewski, T. A., Fluid Dynamics Res. 17, 121 (1996).
5. Notz, P. K., Chen, A. U., and Basaran, O. A., Phys. Fluids 13, 549 (2001).
6. Dong, H., Drop-on-demand inkjet drop formation and deposition, Doctorial dissertation, Georgia Institute of Technology, Atlanta, (2006).
7. Dong, H., Carr, W. W., and Morris, J. F., Rev. Sci. Instrum.77, 85101 (2006).
8. Chen, A. U., Basaran, O. A., Phys. Fluids 14, L1 (2002).
9. Meinhart, C. D. and Zhang, H., J. Microelectromech. Syst. 9, 67 (2000).
10. Xu, Q. and Basaran, O. A., Phys. Fluids 19, 102111 (2007).
11. de Jong, J., De Bruin, G., Reinten, H., Van Den Berg, M., Wijshoff, H., Versluis, M., and Lohse, D., J. Acoust. Soc. Am. 120, 1257 (2006).
12. de Jong, J., Jeurissen, R., Borel, H., van den Berg, M., Wijshoff, H., Reinten, H., Versluis, M, Prosperetti, A., and Lohse, D., Phys. Fluids 18, 121511 (2006).
13. Beulen, B., de Jong, J., Reinten, H., van den Berg, M., Wijshoff, H., and van Dongen, M. E. H., Exp. Fluids 42, 217 (2007).
14. de Jong, J., Reinten, H., Wijshoff, H., van den Berg, M., Delescen, K., van Dongen, R., Mugele, F., Versluis, M., and Lohse, D., Appl. Phys. Lett. 91, 204102 (2007).
15. Furbank, R. J. and Morris, J. F., Phys. Fluids 16, 1777 (2004).
16. Furbank, R. J. and Morris, J. F., Int. J. Multiphas. Flow 33, 448 (2007).
17. Dhont, J., Private communication.
18. Reis N., Ainsley, C., and Derby, B., J. Am. Ceram. Soc. 88, 802 (2005).
19. Kytomaa, H. K., Powder Technol. 82, 115 (1995).

20. Mourougou-Candoni, N., Prunet-Foch, B., Legay, F., Vignes-Adler, M., and Wong, K., J. Colloid Interface Sci. 192, 129 (1997).
21. Morris J. F., Private communication.
22. Miller R., Private communication.

CHAPTER 5

EFFECTS OF SIGNAL AMPLITUDE AND JETTING FREQUENCY ON DOD DROP FORMATION

5.1 Introduction

DOD drop formation is a transient process starting from highly unsteady yet periodic [1] flow field in the nozzle induced by rapid motion of a piezoelectric actuator at frequency typically higher than 1 kHz [2]. When an actuating signal or waveform is sent to the piezoelectric actuator, the actuator conducts corresponding movements and as a result, the pressure inside the printhead chamber or manifold varies. The inkjet ink inside the chamber responds to this pressure variation and is ejected from the nozzle. Thus, for a defined piezoelectric inkjet nozzle, DOD drop formation dynamics is highly affected by the actuating waveform, including amplitude [3, 5], shape [4, 5, 6, 7], and frequency [8, 9].

5.2 Objective

Electrical signal for actuating piezoelectric actuator in the inkjet nozzle can greatly affect DOD drop formation dynamics, i.e., evolution of ejected liquid thread. Previously, Dong [6] studied DOD drop formation of pure Newtonian fluids in great detail, and analysis was oriented to understand the characteristics of the evolution of ejected liquid thread. The objective of this chapter is to contribute to the understanding of DOD drop formation dynamics of pure Newtonian fluids, building on the work done previously in our group. The focus is on the effects of signal amplitude and jetting

frequency. Some important and unique features of DOD drop formation process are addressed.

5.3 Experimental

The imaging system originally developed by Dong *et al.* [10] was modified and used in this study. Detailed information related to the imaging system, inkjet nozzle, and the functionality and actuating mechanism of the double-peak waveform signal (see Figure 4-2) is available in references 3, 6, and 10. Modifications to the imaging system were made so that DOD drop formation dynamics at various jetting frequencies can be studied. The temporal and spatial resolutions of the imaging system are 1 μs and 0.81 μm/pixel, respectively.

The Newtonian fluid used in this study was a mixture of glycerin (43.7 wt%), isopropanol (11.4 wt%) and DI water (44.9 wt%) with shear viscosity of 6.3 cP measured using a Brookfield Part No. LVDVI+ Couette viscometer at shear rate of 52.3 s^{-1}. surface tension of 32 mN/m measured using a KRUSS Bubble Pressure Tensiometer BP2, and density of 1.067 g/mL.

5.4 Results and Discussion

5.4.1 Effect of Signal Amplitude

Using the double-peak waveform shown in Figure 4-2 at a jetting frequency of 10 kHz, the Newtonian fluid was jetted at 15 signal amplitudes. The images are shown in Figure 5-1. Since large amount of images are presented, for better clarification, the data are divided into a few figures. Each figure illustrates two columns of images of the ejected liquid thread at two time intervals starting at the point of the emergence of ink

from the nozzle. Each column illustrates 15 images corresponding to 15 signal amplitudes, and the voltage amplitude increases gradually with a 0.6 Volts step.

The size of all the images in Figure 5-1 is 57 μm × 389 μm. When the positions of the camera and inkjet nozzle are fixed, the size of the CCD sensor is not large enough for imaging the ejected liquid thread at various time intervals. For that reason, the nozzle was lifted up at different time intervals to allow capturing the liquid thread. However, for different signal amplitudes, the vertical positions of the nozzle were identical.

Figure 5-1 (a) shows the images at time intervals of 10 and 20 μs, where ejection and stretching of liquid thread took place. According to Figure 4-12 and the data of Dong *et al.* [3], the maximum liquid volume ejected occurred at time interval of about 15 μs using the double-peak waveform, which indicates that the ejection process was finished before 20 μs. The images indicate that during the ejection process, signal amplitude affects the length of the ejected liquid thread, but does not affect the shape of the leading part.. Higher signal amplitude leads to a longer liquid thread formation and larger ejected liquid volume. Before the time interval of 20 μs, the leading part of the liquid thread has already started the necking process. Above the necking point, the liquid thread is thinner than below the necking point.

Figure 5-1 (b) shows the further development of the necking process at time intervals of 30 and 40 μs. Compared to the images taken at time interval of 20 μs, the liquid thread has shrunk, i.e., the diameter of the liquid thread is smaller, and the shape of the leading part is a spherical cap due to surface tension. At both time intervals, the shapes of the liquid threads are similar except that higher voltage amplitude led to longer liquid thread.

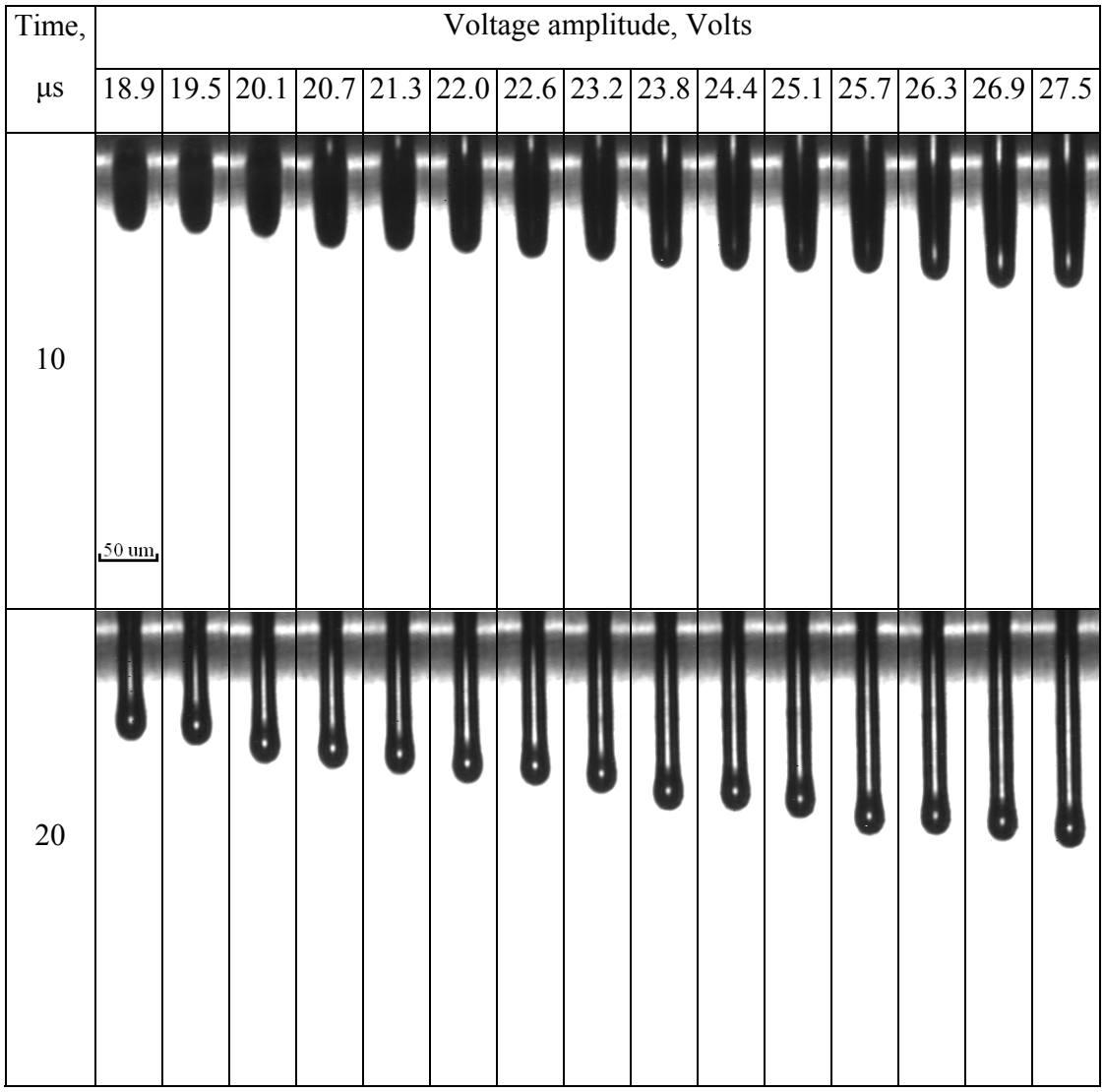

Figure 5-1 (a): Images of a Newtonian fluid being ejected from a DOD inkjet nozzle using the double-peak waveform shown in Figure 4-2 at 15 signal amplitudes and frequency = 10 kHz. The time intervals shown in this figure are 10 and 20 μs.

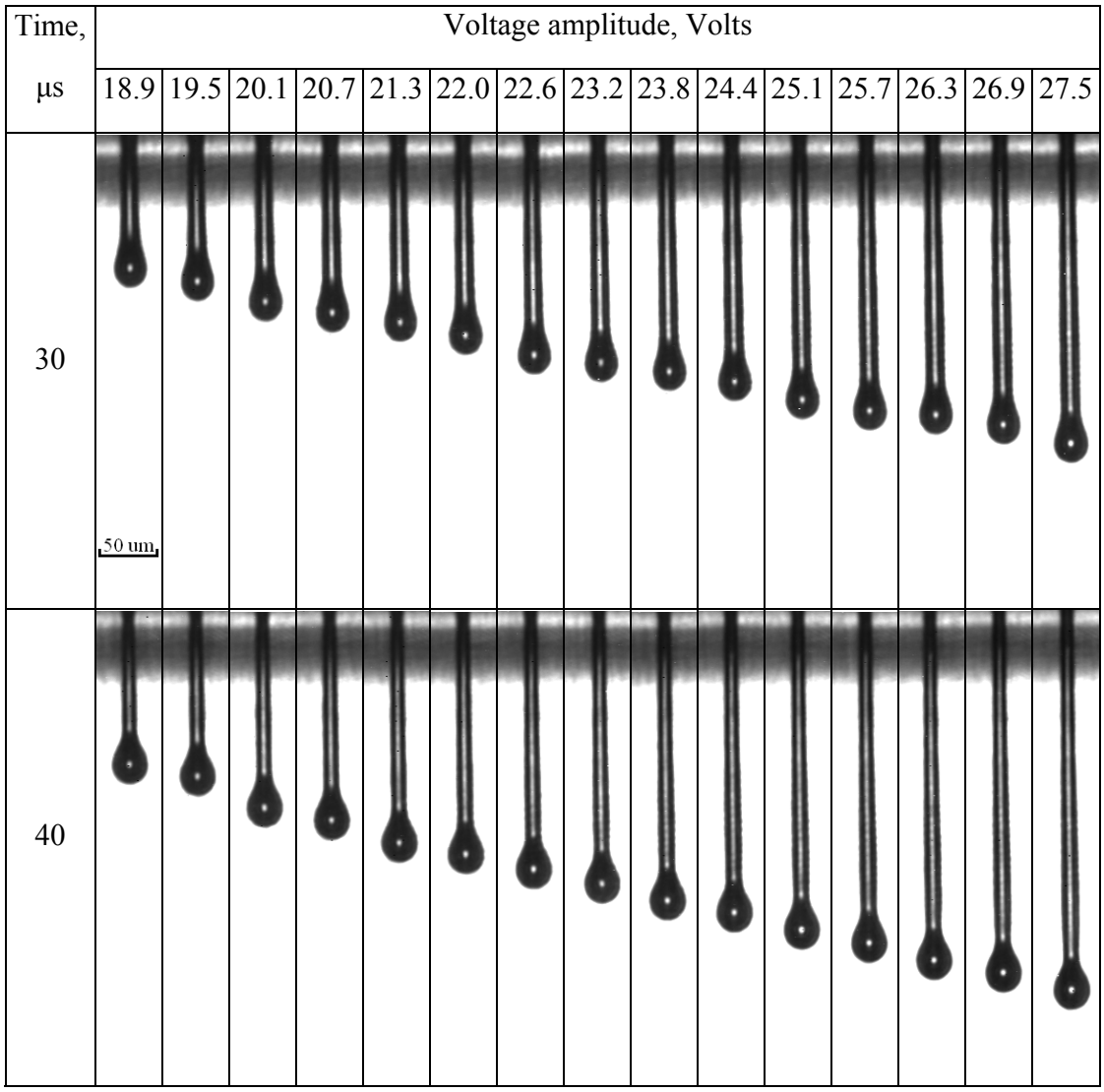

Figure 5-1 (b): Images of a Newtonian fluid being ejected from a DOD inkjet nozzle using the double-peak waveform shown in Figure 4-2 at 15 signal amplitudes and frequency = 10 kHz. The time intervals shown in this figure are 30 and 40 μs.

Figure 5-1 (c) shows the images at time intervals of 50 and 60 μs after the first breakup (at about 46 μs) occurring at the nozzle exit. The breakup point formed the tail of the ejected liquid thread, and due to the high curvature and resulting high capillary pressure at the pinch-off point, the tail recoiled into a spherical cap. Our data indicate that the first breakup took place at the same instant. Dong's data [6] show that the first breakup time can be affected by the shape of actuating signal and the fluid properties of the ejected liquid including surface tension and viscosity; however, voltage amplitude of the actuating signal did not significantly change the first breakup time. The images in Figure 5-1 (c) shows that the vertical positions of the tails at the same time interval were identical for all of the signal amplitudes. At time interval of 60 μs, the shapes of both ends of the liquid thread are spherical, and the necking process has continued. These observations may imply an identical recoiling process for a range of voltage amplitudes.

When the image taken at 50 μs is compared with the one taken at 60 μs, for V = 18.9 Volts, the length of liquid thread at 50 μs is longer; however, as voltage amplitude increases, the length of liquid thread is longer at 60 μs, indicating a further stretching process. As a result, at low signal amplitudes, the tail catches the leading point, resulting in recombination of the primary drop and the satellite if a satellite forms. However, at high signal amplitudes, no recombination occur; instead, depending on jetting frequency, the primary drop may catch the satellite formed by the previous drop formation process. This is called "rear recombination". An example taken by a camera with a larger field of view is shown in Figure 5-2.

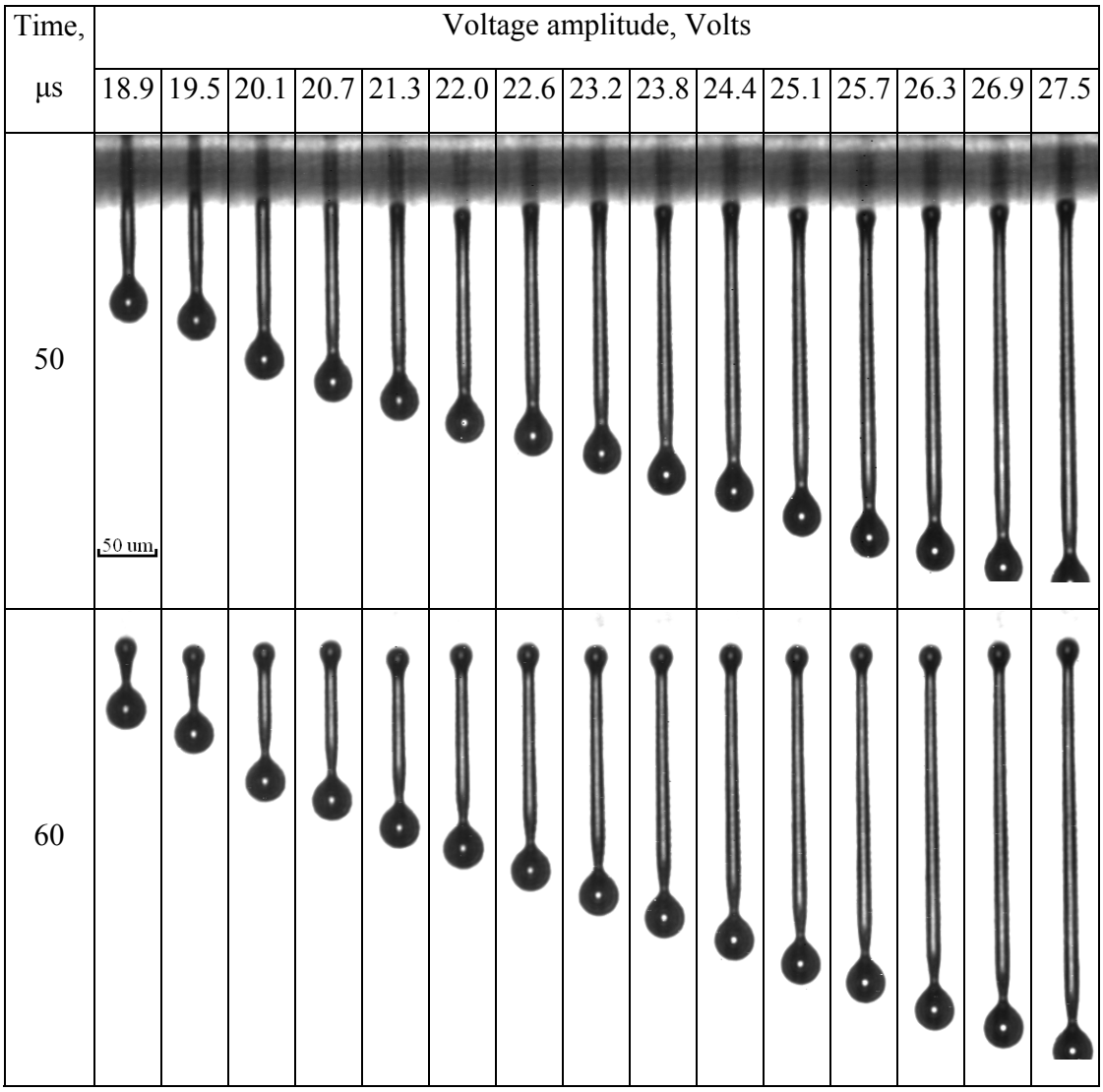

Figure 5-1 (c): Images of a Newtonian fluid being ejected from a DOD inkjet nozzle using the double-peak waveform shown in Figure 4-2 at 15 signal amplitudes and frequency = 10 kHz. The time intervals shown in this figure are 50 and 60 μs.

Figure 5-1 (d) shows the images at time intervals of 70 and 75 μs. The secondary breakup occurred except for the case of voltage amplitude of 18.9 Volts. The type of the secondary breakup in this case was "end pinching" [3] where the breakup point was at the necking point of the thread. The images indicate that except at voltage amplitudes of 18.9 and 19.5 Volts, the secondary breakup occurred at the same time interval (~71 μs). After the secondary breakup, a primary drop and a secondary thread formed. Due to the high curvature and resulting high capillary pressure at the pinch off point, the leading point of the secondary thread recoiled into a spherical cap, similar to what occurs at the tail of the thread after the first breakup. However, no secondary breakup occurred for V = 18.9 Volts and the secondary breakup time V = 19.5 Volts is earlier (67 μs).

Except in the cases where voltage amplitudes were 18.9 and 19.5 Volts, the shape of the liquid threads was similar except that higher signal amplitude led to longer thread length. Also, the vertical positions of the tails were almost the same. These two observations further indicate a similar recoiling process. The size of primary drop was identical, i.e., independent of voltage amplitude.

The detailed analysis of liquid thread breakup can be found in numerous places in the literature [3, 11-16]. Both the first and second breakups are induced by capillary forces and the liquid filament at the necking position shrinks until it vanishes, leading to a finite time singularity [14]. Burton *et al.* [15] conducted experimental investigation and found that near pinch off point, for inviscid flow (fluid with low shear viscosity such as inkjet inks), the similarity solution [16] was found satisfied at nanometer length scales.

Figure 5-1 (e) shows the further evolution of ejected liquid threads at time intervals of 80 and 95 μs. At comparably lower voltage amplitudes, the secondary thread formed after the secondary breakup contracted and its tail and leading point combined, leading to the formation of single satellite. At time interval of 80 μs, recombination occurred for the case of V = 19.5 Volts. At V = 20.1 Volts, the satellite was approaching the primary drop. Recombination of primary drop and satellite exists at low voltage

amplitudes where the speed of primary drop is low. Dong et al. [3, 6] gave a criterion for the occurrence of recombination of primary and satellite drops where low primary drop speed is required. Although lowering voltage amplitude leads to lower primary drop speed and the elimination of satellites, it also leads to a lower impaction accuracy of ejected fluid onto substrate. At higher voltage amplitudes, both the tail and the leading point of the secondary thread increased with voltage amplitude, and their shapes were spherical caps. The liquid bridge in between the two ends of the secondary thread continued shrinking in diameter. The relative vertical position of the primary drop at a single time interval indicates that the primary drop speed varies linearly with voltage amplitude.

Figure 5-1 (f) shows the images at time intervals of 110 and 120 μs. Due to the limited field of view of the camera, in some images, the primary drop and even part of the secondary thread were left out. At time interval of 110 μs, recombination was already finished for V = 19.5 Volts. For V = 20.1 Volts, the satellite continued approaching the primary drop. For V ≤ 23.2 Volts, the contraction of the secondary thread was finished before the time interval of 120 μs was reached, and a single satellite drop was formed. For V > 23.2 Volts, the contraction of the secondary thread was still occurring at the time interval of 120 μs. The secondary thread was not only axi-symmetrical, but the sizes of the spherical caps in the tail and leading point were almost identical. The liquid bridge in between the two ends of the secondary thread continued shrinking in diameter.

Time,	Voltage amplitude, Volts													
μs	18.9	19.5	20.1	20.7	21.3	22.0	22.6	23.2	23.8	24.4	25.1	25.7	26.3	26.9	27.5
70	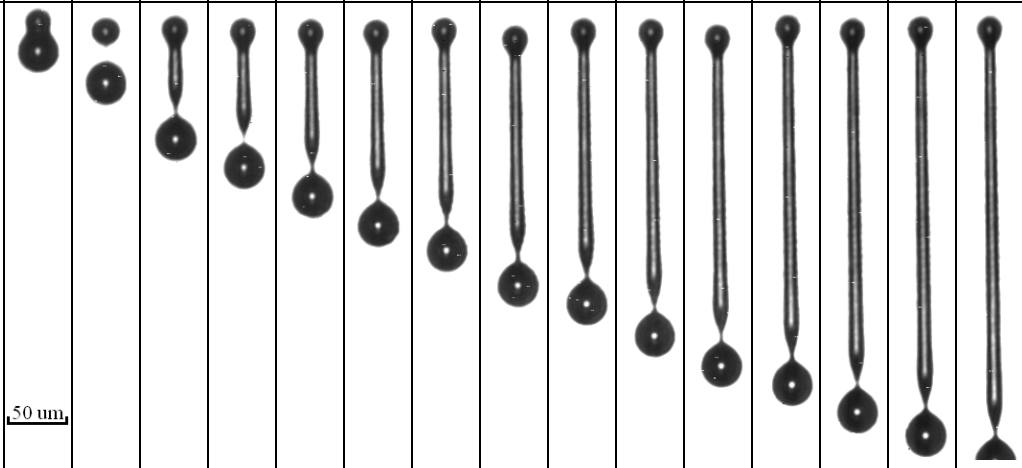														
75	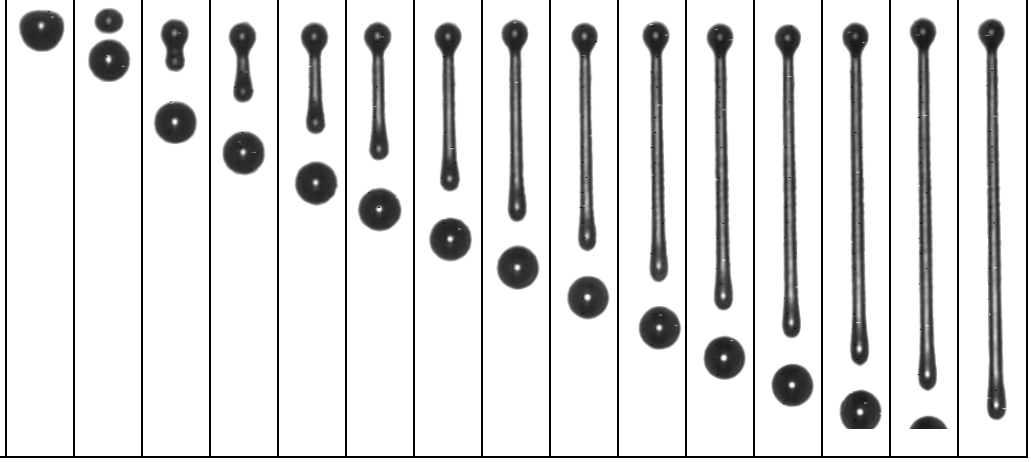														

Figure 5-1 (d): Images of a Newtonian fluid being ejected from a DOD inkjet nozzle using the double-peak waveform shown in Figure 4-2 at 15 signal amplitudes and frequency = 10 kHz. The time intervals shown in this figure are 70 and 75 μs.

Time, Ms	Voltage amplitude, Volts													
	18.9	19.5	20.1	20.7	21.3	22.0	22.6	23.2	23.8	24.4	25.1	25.7	26.3	26.9	27.5
80	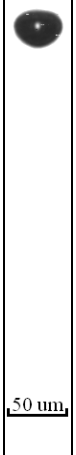	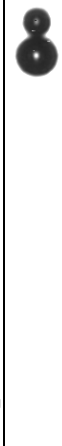	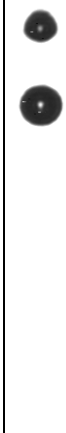	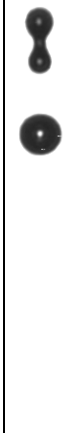		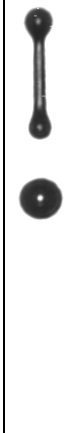	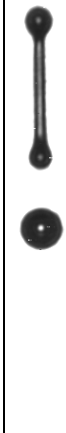	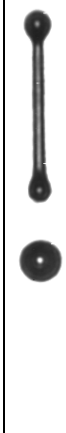			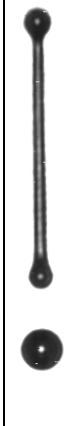		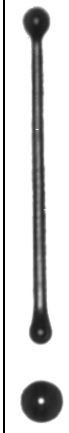		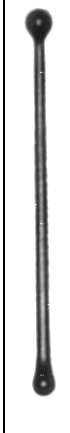
95	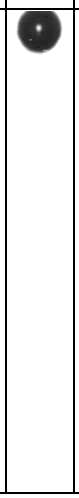				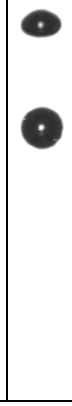	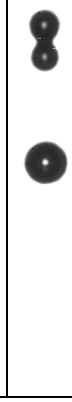	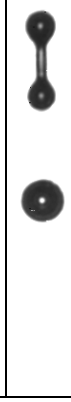	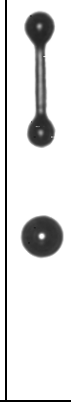	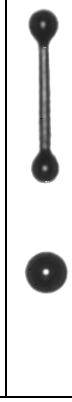			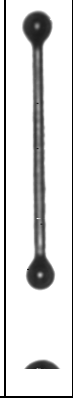	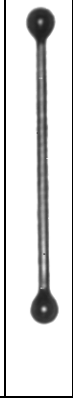	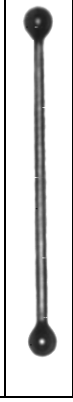	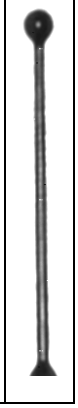

Figure 5-1 (e): Images of a Newtonian fluid being ejected from a DOD inkjet nozzle using the double-peak waveform shown in Figure 4-2 at 15 signal amplitudes and frequency = 10 kHz. The time intervals shown in this figure are 80 and 95 μs.

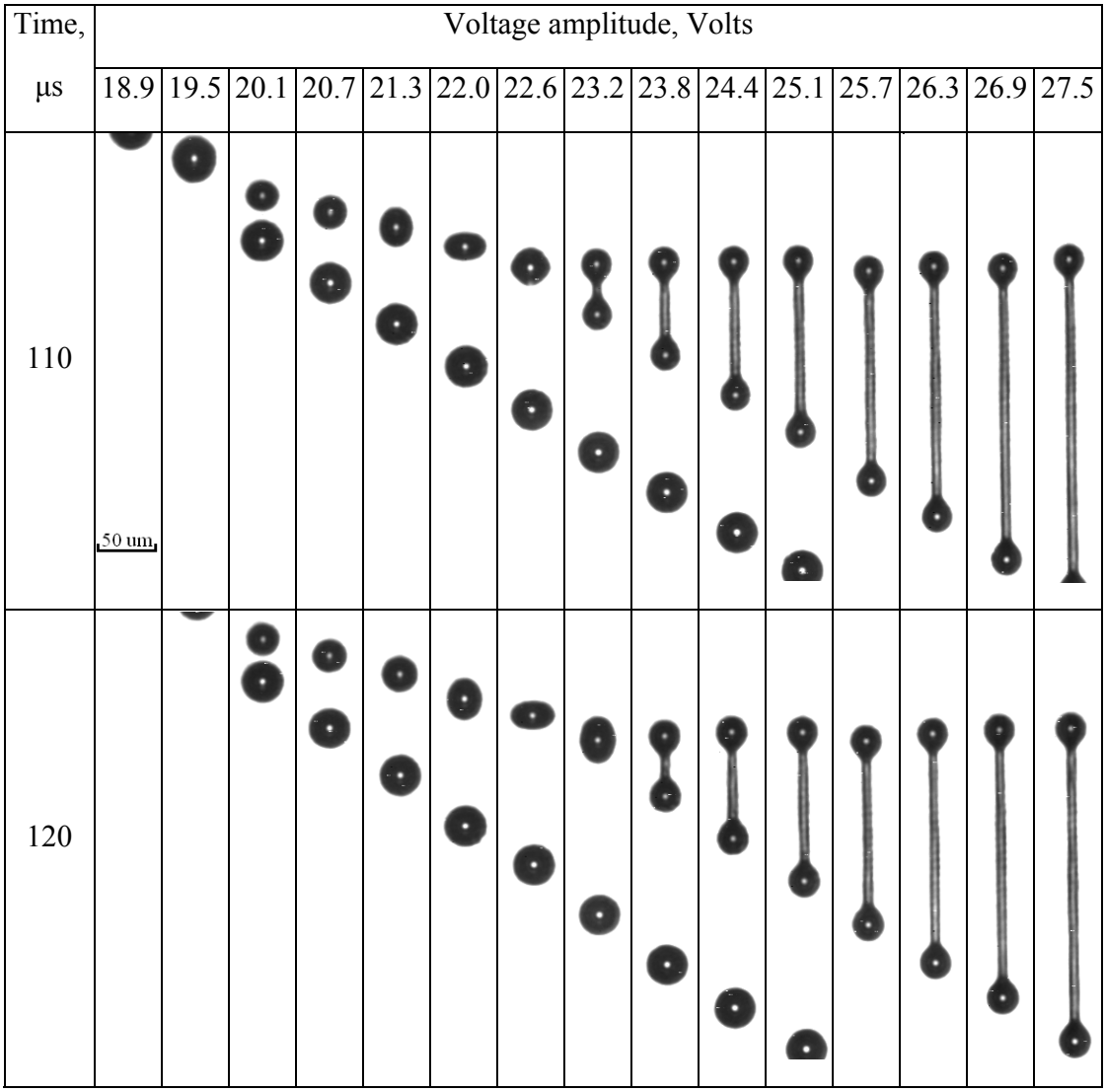

Figure 5-1 (f): Images of a Newtonian fluid being ejected from a DOD inkjet nozzle using the double-peak waveform shown in Figure 4-2 at 15 signal amplitudes and frequency = 10 kHz. The time intervals shown in this figure are 110 and 120 μs.

Figure 5-1 (g) shows the images at time intervals of 130 and 140 μs, primary the shapes of the secondary threads. For V ≤ 24.4 Volts, the secondary thread contracted to form a single satellite before the time interval of 140 μs was reached ; however, for V > 24.4 Volts, the liquid bridge between the tail and leading point of the secondary thread thinned out. For V = 25.1 and 25.7 Volts, end-pinching had occurred in the liquid bridge, resulting in two satellites. End pinching appears to be occurring for V = 26.3 Volts, and capillary waves appear to be in the liquid bridges for V = 26.9 and 27.5 Volts.

Figure 5-1 (h) shows the images at time intervals of 150 and 160 μs. Notice the shapes of the secondary threads. At the time interval of 150 μs and V = 25.1 Volts, the two satellites have recombined, forming a single satellite. For V = 25.7 Volts, the satellite formed by the tail of the secondary thread was approaching the satellite formed by the leading point of the secondary thread, suggesting a recombination of satellites in the future. For V = 26.3 Volts, end-pinching appears to be completed with the formation of two satellites. For V = 26.9 and 27.5 Volts, the secondary threads appear to be breaking up into multiple satellites.

At the time interval of 160 μs, there were: no satellites for V = 18.9, 19.5, and 20.1 Volts; one satellite for V = 21.3 – 25.1 Volts; and two or more satellites for V = 25.7 – 27.5 Volts. For V = 26.9 and 27.5 Volts, multiple breakup appears to be due to wave-like instability. The capillary waves do not show preferred wavelength, and the liquid thread breaks up at several locations at different times, forming satellites of varying sizes as indicated by Figure 5-3, where randomly selected images of the secondary thread for V = 26.9 and 27.5 Volts and time intervals of 140, 150, and 160 μs are shown. The longer the liquid thread, the more satellites are formed when breakup is due to wave-like instability [3]. Thus if voltage amplitude had been increased beyond 27.5 Volts, the liquid thread might be expected to be longer and breakup into more satellites. Since the multiple breakup is due to wave-like instability without preferred wavelength, the location and number of breakup along the thread varies from ejection to ejection.

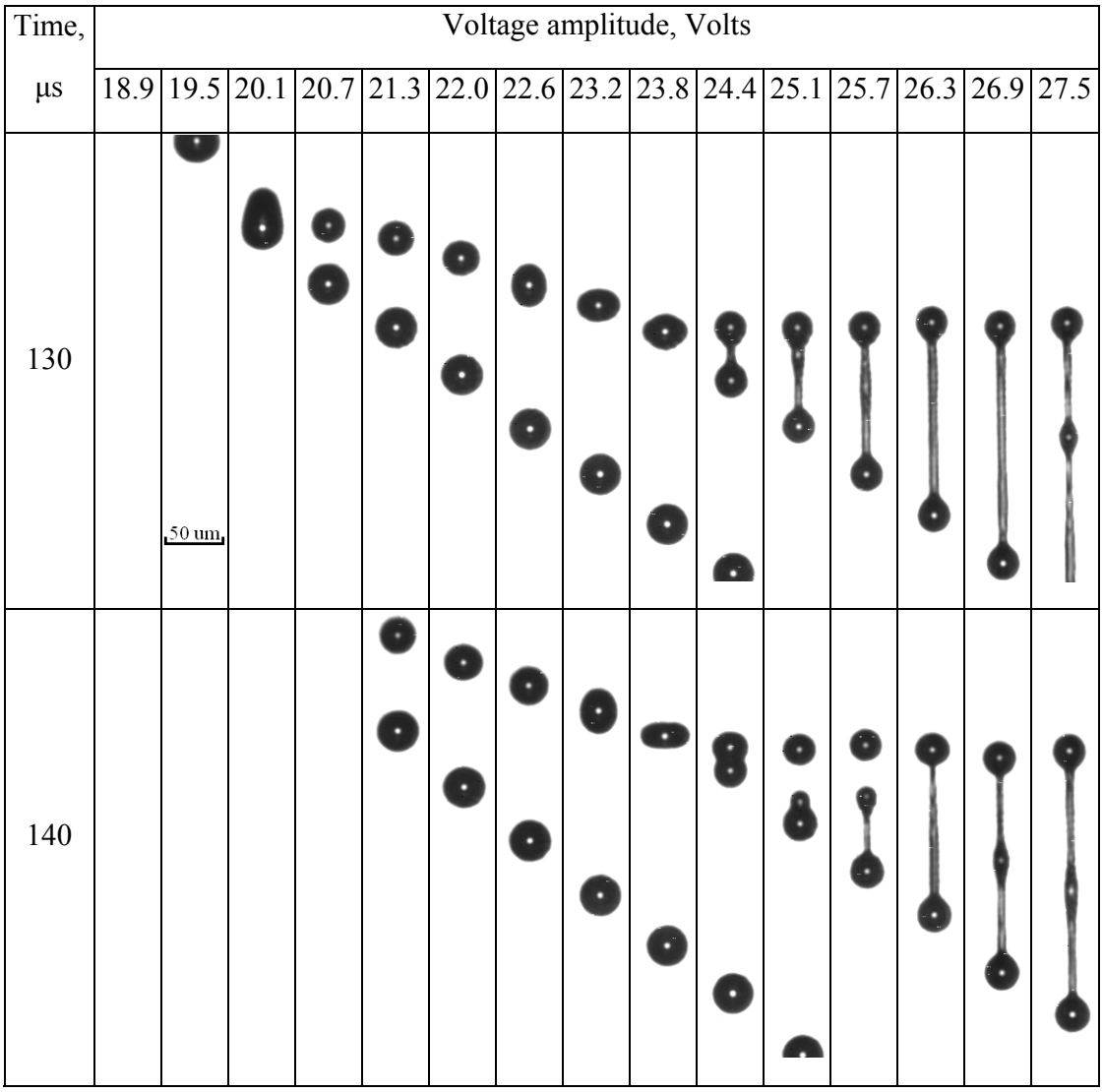

Figure 5-1 (g): Images of a Newtonian fluid being ejected from a DOD inkjet nozzle using the double-peak waveform shown in Figure 4-2 at 15 signal amplitudes and frequency = 10 kHz. The time intervals shown in this figure are 130 and 140 μs.

Time,	Voltage amplitude, Volts													
μs	18.9	19.5	20.1	20.7	21.3	22.0	22.6	23.2	23.8	24.4	25.1	25.7	26.3	26.9	27.5
150						50 um									
160															

Figure 5-1 (h): Images of a Newtonian fluid being ejected from a DOD inkjet nozzle using the double-peak waveform shown in Figure 4-2 at 15 signal amplitudes and frequency = 10 kHz. The time intervals shown in this figure are 150 and 160 μs.

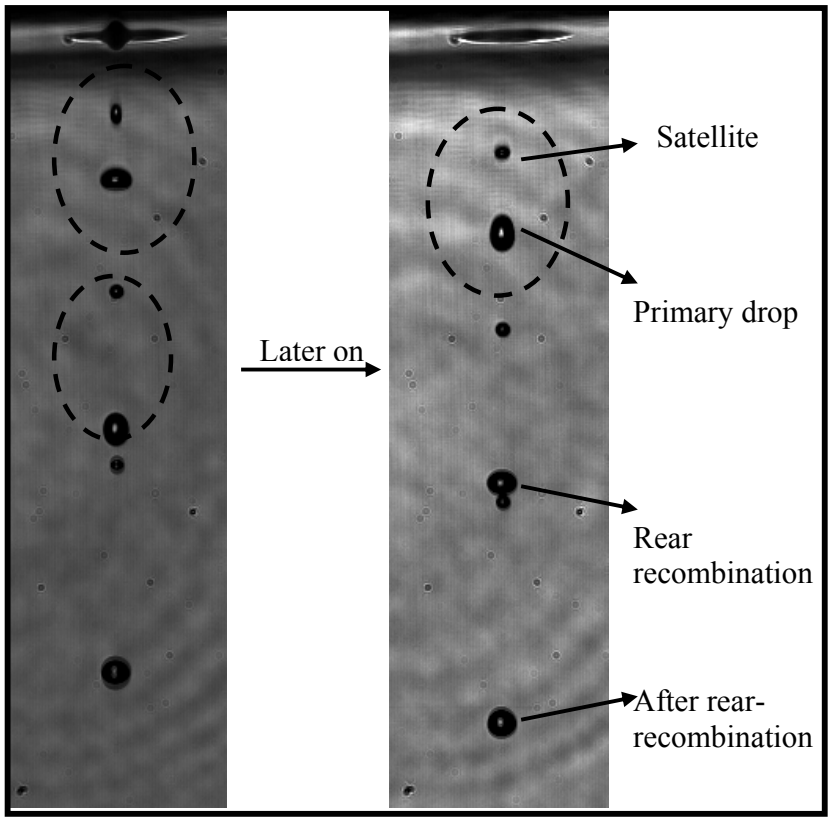

Figure 5-2: An example of "rear recombination", i.e., primary drop catches the satellite formed in the previous drop formation process. Drops in the dashed circles were formed by one pulse.

Experimental data at time interval higher than 160 μs indicate that recombination of satellites occurred for the cases where the secondary thread broke down and multiple satellites were formed. Depending on voltage amplitudes, after recombination(s) of satellites, only one or two satellites existed. The numbers of satellites formed and recombinations of 1) primary drop and satellite and 2) satellites are summarized in Table 5-1.

Figure 5-4 shows the relationships of primary drop speed, satellite drop speed, and total volume of ejected liquid body versus voltage amplitude. The correlations show that the relationships are linear.

Time	Voltage amplitude = 26.9 Volts	Voltage amplitude = 27.5 Volts
140 μs	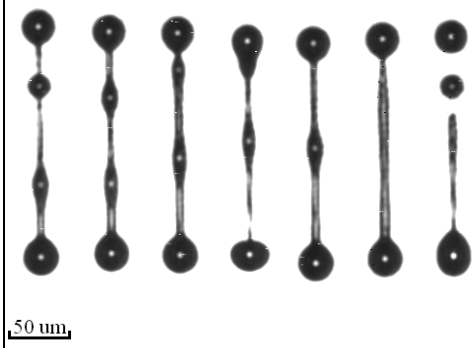	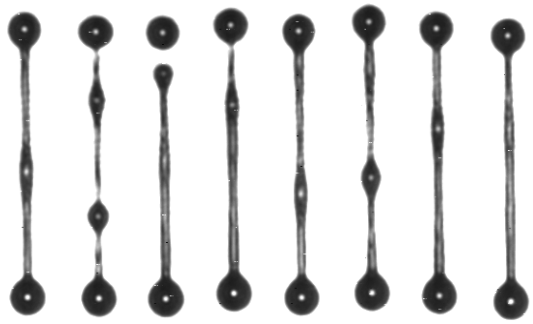
150 μs	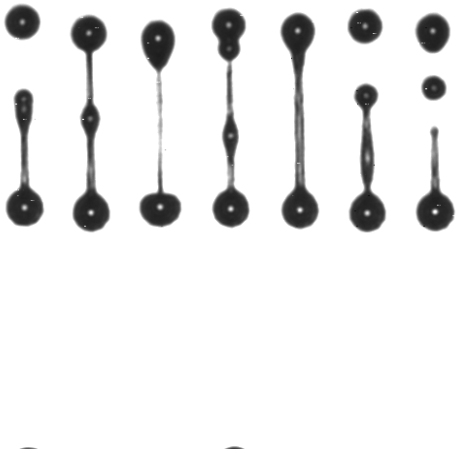	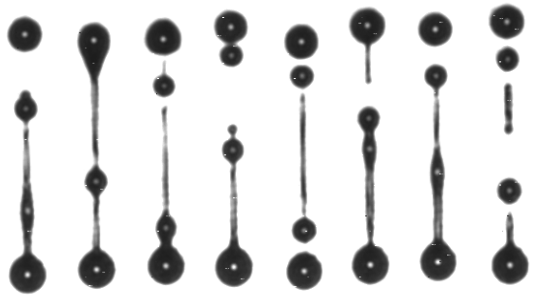
160 μs		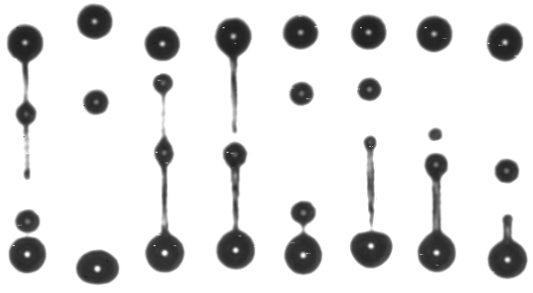

Figure 5-3: Randomly selected images of the secondary thread at V = 26.9 and 27.5 Volts and time intervals of 140, 150, and 160 μs.

Table 5-1: Number of satellites and recombinations at various voltage amplitudes

Voltage, amplitudes, Volts	Number of satellites formed before any recombination	Recombination of primary drop and satellite	Recombination of satellites	Number of satellites after all recombinations
18.9	0	--	--	0
19.5	1	Yes	--	0
20.1	1	Yes	--	0
20.7	1	Yes	--	0
21.3	1	Yes	--	0
22.0	1	No	--	1
22.6	1	No	--	1
23.2	1	No	--	1
23.8	1	No	--	1
24.4	1	No	--	1
25.1	2	No	Yes	1
25.7	2 ~ 3	No	Yes	1
26.3	3	No	Yes	1
26.9	3 ~ 4	No	Yes	2
27.5	> 4	No	Yes	2

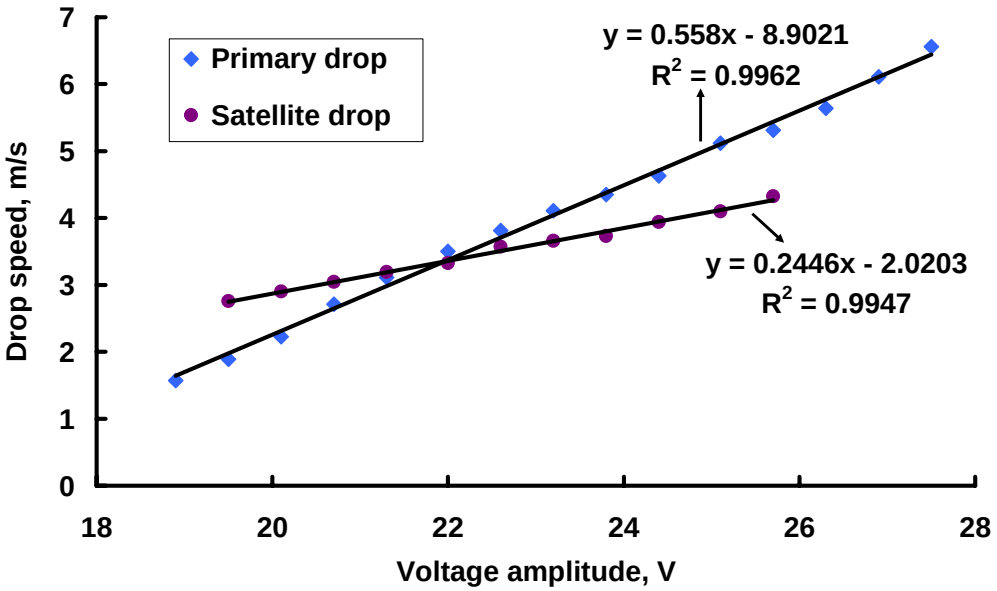

(a)

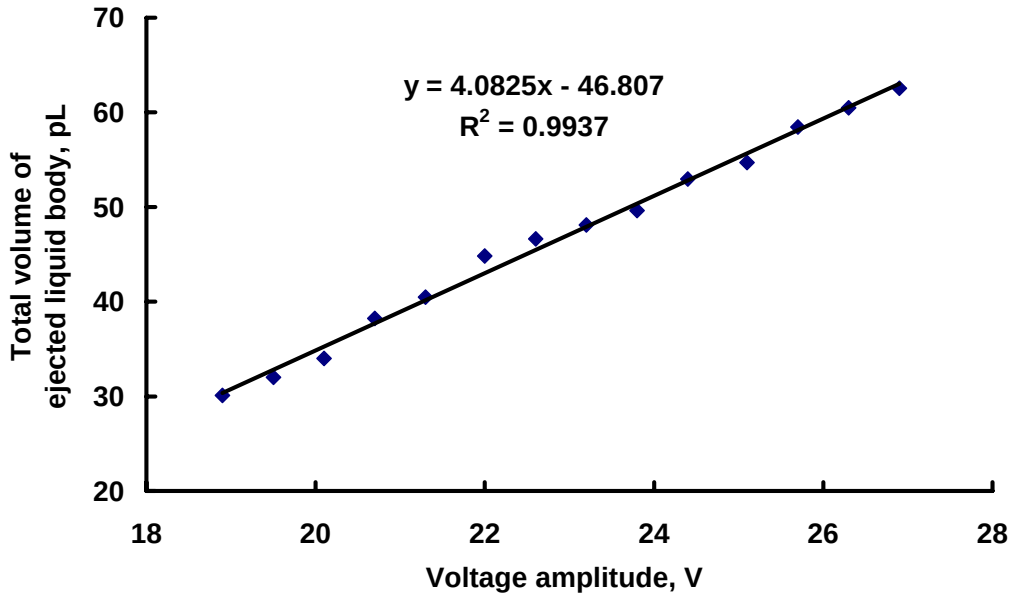

(b)

Figure 5-4: (a) Primary drop and satellite speeds and (b) total volume of ejected liquid body versus voltage amplitudes using the double-peak waveform shown in Figure 4-2 with jetting frequency = 10 kHz.

5.4.2 Effect of Jetting Frequency

The frequency of the actuating signal greatly affects DOD drop formation dynamics. As jetting frequency increases, the time between two consecutive signals decreases. When jetting frequency gets sufficiently high, the time interval between two consecutive signals is not long enough for pressure variation inside the nozzle chamber due to the previous pulse to be fully damped by viscous dissipation before the next pressure pulse is produced. As a result, the pressure waves due to consecutive pulses interact. This coupling varies as frequency changes, which leads to different DOD drop sizes and velocities.

Shin *et al.* [8] showed that the mass transport rate of DOD printhead is a function of the actuating frequency for a defined waveform. The relation is not linear, but with several local optimum peaks of productivity. Wassink *et al.* [9] maximized the jetting frequency while maintaining the reliability of DOD drop formation. By accelerating the damping process of residual vibrations between two consecutive pulses, a quicker rest was successfully brought for the printhead chamber.

During the inkjet printing process, an individual nozzle is not continuously firing; instead, it jets for a period of time at a certain frequency followed by an idle period. If the idle time is long enough, a so-called "first-drop" problem occurs. Dong *et al.* [3, 6] found that "first-drop" problem leads to low reproducibility of DOD drop formation for the first few drops, which is primarily caused by the evaporation of ink at the nozzle exit. When the inkjet nozzle is idle for sufficiently long period of time, solvent evaporation leads to higher ink viscosity and change in surface tension. Kang [17] found that "first-drop" problem can be reduced by a proper ink formulation.

When the idle time is sufficiently short that the "first-drop" problem is insignificant, at sufficiently high jetting frequency, the drop triggered by the first pulse after the nozzle is idle is identical to the drop fired at low frequency; however, the drop

formation process varies until it stabilizes at a dynamic equilibrium, where DOD drop formation is periodic and highly reproducible. Dijksman *et al.* [18] gave a theoretical analysis on the start-stop behavior of a print head. They found that when the inkjet nozzle is transient from idle to a stable running situation, the drop size and velocity change. They pointed out that for fluids with low shear viscosity, damping is poor and the transition from idle to jetting lasts longer.

5.4.2.1 Effect of Jetting Frequency on Steady State DOD Drop Formation Dynamics

In order to study the effect of jetting frequency on DOD drop formation, a signal sequence (shown in Figure 5-5) composed of multiple double-peak waveforms as shown in Figure 4-2 was used to trigger the inkjet nozzle. Through changing the interval time between two consecutive signals, the jetting frequency was adjusted.

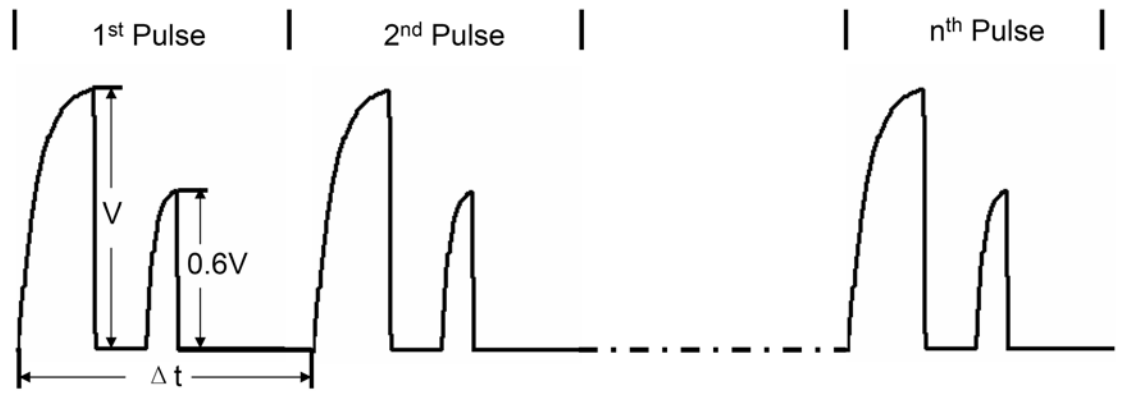

Figure 5-5: A signal sequence composed of multiple double-peak waveforms (see Figure 4-2). Decreasing Δt corresponds to increasing jetting frequency.

In order to show with better clarification the effect of jetting frequency on steady state DOD drop formation, the images used in the discussion are processed in such a

fashion that the irrelevant information in each image is left out. An example of such a process is shown in Figure 5-6.

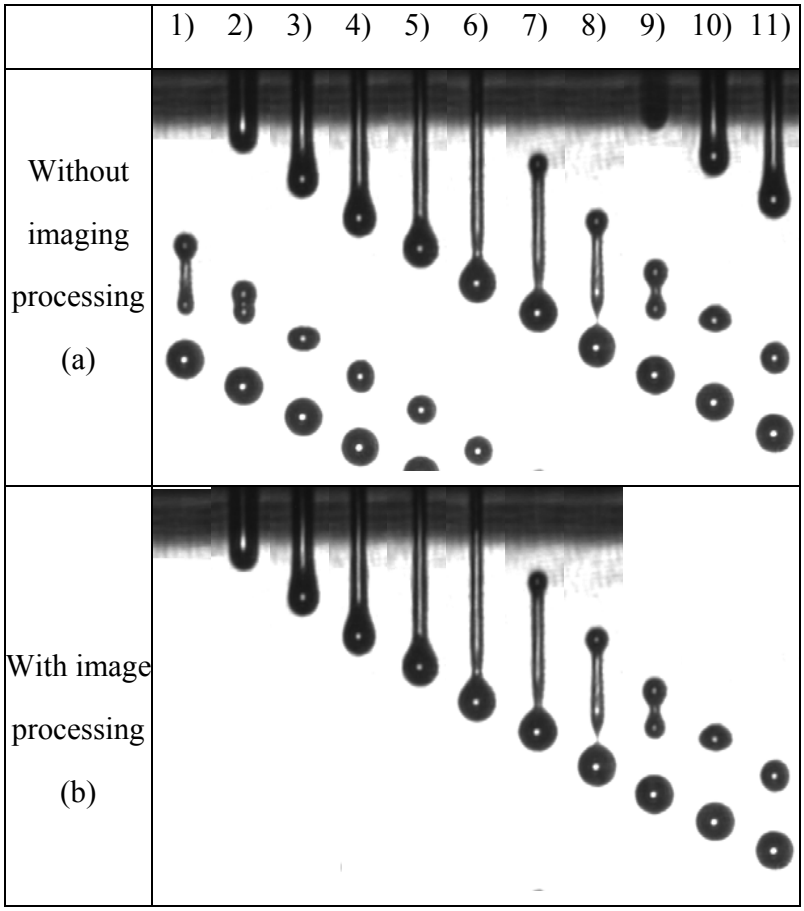

Figure 5-6: Sequence of images of DOD drop formation using the double-peak waveform shown in Figure 4-2 with voltage amplitude = 19.50 Volts and frequency = 13.3 kHz. Interframe time = 10 μs and image size = 57 μm × 389 μm. The images in (a) have not been image processed while those in (b) were image processed.

Figure 5-7 shows the sequence of images of DOD drop formation at voltage amplitude of 19.50 Volts for 6 different jetting frequencies. The data, collected at steady state conditions where the dynamics is periodic and highly reproducible, indicate that jetting frequency has a great effect on DOD drop formation dynamics. At jetting frequency of 0.02 kHz, the time interval between two consecutive signals is long enough

for pressure variation inside the nozzle chamber to be fully damped by viscous dissipation. Thus, DOD drop formation process at this frequency is used as a reference. Among all the differences in DOD drop formation at varied jetting frequencies, a few observations are addressed here.

At the jetting frequency = 0.02 kHz, the secondary breakup occurred before time interval of 70 μs (see No.8 image in Figure 5-7 (a)); however, at the other 5 jetting frequencies, it had not occurred. Dong *et al.* [3, 6] discussed breakup time of liquid threads during DOD drop formation process and pointed out that the breakup time of a liquid thread should depend only on the capillary time and the fastest growth rate of disturbance. Our results (see Figure 5-7) indicate that the secondary breakup time can be slightly affected by jetting frequency.

The second observation is that the length of liquid thread ejected varied with jetting frequency. The length of ejected liquid threads at jetting frequency of 13.3 kHz (Δt = 75 μs) are longer than that at jetting frequency of 0.02 kHz. However, at jetting frequencies of 10 kHz (Δt = 100 μs) and 20 kHz (Δt = 50 μs), it is significantly shorter.

The third observation is that corresponding to the length of ejected liquid thread, the speed of ejected liquid body varied with jetting frequency, which is indicated by the vertical position of the primary drop at time interval of 100 μs (see No.11 images in Figure 5-7 (a) and (b). The drop speed at jetting frequencies of 13.3 kHz (Δt = 75 μs) is faster than that at jetting frequency of 0.02 kHz. However, at jetting frequencies of 10 kHz (Δt = 100 μs) and 20 kHz (Δt = 50 μs), it is slower than that at jetting frequency of 0.02 kHz. Also, at jetting frequencies of 10 kHz (Δt = 100 μs) and 20 kHz (Δt = 50 μs), due to the slower primary drop speed and shorter ejected liquid thread, recombination of primary drop and satellite occurred before time interval of 80 μs (see No.9 image in Figure 5-7 (a)).

The above observations indicate that a destructive effect between pressure pulses produced by two consecutive DOD drop formation processes existed for jetting

frequencies of 10 kHz (Δt = 100 μs) and 20 kHz (Δt = 50 μs) and a constructive effect between pressure pulses existed for jetting frequency of 13.3 kHz (Δt = 75 μs). The effect of jetting frequency on DOD drop formation dynamics depends on the nozzle geometry and the acoustic wave speed of the fluid [19].

Figure 5-8 shows the variations of drop speed and total volume of the ejected liquid body with jetting frequency using the double-peak waveform shown in Figure 4-2 with voltage amplitude = 19.50 Volts. At all jetting frequencies, if satellite existed, recombination of primary drop and satellite occurred. The drop speed in Figure 5-8 (a) is the speed of the recombined drop.

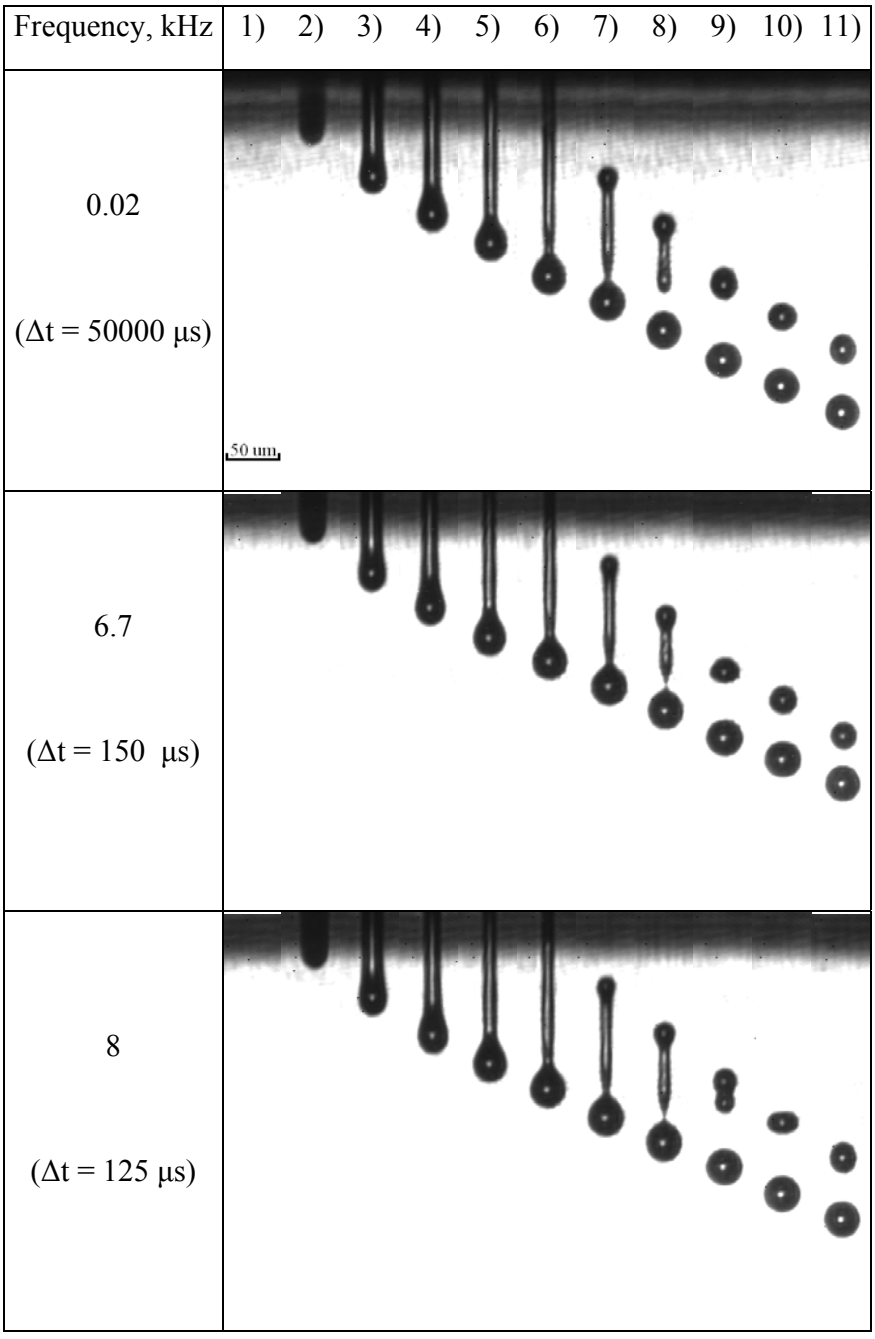

Figure 5-7 (a): Sequence of images of DOD drop formation using the double-peak waveform shown in Figure 4-2 with voltage amplitude = 19.50 Volts at jetting frequencies of 0.02, 6.7, and 8 kHz. Interframe time = 10 μs and image size = 57 μm × 389 μm.

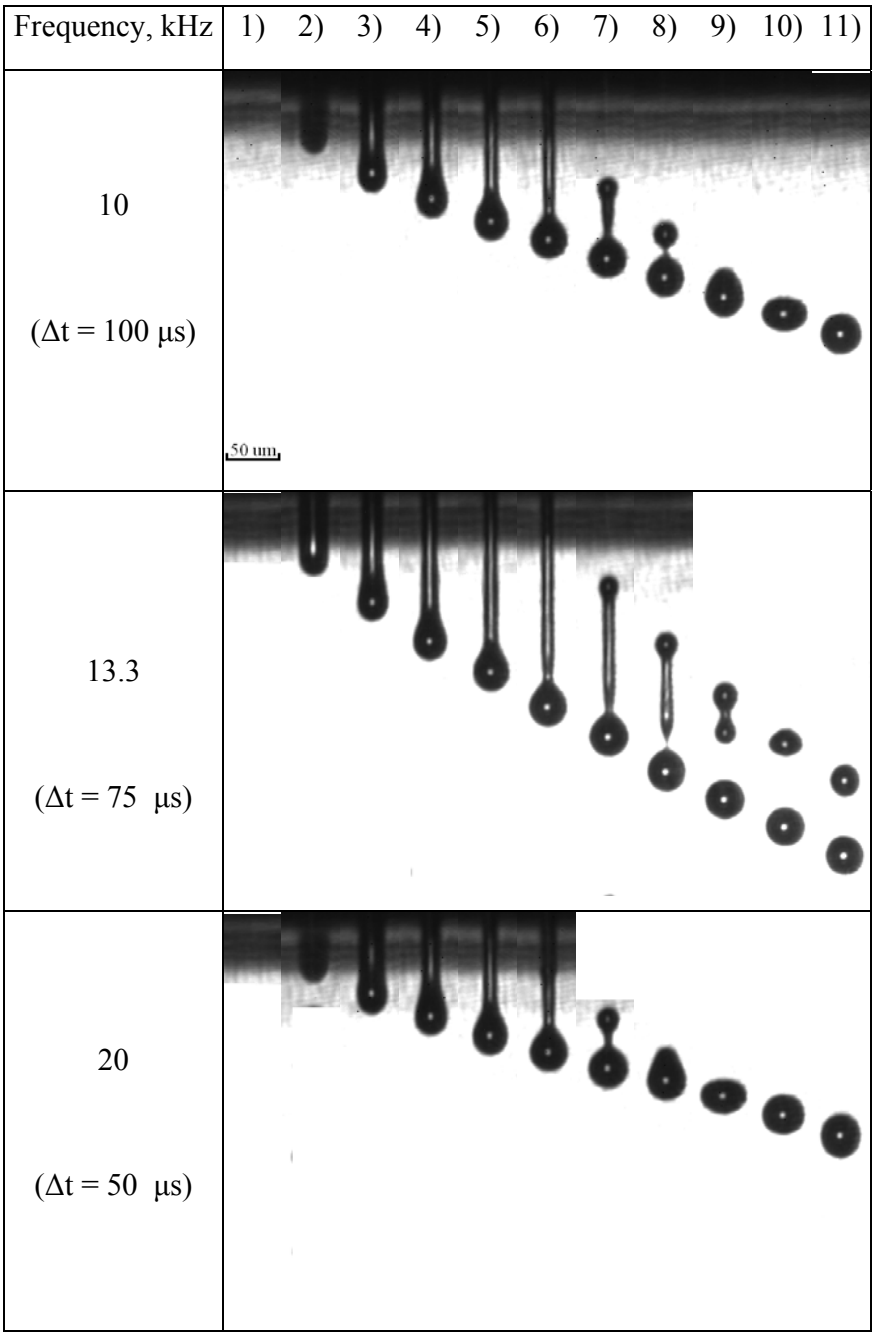

Figure 5-7 (b): Sequence of images of DOD drop formation using the double-peak waveform shown in Figure 4-2 with voltage amplitude = 19.50 Volts at jetting frequencies of 10, 13.3, and 20 kHz. Interframe time = 10 μs and image size = 57 μm × 389 μm.

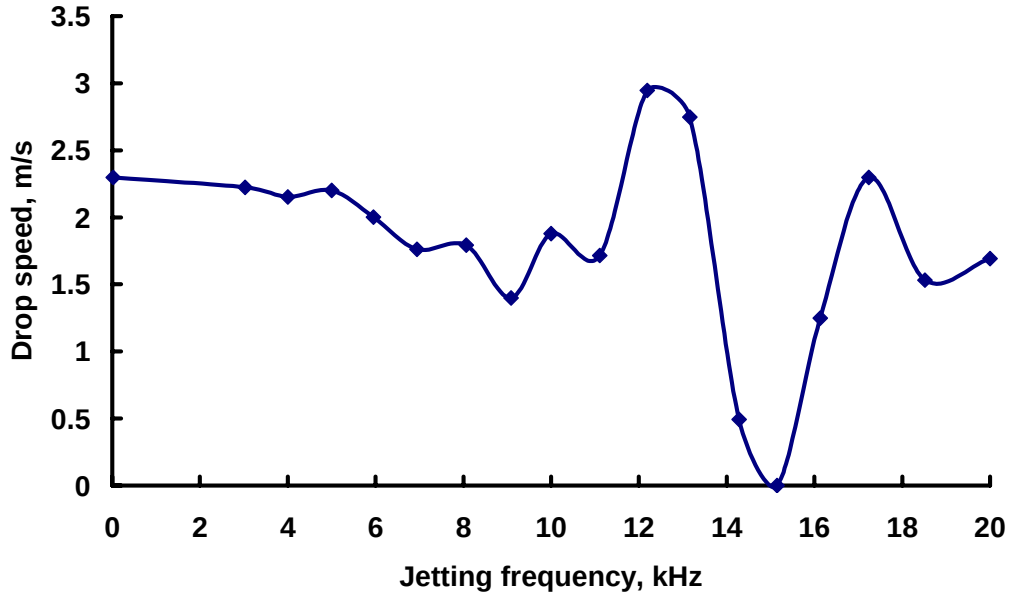

(a)

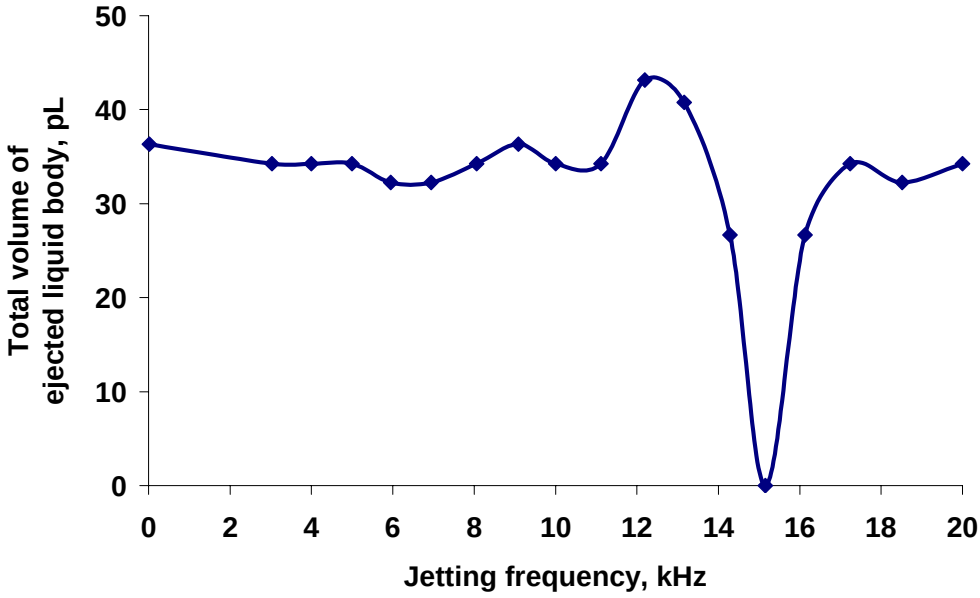

(b)

Figure 5-8: Effects of jetting frequency on a) drop speed and b) total volume of ejected liquid body using the double-peak waveform shown in Figure 4-2 with voltage amplitude = 19.50 Volts.

5.4.2.2 Transition of DOD Drop Formation Dynamics from Idle to Jetting

Figure 5-9 shows sequences of images of DOD drop formation of the first four pulses at jetting frequencies of 6.7, 8, 10, 13.3, and 20 kHz (Δt = 150, 125, 100, 75, and 50 μs, correspondingly) after an idle time of close to 50 ms. The double-peak waveform shown in Figure 4-2 with voltage amplitude of 19.50 Volts was used. For better clarification, the images used in the discussion are processed in such a fashion that the irrelevant information in each image is left out (see Figure 5-6 as an example).

The data indicate that although the jetting frequencies were different, the drop triggered by the first pulse after idle had the same drop formation dynamics as the case of jetting frequency of 0.02 kHz. For each jetting frequency, the drop formation process varied after the first pulse until it stabilized to a dynamic equilibrium. Comparing the data shown in Figure 5-7 where steady state DOD drop formation dynamics is shown with the data shown in Figure 5-9 where DOD drop formation dynamics of the first four pulses is shown. After the fourth pulse, DOD drop formation dynamics for jetting frequencies of 6.7, 8, 10, 13.3, and 20 kHz has almost reached dynamic equilibrium.

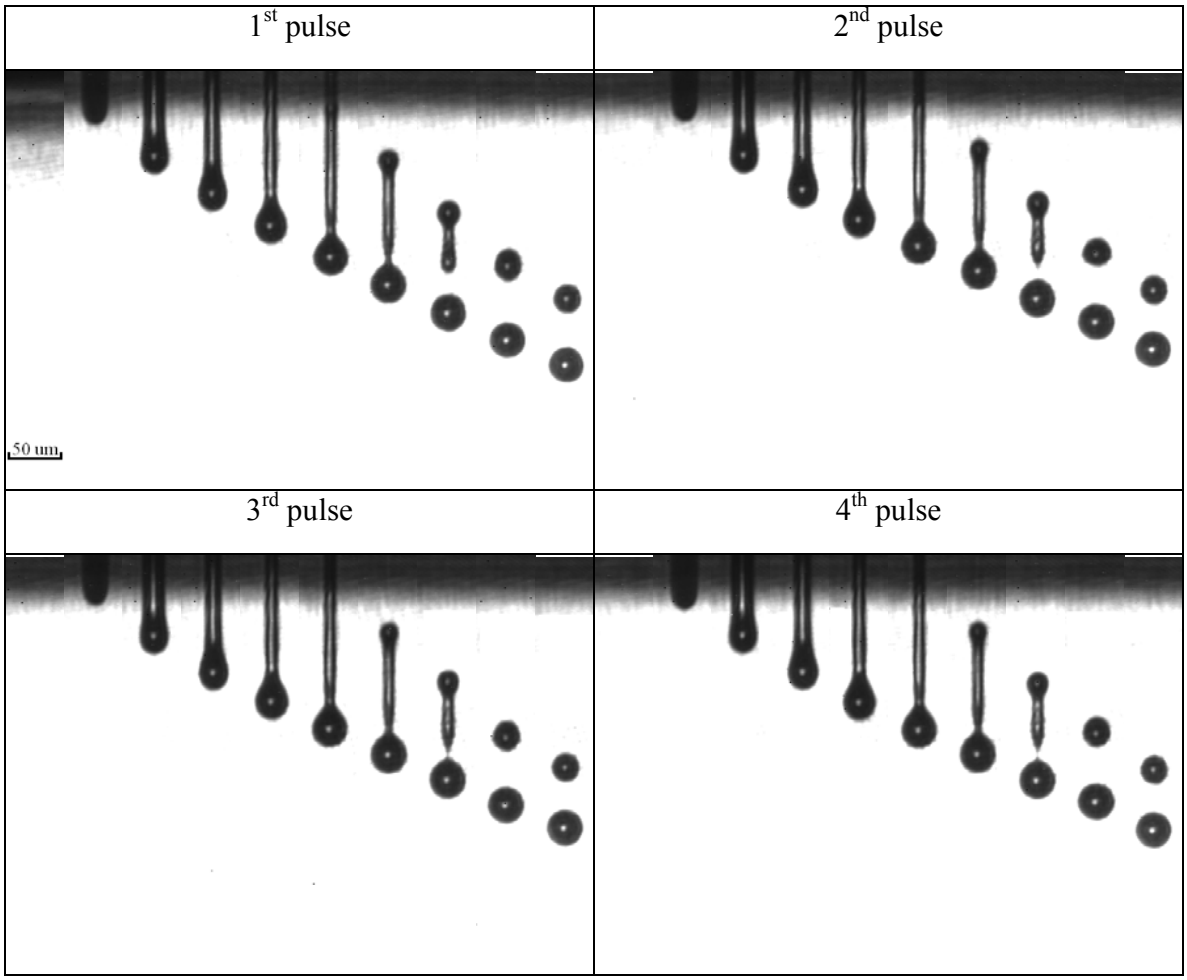

Figure 5-9 (a): Sequences of images of DOD drop formation of the first four pulses at jetting frequency of 6.7 kHz (Δt = 150 μs) after an idle time of close to 50 ms. The double-peak waveform shown in Figure 4-2 with voltage amplitude = 19.50 Volts was used. Interframe time = 10 μs and image size = 57 μm × 389 μm.

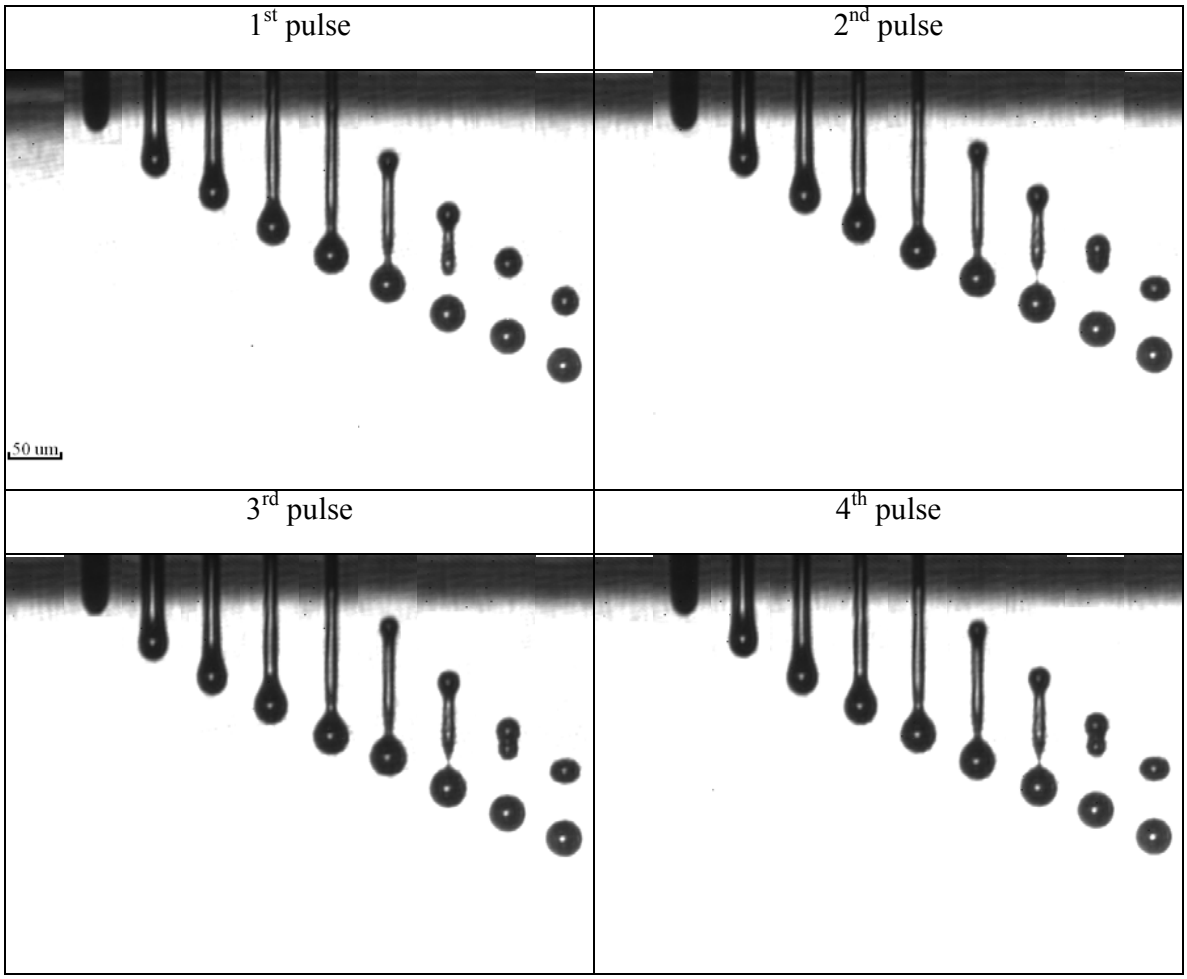

Figure 5-9 (b): Sequences of images of DOD drop formation of the first four pulses at jetting frequency of 8 kHz (Δt = 125 μs) after an idle time of close to 50 ms. The double-peak waveform shown in Figure 4-2 with voltage amplitude = 19.50 Volts was used. Interframe time = 10 μs and image size = 57 μm × 389 μm.

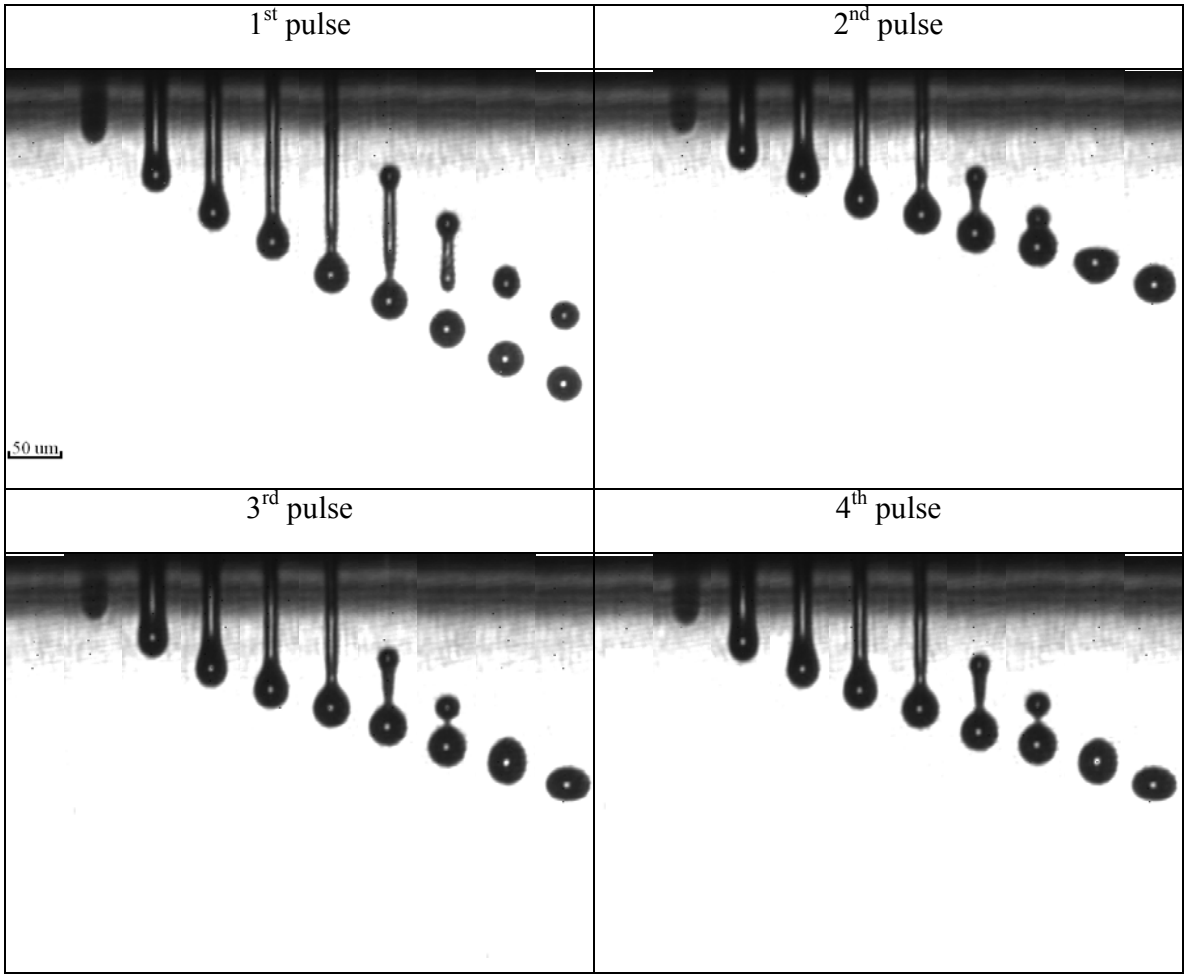

Figure 5-9 (c): Sequences of images of DOD drop formation of the first four pulses at jetting frequency of 10 kHz (Δt = 100 μs) after an idle time of close to 50 ms. The double-peak waveform shown in Figure 4-2 with voltage amplitude = 19.50 Volts was used. Interframe time = 10 μs and image size = 57 μm × 389 μm.

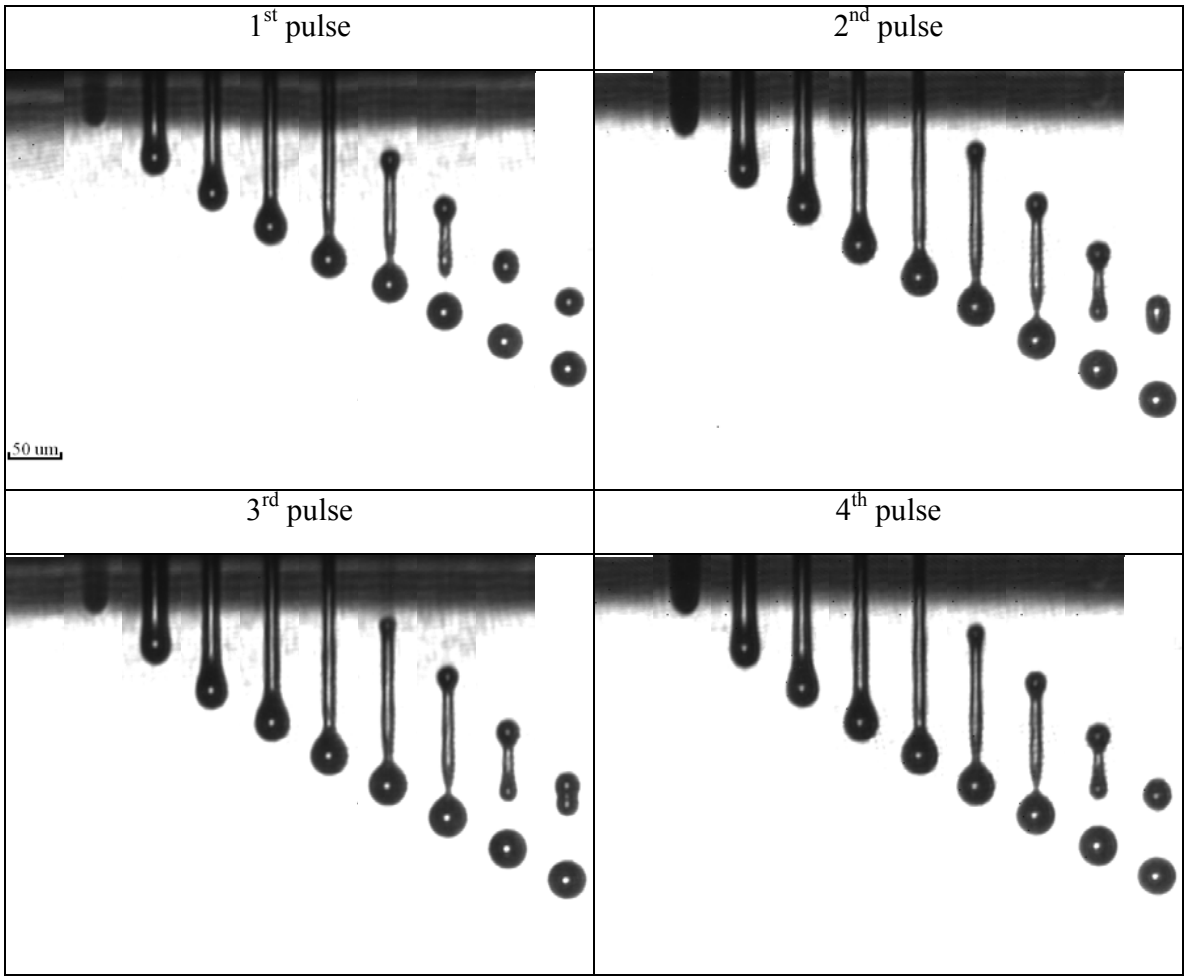

Figure 5-9 (d): Sequences of images of DOD drop formation of the first four pulses at jetting frequency of 13.3 kHz (Δt = 75 μs) after an idle time of close to 50 ms. The double-peak waveform shown in Figure 4-2 with voltage amplitude = 19.50 Volts was used. Interframe time = 10 μs and image size = 57 μm × 389 μm.

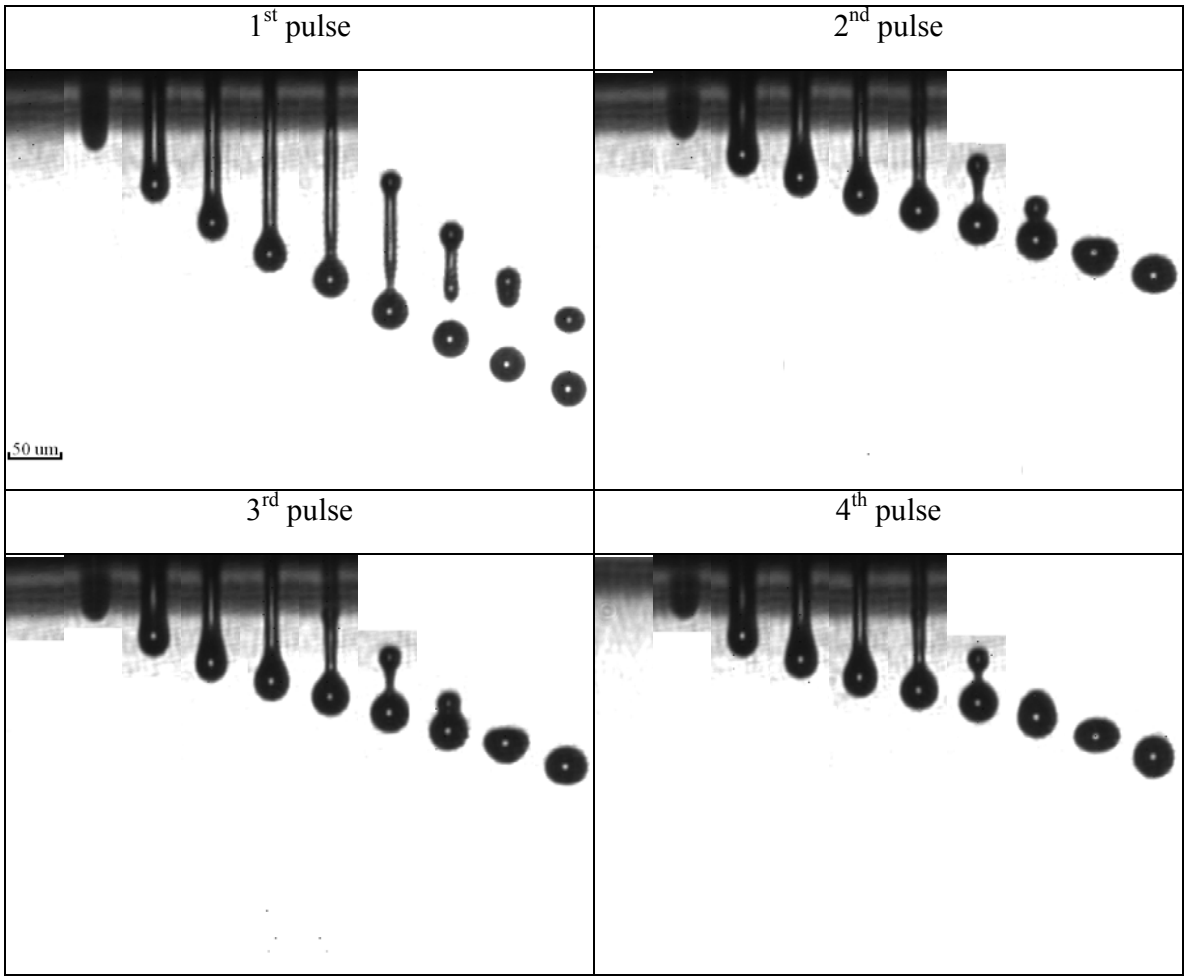

Figure 5-9 (e): Sequences of images of DOD drop formation of the first four pulses at jetting frequency of 20 kHz (Δt = 50 μs) after an idle time of close to 50 ms. The double-peak waveform shown in Figure 4-2 with voltage amplitude = 19.50 Volts was used. Interframe time = 10 μs and image size = 57 μm × 389 μm.

5.4.2.3 Effect of Modulation Pulse on DOD Drop Formation of the First Pulse during the Transition from Idle to Jetting

As pointed out by Dijksman *et al.* [18], for DOD inkjet printing of highly functional materials such as light emitting polymer, every drop counts. For a sufficiently high jetting frequency, DOD drop formation of the first several pulses after idle is not identical to that in equilibrium. To solve this problem, a method is proposed here based on the observations made in section 5.4.2.1. When time interval between two consecutive pulses was 100 μs (jetting frequency = 10 kHz) and 50 μs (jetting frequency = 20 kHz), a destructive effect was observed; when time interval was 75 μs (jetting frequency = 13.3 kHz), a constructive effect was observed.

For jetting frequency of 10 kHz (Δt = 100 μs), the speed and volume of DOD drops formed by the first pulse are higher than those formed when for equilibrium has been reached in the nozzle (see Figure 5-9 (c)). In order for the drop formation process of the first pulse, as shown in Figure 5-9, to be similar to that once the system is in equilibrium, a modulating pulse was added at 75 μs before the first pulse, and it was an inverse double-peak waveform (see Figure 4-2). It was conjectured that a destructive effect could be produced using an inverse pulse. Since a pulse imposed at a time interval of 75 μs would lead to a constructive effect, then a destructive effect should be produced by adding a negative pulse. The magnitude of destructive effect should vary with the amplitude of the modulating pulse. Thus, three amplitudes were tested, which are 30%, 50%, and 70% of the voltage amplitude of the first pulse (see Figure 5-10). The effect of modulating pulse at three different signal amplitudes on DOD drop formation of the first pulse at jetting frequency of 10 kHz is shown in Figure 5-11.

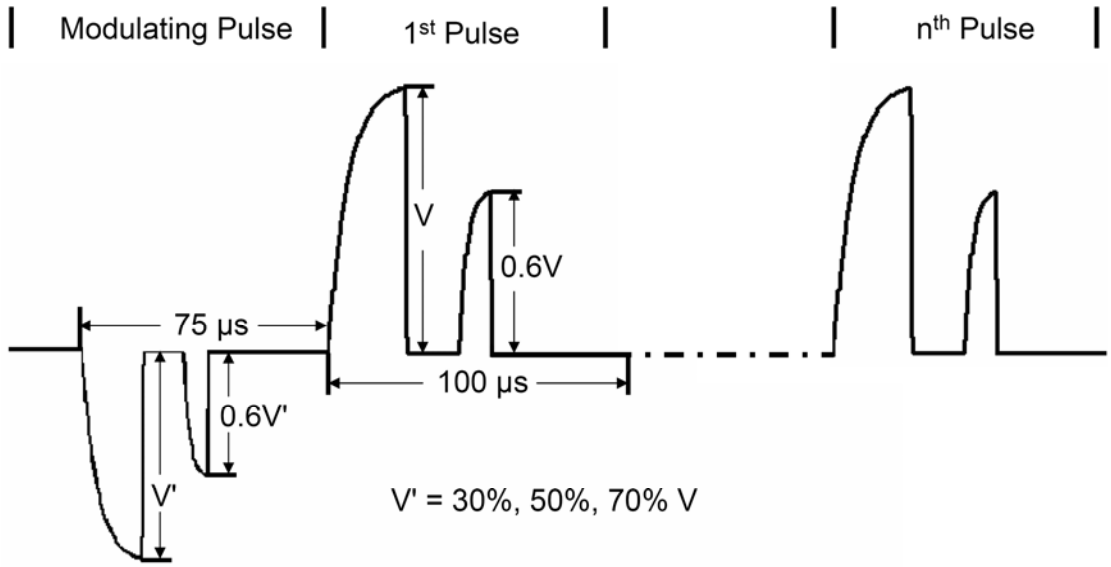

Figure 5-10: A signal sequence composed of multiple double-peak waveforms at jetting frequency of 10 kHz. A modulating pulse is added at 75 µs before the first pulse.

Figure 5-11 shows that the modulating signal in Figure 5-10 had a destructive effect on DOD drop formation of the first pulse, and the higher the signal amplitude of the modulating pulse, the bigger the destructive effect. At signal amplitude of -70% V, the length of the ejected liquid body was shortest and the speed was lowest, which was the close to what occurs for DOD drop formation in equilibrium at jetting frequency of 10 kHz. It is also noticed that the secondary breakup time was affected by the signal amplitude of the modulating pulse. The data indicate that the modulating pulse itself did not lead to DOD drop formation, and DOD drop formation of the second pulse was the same as the one in steady state for the case where the signal amplitude of the modulating pulse equaled to -70% V (see Figure 5-10).

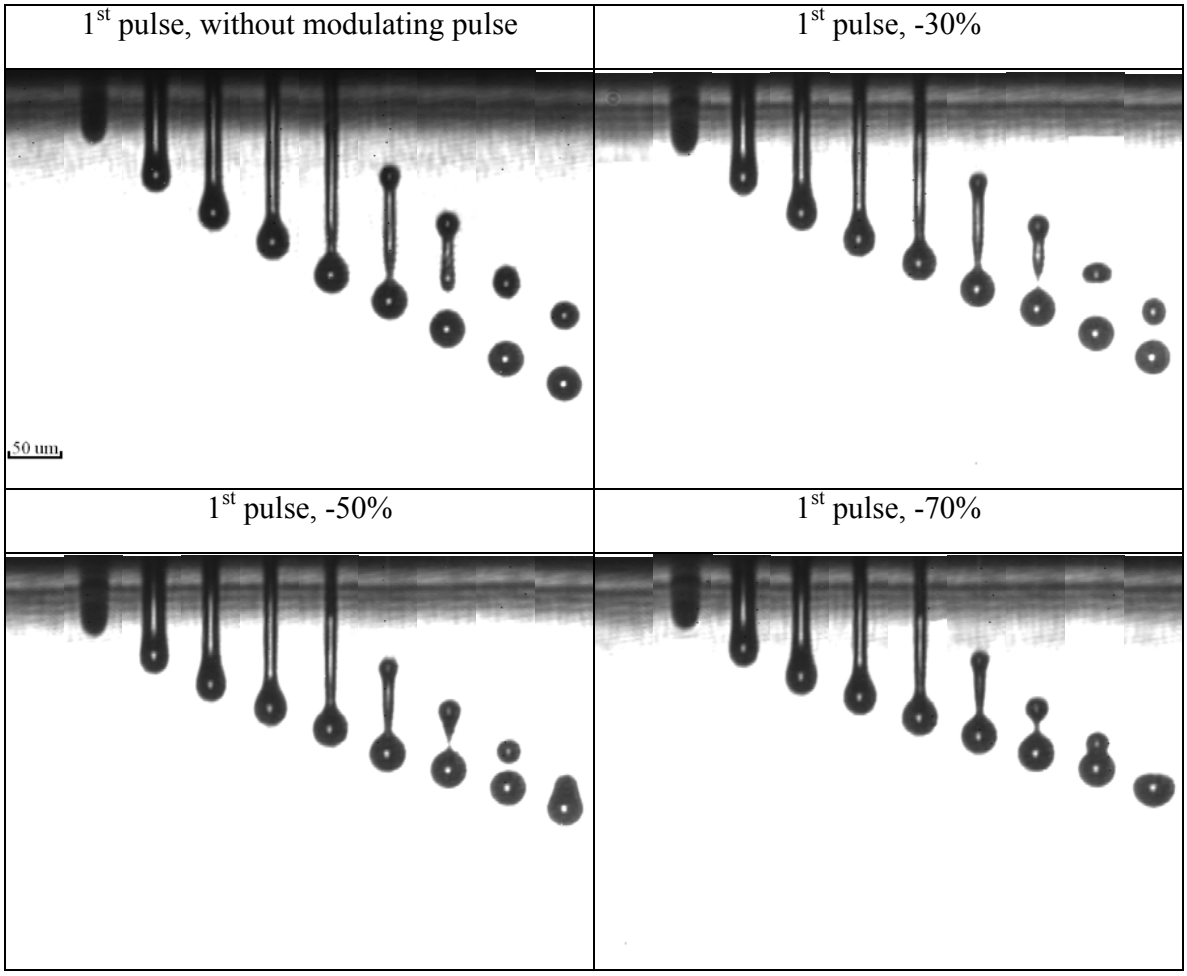

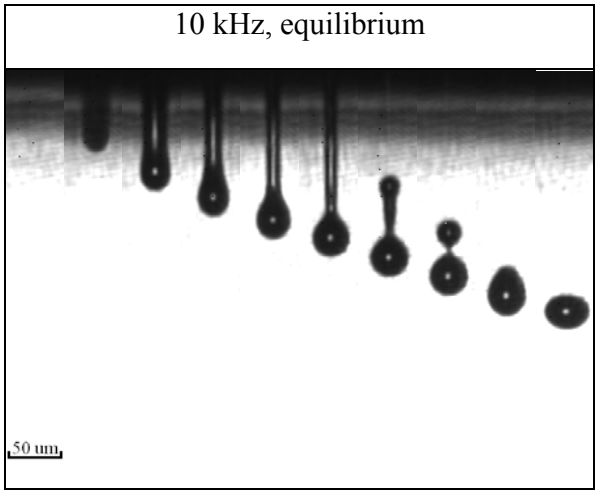

Figure 5-11: Effect of modulating pulse shown in Figure 5-10 on DOD drop formation of the first pulse at jetting frequency of 10 kHz (Δt = 100 μs). Voltage amplitude = 19.50 Volts. Interframe time = 10 μs and image size = 57 μm × 389 μm.

For jetting frequency of 13.3 kHz (Δt = 75 μs), the speed and volume of DOD drops formed by the first pulse is lower than that formed in equilibrium (see Figure 5-9(d)). In order to constructive the drop formation process of the first pulse, as shown in Figure 5-12, a modulating pulse was added at 75 μs before the first pulse and it was a positive double-peak waveform (see Figure 4-2). It was conjectured that time interval of 75 μs would lead to a constructive effect, and the higher the amplitude of the modulating pulse, the bigger the constructive effect. Thus, three amplitudes were tested, which are 30%, 50%, and 70% of the voltage amplitude of the first pulse (see Figure 5-12). The effect of modulating pulse at three different signal amplitudes on DOD drop formation of the first pulse at jetting frequency of 13.3 kHz is shown in Figure 5-13.

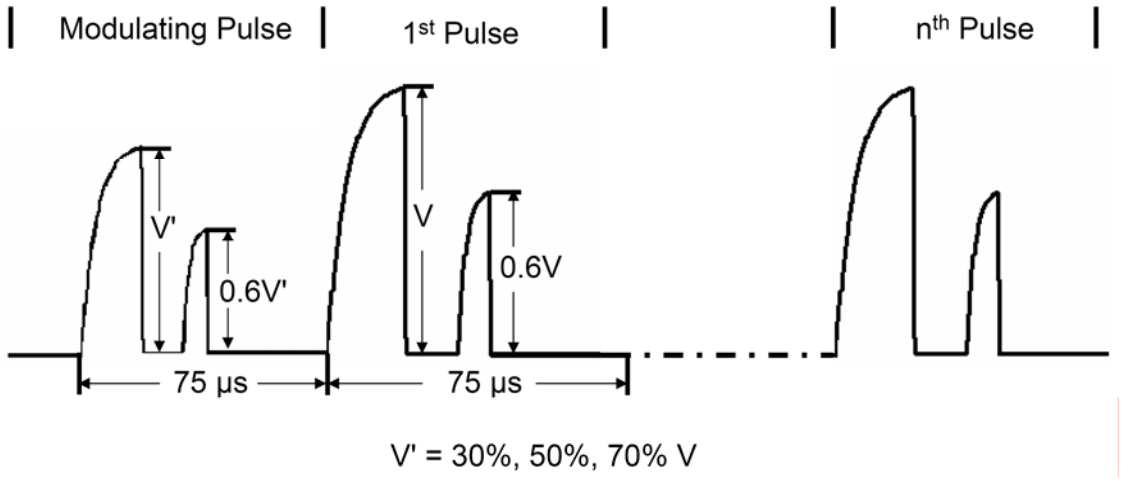

Figure 5-12: A signal sequence composed of multiple double-peak waveforms at jetting frequency of 13.3 kHz. A modulating pulse is added at 75 μs before the first pulse.

Figure 5-13 shows that the modulating signal in Figure 5-12 had a constructive effect on DOD drop formation of the first pulse. However, when the signal amplitude of the modulating pulse was 50% V, the constructive effect was maximized as indicated by the longest length of ejected liquid thread and highest speed of the ejected liquid body. When the signal amplitude of the modulating pulse was 70% V, DOD drop formation

induced by modulating pulse was observed. Thus, part of energy of the propagating wave was transformed into the energy for DOD drop formation; as a result, the constructive effect on DOD drop formation of the first pulse was less than the case where the signal amplitude of the modulating pulse was 50% V. At signal amplitude of 30% V, DOD drop formation of the first pulse was closest to DOD drop formation in equilibrium at jetting frequency of 13.3 kHz. Similar to the case where jetting frequency was 10 kHz, the secondary breakup time was affected by the signal amplitude of the modulating pulse. The data also indicate that DOD drop formation of the second pulse was the same as the one in steady state.

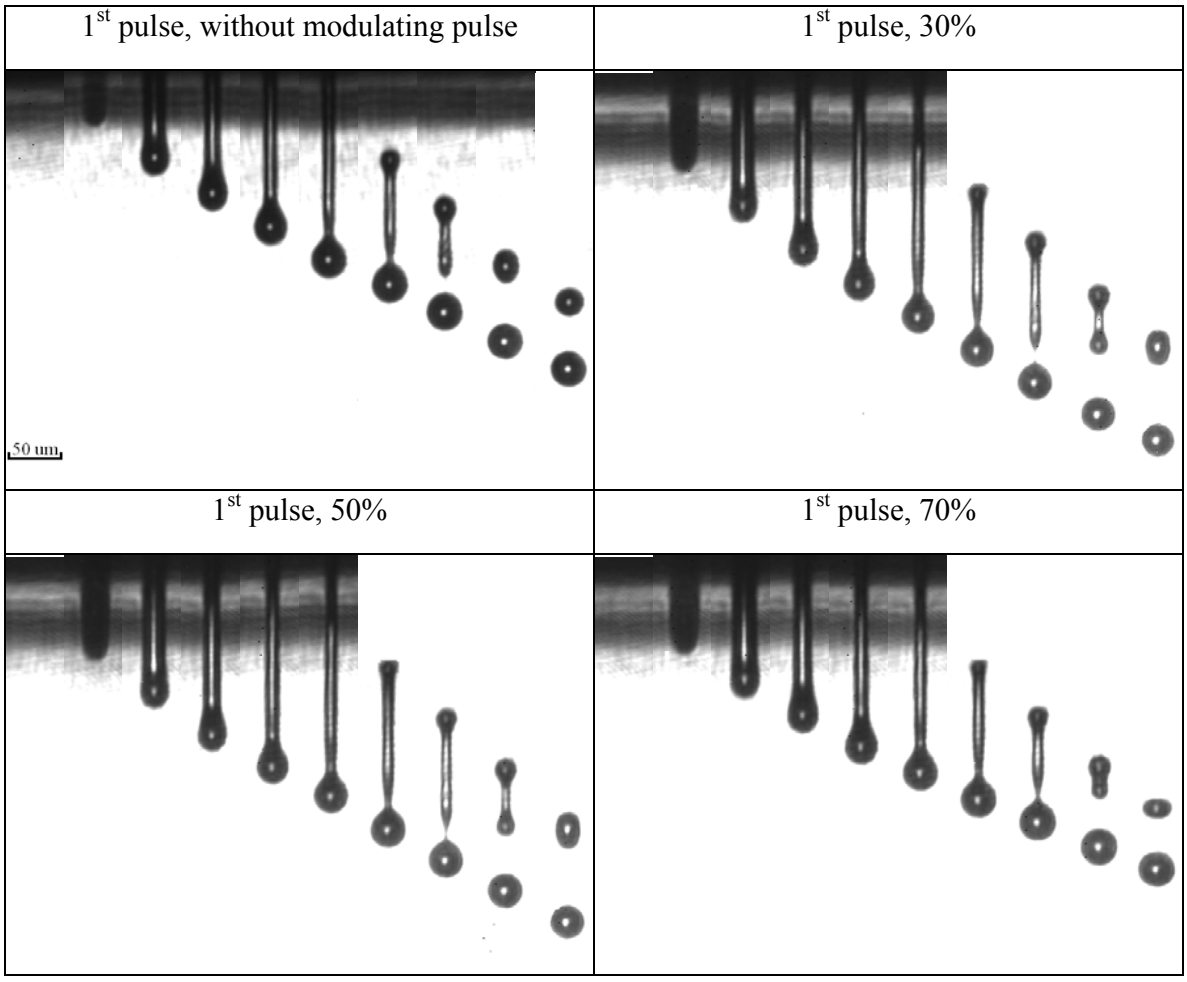

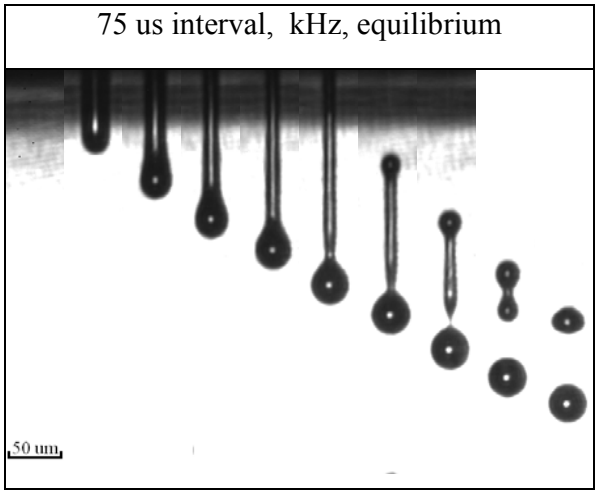

Figure 5-13: Effect of modulating pulse shown in Figure 5-12 on DOD drop formation of the first pulse at jetting frequency of 13.3 kHz (Δt = 75 μs). Voltage amplitude = 19.50 Volts. Interframe time = 10 μs and image size = 57 μm × 389 μm.

5.5 Conclusions

In this chapter, the effects of signal amplitude and jetting frequency of actuating waveform on DOD drop formation of a Newtonian fluid with shear viscosity of 6.3 cP and surface tension of 32 mN/m were studied. The effect of adding a modulating pulse on DOD drop formation of the first pulse after idle was investigated.

It was found that at different signal amplitudes, the shape of being ejected liquid thread was the same except that the thread length was longer when the signal amplitude was higher. Both the first and second breakup times were independent of signal amplitudes for the fluid, actuating waveform and jetting frequency used in this study. After the first and second breakups, recoil at the tip of the liquid thread occurred due to the high local capillary pressure and the recoiling process was identical and independent of signal amplitudes.

The satellite formation was due to end-pinching at the lower voltage amplitudes, but as voltage amplitude was increased, the ligament length increased, and multiple breakup occurred, apparently due to wave-like instability. The capillary waves do not show preferred wavelength, and the liquid thread breaks up at several locations at different times, forming satellites of varying sizes. The reproducibility of evolution of the secondary liquid thread became very low once voltage amplitude was increased to a level where the wave-like instability breakup occurred.

Jetting frequency was found to have a great effect on DOD drop formation dynamics. When jetting frequency was low, DOD drop formation was found to be identical; however, at sufficiently high jetting frequency, the propagating wave induced by consecutive pulses interacted with each other in the inkjet nozzle before being damped out, leading to a frequency dependent jetting behavior. Jetting frequency was found to affect the volume and speed of ejected liquid body.

After idle for a short period of time, the drop triggered by the first pulse was found to be identical and independent of jetting frequency. However, at sufficiently high jetting frequency, a transition of DOD drop formation dynamics from idle to jetting was observed. For the particular inkjet ink, inkjet nozzle, actuating waveform and signal amplitude used in this study, the transition was found to be almost finished after the first four pulses after idle.

In order to have DOD drop formation of the first pulse after idle identical to DOD drop formation in equilibrium at sufficiently high jetting frequency, a method using a modulating pulse before the first pulse was proposed. The results show that it was effective.

5.6 References

1. Meinhart, C. D. and Zhang, H., J. Microelectromech. Syst. 9, 67 (2000).
2. Reis N., Ainsley, C., and Derby, B., J. Am. Ceram. Soc. 88, 802 (2005).
3. Dong, H., Carr, W. W., and Morris, J. F., Phys. Fluids 18, 072102 (2006).
4. Chen, A. U., Basaran, O. A., Phys. Fluids 14, L1 (2002).
5. Chen, P. H., et al., Int. J. Mech. Sci. 41, 235 (1999).
6. Dong, H., Drop-on-demand inkjet drop formation and deposition, Doctorial dissertation, Georgia Institute of Technology, Atlanta, (2006).
7. Yang, A., et al., J. Micromechanics and Microengineering 16, 180 (2006).
8. Shin, D.Y., Grassia, P., Derby, B., Int. J. Mech. Sci. 46, 181 (2004).
9. Wassink, M.B.G., Bosgra, O.H., Slot, M. Final Program and Proceedings of IS&T NIP21, 273 (2005).
10. Dong, H., Carr, W. W., and Morris, J. F., Rev. Sci. Instrum.77, 85101 (2006).
11. Henderson, D., Segur, H., Smolka, L. B., and Wadati, M., Phys. Fluids 12, 550 (2000).
12. Notz, P. K. and Basaran, O. A., J. Fluid Mech. 512, 223 (2004).
13. Schulkes, R. M. S. M., J. Fluid Mech. 309, 277 (1996).
14. Eggers, J., Rev. Mod. Phys. 69, 865 (1997).
15. Burton, J. C., Rutledge, J. E., and Taborek, P., Phys. Rev. Lett. 92, 244505-1 (2004).
16. I. Cohen and S. R. Nagel, Phys. Fluids 13, 3533 (2001).
17. Kang, H. R., J. Imaging Sci. 35, 195 (1991).
18. Dijksman, J. F., Duineveld, P. C., Hack, J. J., Pierik, A., Rensen, J. Rubingh, J.-E., Schram, I., Vernhout, M. M., J. Mater. Chem. 17, 511 (2007).
19. Letendre, W., Private communication.

CHAPTER 6

DYNAMICS OF IMPACTION AND POST-IMPACTION BEHAVIOR OF DROP-ON-DEMAND (DOD) INKJET DROPS ON TEXTILES

6.1 Introduction

Textile digital printing, with ink jet printing as the mode of application, has become an accepted technology. Research and development is being conducted in the following areas: a) design of inkjet printers specifically for digital printing of textiles [9, 14], b) formulation of novel inkjet inks for textiles [10, 13, 15], c) upgrading of polymer dispersant agents for textile pigment inks with lowered viscosity profiles suitable for piezo-printheads [11], and d) image quality evaluation of textile inkjet printing [12]. Yet the broad utilization of this flexible method of printing on textiles faces a number of barriers. Research is needed to better understand the dynamics of DOD drop impaction and post-impaction (spreading, wicking and drying) of solids-laden inks, as well as the role of the surface morphology and surface chemistry encountered in printing of textile materials.

Drop impaction dynamics on flat surfaces has been studied extensively for over 100 years beginning with the early works of Worthington [1]. Recently, Yarin [2] gave a comprehensive review on drop impaction on thin liquid layers and dry surfaces, including solid surfaces with roughness and chemical heterogeneity. Although much research has been conducted on drop impaction on flat surfaces, much of the results can not be expected to apply to the DOD drop deposition process as the substrates encountered are often with high roughness and porosity such as paper and textiles.

In inkjet printing on paper, ink drops impacting on paper surfaces tend to spread in the direction of fiber orientation and to penetrate into size coating and then into the

pores and voids of the paper. In digital printing on textiles, impacting drops also tend to spread in the direction of fiber orientation and into the pore and voids between fibers; however, the dimensions of the capillarity and pores are much larger than those in paper. The absolute roughness R_a for inkjet paper for color printing is about 1 μm [3], and paper fibers are randomly oriented on the surface of the paper. The absolute roughness R_a for textiles is typically much larger (< 20 μm) and varies considerably, depending on the type of textile. Textiles are complex substrates. Factors affecting fabric surface characteristics include fiber parameters such as diameter (typically ranging from 10 to 30 μm), cross-section shape, material, and surface morphology, yarn parameters such as yarn diameter (typically ranging from 100 to 1000 μm) and linear density, and fabric construction. Typically, a DOD drop has the size of less than 100 μm and a single textile fiber has the size of 10 – 30 μm. Compared to drop impaction on flat surfaces, the dynamics of drop impaction on textiles thus highly depend on local surface characteristics. In closer, the interaction between a DOD inkjet drop and a single or several textile fiber(s) dominates the DOD drop impaction process.

No refereed literature was found on drop impaction dynamics on textile substrates, including inkjet drop. Park *et al*. [4, 5] attempted to visualize continuous inkjet drop impaction on a rayon fabric, but due to the limited temporal and spatial resolutions of their imaging system, no high quality images were recorded. Instead, they scaled up both the inkjet drop and textile fibers to bigger dimensions by using drop size of 2.3 mm and parallel arranged monofilament of 1.3 mm. They found that more liquid flows in the filament axial direction than in the radial direction and that the spreading and retracting shapes and maximum spreading ratios depend on impact position. Part *et al*. [24] also studied the effects of printing direction, weave structure, and finishing on image quality of lines inkjet printed on polyester woven fabric. They found that "*when ink drops impact yarns running transversely to the printing direction, wicking in the transverse direction may occur and reduce image quality*".

Although study on drop impaction on textiles has not been conducted, work has been done on observing wicking of tens of picoliter liquid on textiles. Minor and his co-workers [6-8] conducted a series of studies on the migration of liquids in textile assemblies. They investigated the effects of yarn tightness, shape of fiber cross-section, and rheological properties of liquid on wicking, which is relevant to DOD drop deposition on textiles as both spreading (forced wetting due to inertial force) and wicking (spontaneous wetting due to capillary force) processes are presented.

In this study, a high-resolution high-speed continuous imaging system was developed and was used for studying multi-DOD drop impaction on textiles. Design consideration of the setup is given in detail. The number of DOD drops deposited onto these substrates was varied and the dynamical processes of accumulation of inkjet ink, spreading and wicking were recorded.

6.2 Objective

An important application of inkjet printing is digital textile printing. Compared with inkjet paper, textiles has much higher length scale of both capillarity and porosity, which leads to dramatic differences in drop impaction and post-impaction behaviors on these two substrates. The objectives of the study discussed in this chapter are: 1) to establish an experimental approach for investigating DOD drop impaction dynamics on textile substrates; and 2) to investigate the fundamental aspects of DOD drop impaction and equilibrium inkjet ink distribution on selected textiles.

6.3 Experimental

6.3.1 Design Considerations of Imaging System

Previously, Dong *et al.* [18, 19] successfully studied DOD drop impaction on smooth surfaces. The imaging system they developed requires a high reproducibility of drop impaction dynamics so that temporally resolved images can be taken to be reassembled for representing a single DOD drop impaction process. However, this approach is not applicable if the substrate has a morphological and/or chemical unevenness at a length scale comparable to the size of a single DOD drop.

Textile substrates are complex. To visualize single DOD drop impaction on textiles, obstacles exist due to the larger dimension of surface roughness (higher than 100 μm) of textiles compared with that of DOD drop (typically less than 100 μm). This creates three uncertainties: 1) the time when a single DOD drop impacts; 2) the vertical position where a single DOD drop impacts; and 3) the impaction dynamics.

As a result, high-speed imaging system based on flash photography technique where high reproducibility is required [16] can not be used. Since the time duration of DOD drop impaction and post impaction is extremely short (< 100 μs) [18, 19], the process is also difficult to be visualized using continuous photography techniques. For example, an ultra-high speed imaging system with frame rate of 10^6 frames per second (fps) is required to give a temporal resolution of 1 μs.

Another problem is that the probability of successfully visualizing the impacting drop by a high-magnification lens system is low. For a lens system, the higher the magnification, the lower the depth of view is. Even if the lens is focused on a fixed position of a textile substrate, the uncertain impaction position of DOD drops leads to un-focused recorded images.

In this study, it was found that it was very difficult to image a single DOD drop impaction on textiles due to above reasons. However, an approach to imaging multi-DOD drop impactions on textiles was found to be feasible. It takes 2000 μs to jet a train of 20 DOD inkjet drops jetting at 10 kHz, and the spreading and wicking processes take tens of milliseconds. With more drops deposited, the liquid volume and the surface area

covered by the ink fluid increase, which lowers the requirement for the magnification of the lens and frame rate of the camera. As a result, a higher depth of view can be used, and the impaction accuracy of DOD drops is less important.

Since textile substrates have a much higher porosity than that of inkjet paper, for both graphic and non-graphic (such as printing sensors [20] and conductive patterns [21]) printing on textiles, more ink per unit area is needed. Study of multi-drop impaction on textiles can provide some basic understanding of inkjet printing dynamics on textiles. Thus, an imaging system based on a continuous photographic technique was set up to qualitatively study multi-DOD drop impaction process including ink accumulation, spreading and wicking.

6.3.2 Setup of Continuous Imaging System

A photograph of the continuous imaging system used in this study is shown in Figure 6-1. It has a resolution of 1.2 μm/pixel and can continuously record at frame rate up to 16,000 fps. Frame rates of 1000 and 2000 fps with a shutter time of 500 μs were used in this study.

The equipment consisted of the following:

I. A piezo-electric inkjet head with thirty-two, 53-μm-diameter nozzles and an actuating signal source;
II. A high resolution digital camera and lens;
III. Copper solid-state laser for delivering pulsed laser light of 25-ns duration;
IV. A one-dimensional translational stage with programmable traveling speed and scheme; and
V. A system to delay the camera and laser pulse amplitude for imaging and to control the translational stage for positioning and housing the inkjet drop.

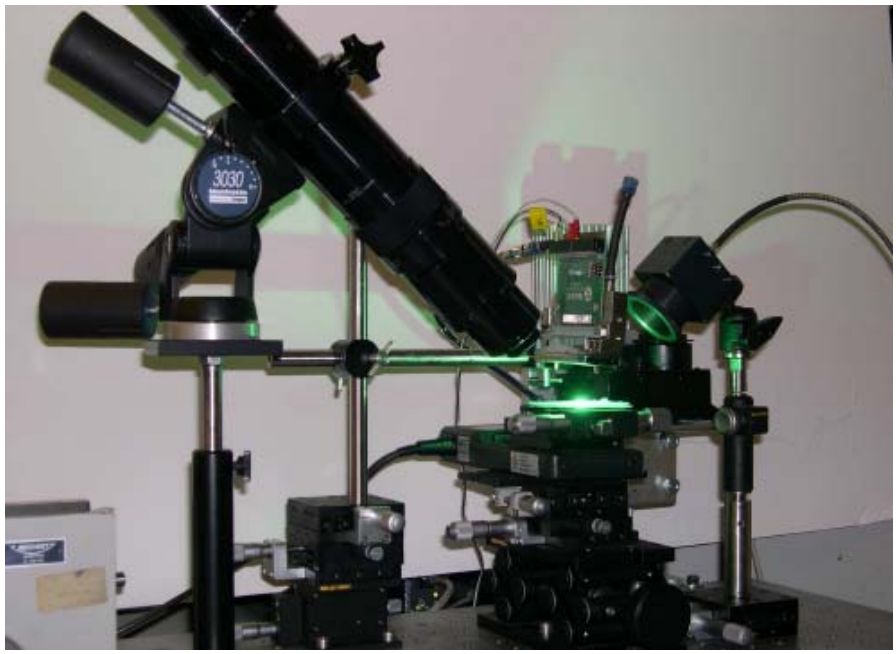

Figure 6-1: Experimental setup for continuous imaging multi-drop impaction.

As shown in Figure 6-1, the CCD camera was mounted so that it had a 45° observation angle to the plane of the substrate. A laser light was projected at almost the same angle and reflected from the substrate to the CCD camera. An example of DOD drop formation process for an actuating voltage of 27 V is shown in Figure 6-2. The clock was started at the point of the emergence of ink from the nozzle. The process of drop formation was highly reproducible for the first 130 μs. For longer times, reproducibility of the formation of satellites decreased due to the long length of the liquid ligament after the secondary breakup (at which the primary drop and the liquid ligament was separated as shown in Figure 6-2 at 75 μs). As a result, the number, sizes and velocities of satellites were different for each actuating signal. In Figure 6-2, six random chosen scenarios of the contracting liquid ligament at time of 160 μs show the

irreproducibility of the formation of satellites at high actuating voltage. However, the size and speed of the primary drop were highly reproducible.

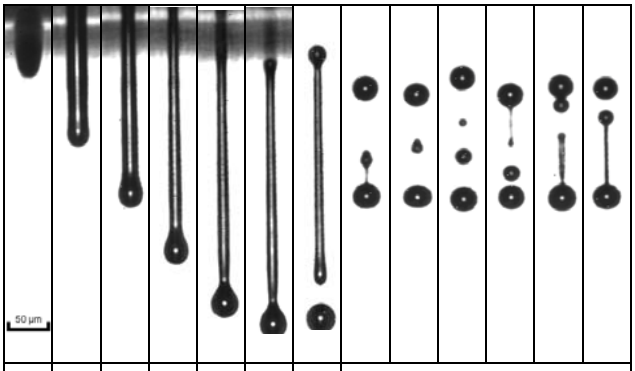

Figure 6-2: An example of DOD drop formation process at actuating voltage of 27 V, jetting frequency of 10 kHz, and waveform show in Figure 4-2. The ink was a Newtonian fluid (a mixture of glycerin (43.7 wt%), isopropanol (11.4 wt%) and DI water (44.9 wt%)) with surface tension of 32 mN/m and viscosity of 6.3 cP. The images were taken using the imaging system developed by Dong *et al.* [22].

In order to visualize the impaction and spreading dynamics of DOD drops on the substrates and to have sufficient space for the laser light to be reflected to the camera (see Figure 6-1), the distance from the nozzle to the substrate was set to be about 6.0 cm, which is much higher than the conventional operation distance. The larger separation distance affected the impact positions of the satellites, but not those of the primary drops which had a much higher speed. As a result, the satellites did not interfere with the observation of the impaction of primary drops, as illustrated in Figure 6-3. In this study, we visualized only impaction dynamics of the primary drops. For studying the final distribution of ink on the surface of the fabric for varied amount of drops, the printing distance from the nozzle to the substrate was maintained at 0.3 cm. At this printing distance, the satellites and the primary drops had the same trajectory and impacted at the same position on the substrate.

A train of actuating signals was designed using a computer-programmed waveform generator and sent to a single piezo-electrical nozzle. The number of actuating signals was varied, which corresponded to the number of primary drops impacting on the substrate. For the printhead used in this study, the drop formation process was independent of drop frequency for frequencies up to about 7 kHz. At higher frequency, the time interval, Δt, between two consecutive actuating signals was not long enough for sufficient acoustic damping in the nozzle chamber, resulting in interaction between two consecutive actuating signals. In this study, Δt, was varied, but chosen to be no less than 150 μs (frequency no higher than 6.7 kHz). By using this strategy, reproducibility of primary drop formation was achieved.

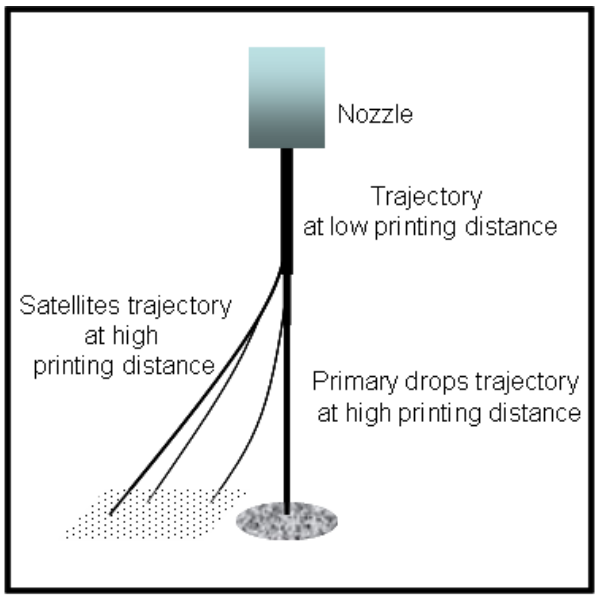

Figure 6-3: Illustration of trajectories of primary drops and satellites.

6.3.3 Preparation of Inkjet Inks and Textile Substrates

The properties of the three inks (two pigmented inkjet inks and distill water) use in this study are given in Table 6-1. The shear viscosity and static surface tension were measured using a Brookfield Part No. LVDVI+ Couette viscometer at shear rate of 52.3 s^{-1} and temperature of 22°C and a KRUSS Bubble Pressure Tensiometer BP2 with capillarity of 1.110 mm at temperature of 23°C, respectively.

Plain woven fabrics with two different materials, cotton and polyester filament, from Testfabrics, Inc. was used as textile substrates. The two fabrics were bleached, mercerized combed cotton broadcloth and filament polyester Oxford weave. A schematic of the cross-section of a plain woven fabric is shown in Figure 6-4. For comparison, Epson high quality inkjet paper was also used.

Table 6-1: Properties of inkjet ink samples used for DOD drop deposition on textiles

# of inks	Surface tension, mN/m	Viscosity, cP	Pigment, % w/w	Dispersion mechanism
1	73	1.0	0	N/A (DI water)
2	33	4.5	5	electrosteric
3	34	5.8	1.5	electrostatic

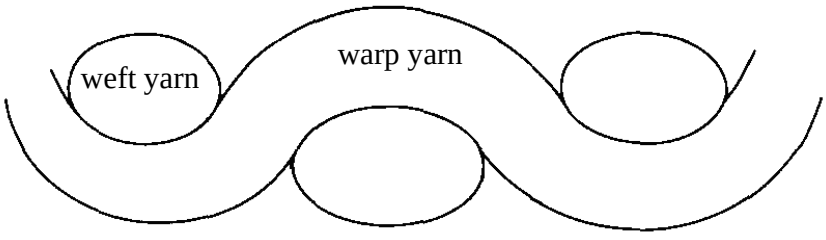

Figure 6-4: Schematic of the cross-section of a plain woven fabric.

For the cotton fabric, yarn size in both warp and filling directions was 40's c.c., and the thread count is 133×72, which means that in the warp direction, there were 133 yarns/inch, and in the filling direction, there were 72 yarns/inch. For the polyester fabric, the yarn size was 250 denier in both warp and filling directions, and the thread count was 56×40. The SEM pictures for both samples are shown in Figure 6-5. Due to the short length of the cotton fibers, fibers protruded from the surface of the cotton yarns, creating a "hairy" fabric.

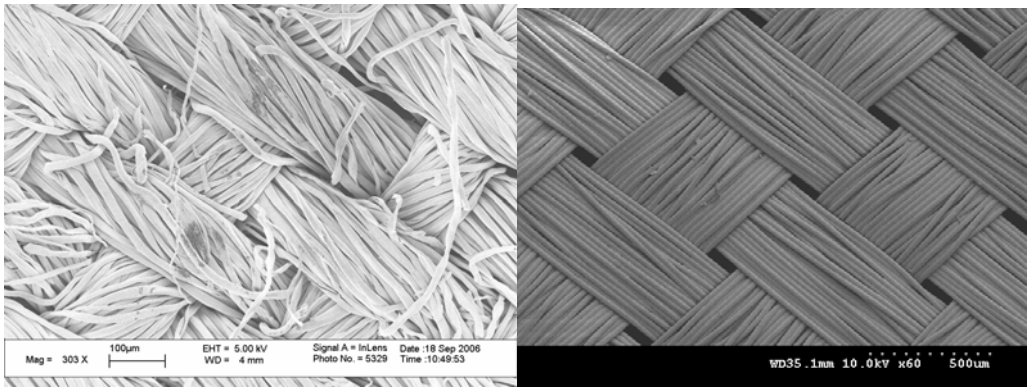

Figure 6-5: SEM pictures for: (left) bleached, mercerized combed cotton broadcloth and (right) filament polyester oxford weave.

6.4 Results and Discussion

6.4.1 Dynamics of DOD Drops Impacting on Inkjet Paper and Textiles

A series of 40 primary drops made of Ink 3 (see Table 6-1) were impacted on inkjet paper, cotton fabric and polyester fabric. The total ink deposited in each case was 1.1 nanoliters. The drops (diameter of 37 µm and speed of 6.1 m/s) were jetted at a frequency of 6.7 kHz, so the time, Δt, between two consecutive actuating signals was 150

μs. The digital camera frame rate and the shutter time were 1000 fps and 500 μs, respectively.

Images taken at a series of times for the accumulation of all 40 drops is shown in Figure 6-6. Time was measured starting at the last frame prior to the first impaction on the substrate. Due to the uncertainty of when the first drop hits the substrate, the first frame with drops may contain one to seven drops. When time reaches 6 ms, all 40 drops will have impacted the substrate.

For all three substrates, as drops accumulated, the diameter of liquid mass increased and the edges were confined by the local surface morphology. The main liquid mass on inkjet paper (Figure 6-6, (a)) appears oval for all 6 images. Note that the camera was arranged to have a 45 degree observation angle to the plane of the substrate. Thus the actual vertical dimension is $\sqrt{2}$ larger than appears in the photograph. When the vertical dimension is increased by this factor, the liquid mass resembles an irregular circle. For the cotton fabric (Figure 6-6, (b)), the drops were deposited on a warp yarn (running in the vertical direction of the images). The fibers acted as barriers for spreading. Due to the fibers' orientation in the vertical direction, the liquid mass spread more in that direction. For the polyester fabric (Figure 6-6, (c)), the drops were deposited on a weft yarn (running in the horizontal direction of the images) with a position very close to the intersection between a warp yarn and a weft yarn. As shown in Figure 6-6 at 2 ms, the accumulated liquid spread to the fibers in the warp yarn, but further spreading in that direction was inhibited by the vertically oriented warp fibers which acted as barriers. As a result, the deposited drops spread more to the left direction in the images where there were no such barriers.

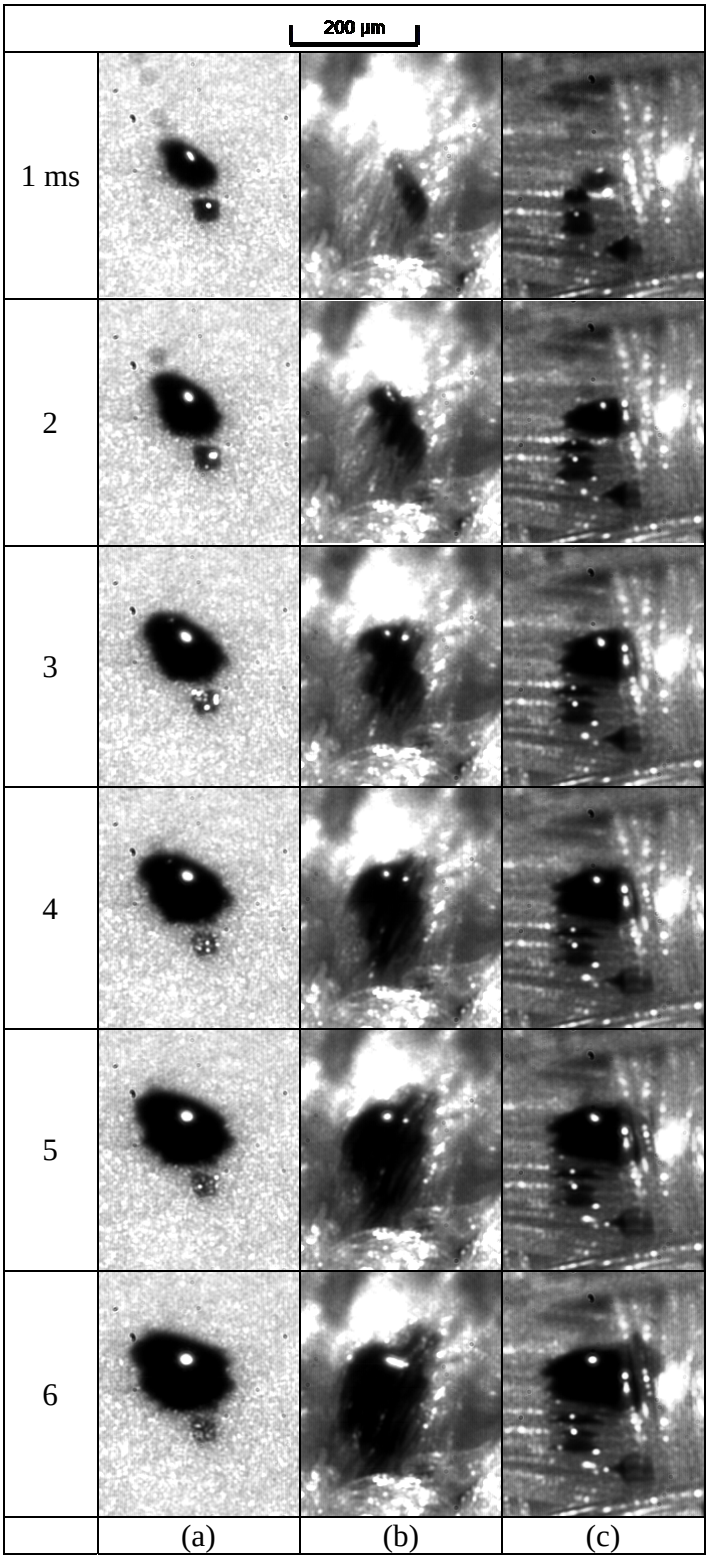

Figure 6-6: First 6 ms of accumulation of a series of 40 primary drops on: a) high quality inkjet paper, b) cotton fabric and c) polyester fabric, respectively. Note that the camera was arranged to have a 45 degree observation angle to the plane of the substrate.

When time reached 6 ms, all 40 drops have impacted the substrate and the impact process driven by inertia was over. Liquid movement was then driven by capillary forces until the ink reached to its final position. Images of the substrate surface at various times are shown in Figure 6-7. The area colored by the ink increased with time for all substrates, but reached the final value much quicker for the inkjet paper.

For inkjet paper, ink spread over the surface in all directions and wicked into the substrate. The fabrics had a much higher mean surface roughness with individual fibers tending to run in the directions of the warp and weft yarns which affected the direction of capillary flow and the pigment distribution (as shown in Figure 6-7, 121 ms). For both fabrics, the ink on the warp yarn flowed in the vertical direction while the ink on weft yarn flowed in the horizontal direction. For polyester fabric (as shown in Figure 6-7, part (c)), at 6 ms, much of the liquid mass was positioned on a weft yarn (on left) which intersected with a warp yarn (on right). A small amount of the liquid was on a few fibers in the warp yarn. When time reached 121 ms, however, more liquid mass was distributed on the warp yarn.

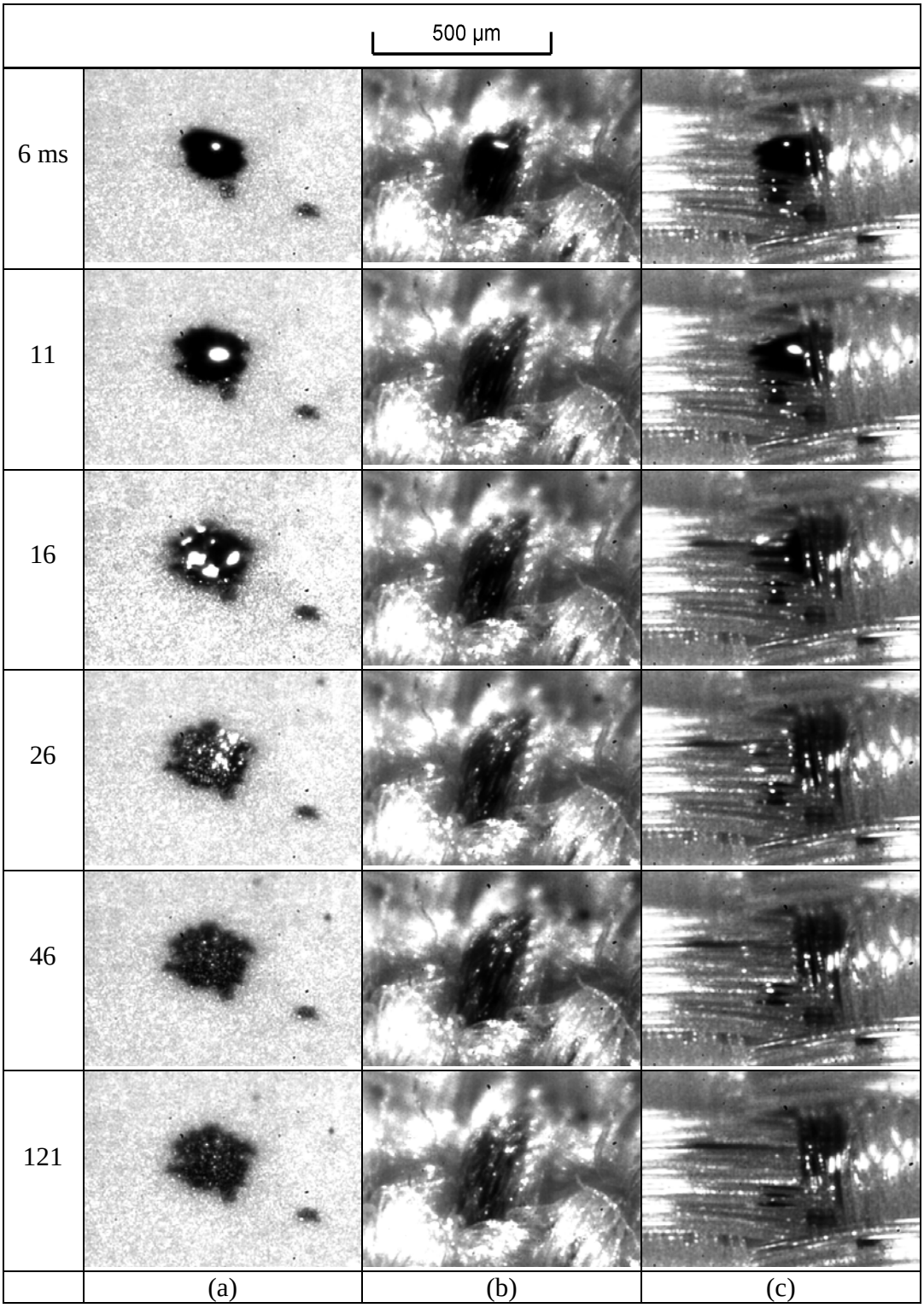

Figure 6-7: Further spreading of the 40 primary drops to the final position on: a) high quality inkjet paper, b) cotton fabric and c) polyester fabric, respectively.

6.4.2 Final Ink Distribution on Inkjet Paper and Textiles

Figure 6-8 shows a SEM picture of a 43-μm (41.6 picoliter) single DOD drop of Ink 2 (see Table 4-3) deposited on inkjet paper and on cotton fabric. No satellite was produced in the drop formation process. The circles in the middle of the pictures indicate the size of the DOD drop. The ink distributions on inkjet paper resembled an irregular circle with diameter approximately doubled that of the impacting drop. The ink distribution for the cotton fiber is not circular. The cotton fiber size is about 20 ± 10 μm and the yarn size is about 200 μm. The size of the DOD drop is about the size of 2 to 3 fibers, including the gap between neighboring fibers, and the yarn size is about 4.7 times bigger than the ink drop. The distribution of the pigment on the surface of the fibers gives a hint for the direction of the spreading process. The impacting ink drops spread further along the fiber direction than in the transverse direction. The fibers acted as a barrier for transverse spreading. This observation agrees well with the phenomena discussed below for the cases of multi-drop impaction on fabrics.

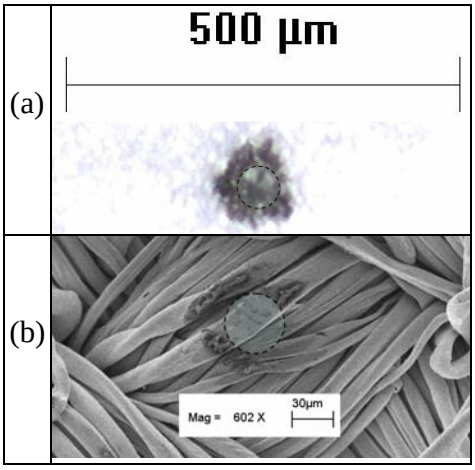

Figure 6-8: Optical microscope picture (a) and SEM picture (b) of a single DOD drop of 43-μm diameter deposited on high quality inkjet paper (top) and cotton fabric (bottom). The dashed circles represent the size of a single drop.

Final ink distribution was studied varying the amount of Ink 3 deposited on cotton fabric and inkjet paper. The printing distance between the nozzle and the substrate was

0.3 cm so that primary drops and satellites were deposited on the same position. Figure 6-9 shows the dried pattern of 20, 40, 60, 80, and 100 drops (approximately 1.1, 2.2, 3.3, 4.4, 5.5 nanoliters, including satellites) deposited on the inkjet paper and Figure 6-10 shows 20, 60, 100 drops (approximately 1.1, 3.3, 5.5 nanoliters, including satellites) deposited on the cotton fabric. The jetting frequency was 1 kHz.

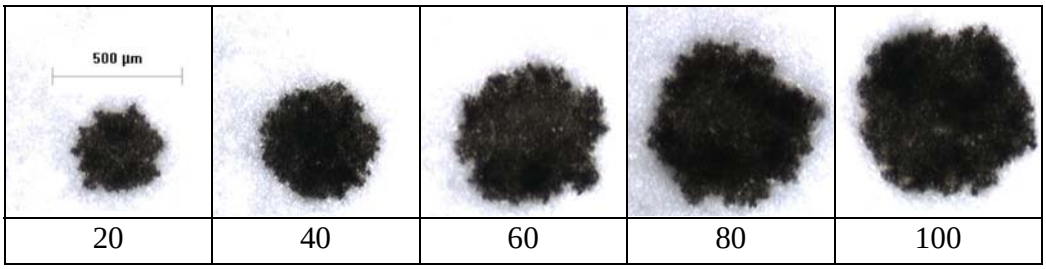

20	40	60	80	100

Figure 6-9: Varied amount of ink deposited on high quality inkjet paper. The number of drops deposited is shown below the image.

The final ink distributions on inkjet paper resembled irregular circles, with their size increasing as the number of drops increased. The final ink distribution on the cotton fabric was greatly affected by the fabric structure, that is, the yarn direction and intersections. The ink tended to stay on one yarn as drops accumulated until excess ink moved to neighboring yarns. As the number of drops increased, the change in the ink distribution on the cotton fabric was mainly the increasing distance over which the ink spread along the yarns.

Figure 6-11 shows three randomly chosen pictures of 100 drops deposited onto the cotton fabric after drying. The distribution of ink depended on the impaction location on the fabric, and the patterns on the three fabrics were different. While the patterns were different, in all three cases, the movement of liquid was along yarns. Sometimes when yarns intersected, some of the ink moving along the yarn changed directions and moved along the intersecting yarn.

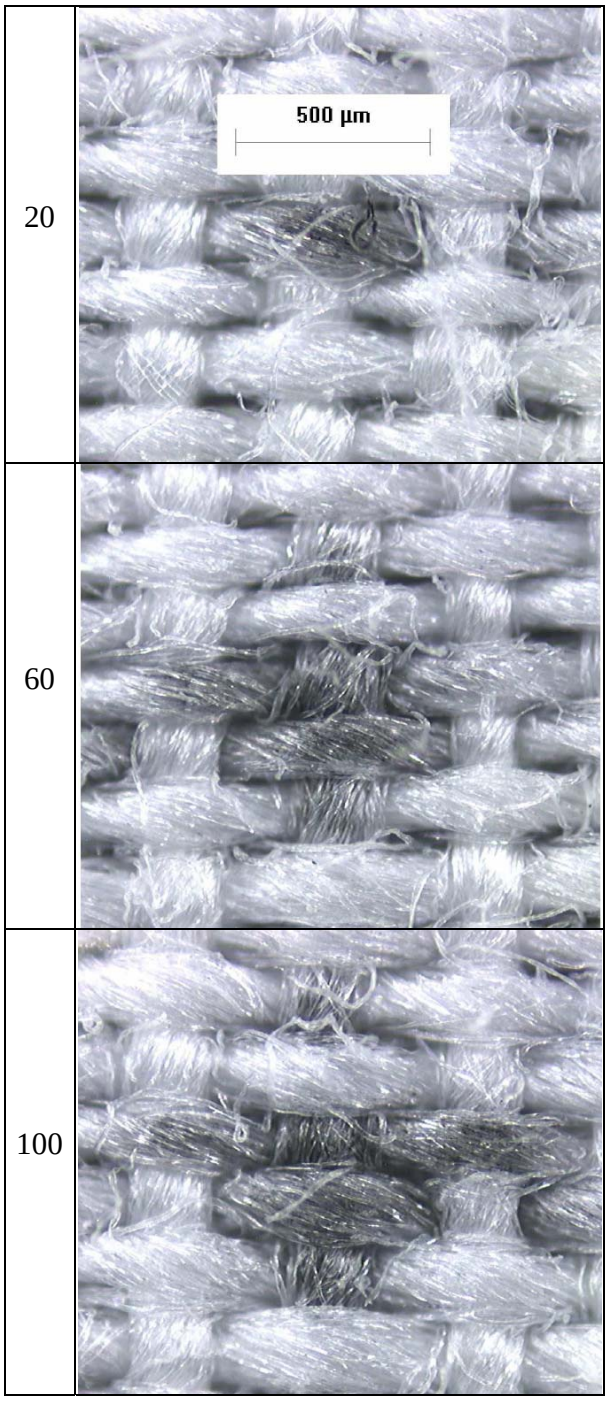

Figure 6-10: Varied amount of DOD drops deposited on the cotton fabric. The number of drops deposited is shown next to the image.

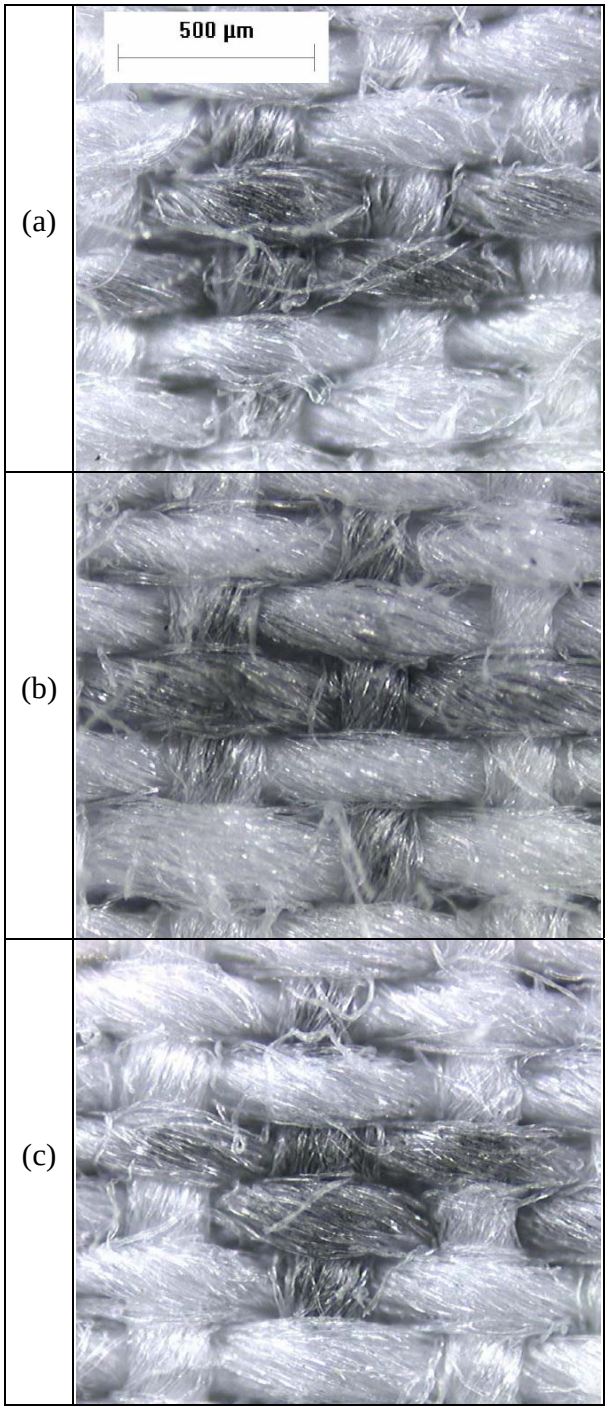

Figure 6-11: Three random chosen cases of 100 drops (including satellites) depositing on cotton fabric.

6.4.3 Role of Yarn Hairiness on Digital Printing on Textiles

As mentioned earlier, due to the short length of the cotton fibers, fibers protrude from the surface of the cotton yarns, creating a "hairy" fabric. These fibers can affect the final ink distribution. Figure 6-12 shows inkjet printed water drops (Ink 1 in Table 6-1) captured by a surface fiber. In case 1, the captured water had a clam-shell shape [17], and remained on the fiber. In some instances, the accumulated water fell from the fiber onto the fabric, as illustrated by case 2 in Figure 6-12.

In both cases shown in Figure 6-12, ink distribution was affected by a surface fiber. In case 1, ink remained on the fiber and did not reach the intended location. While for case 2, the final location of the accumulated ink may be affected by the orientation, diameter, length, and stiffness of the fiber. Figure 6-13 gives several examples for the two cases observed in inkjetting Ink 2 in Table 6-1 onto cotton fabric. All the pictures were taken after the ink was dry. For images (a) and (c), 4 and 6 drops, respectively, were captured and remained on surface fibers. As a result, the fibers were coated with pigment. For image (e), it appears that only part of the captured drops remained on the fiber and the rest fell down to the fabric. The portion left on the fiber dried and formed a barrel-shape [17] pigment body, and the part that fell can be seen as a grey region on the fabric. As a comparison, images (b), (d), and (f) show final ink distribution when the drops were deposited directly to the fabric.

Quéré *et al.* [23] conducted experimental investigation on the dynamics of drops impacting on horizontal fibers. A threshold impact velocity was quantified for identifying whether or not small enough drops can be captured by a fiber. For inkjet ink which has a low viscosity, the threshold velocity depends on inertia, the drag of the fiber, gravity and capillary forces. However, for a drop larger than a critical radius, it cannot be captured no matter what its velocity is. The experimental data obtained in this study indicate that for all three inks tested, a single DOD drop (diameter of less than 50 μm and

speed of less than 10 m/s) was always captured by the protruded fibers (diameter in between 10 to 30 μm). As more and more drops accumulated on the fiber, the size of the liquid body increased until part or all of the liquid body separated from the fiber.

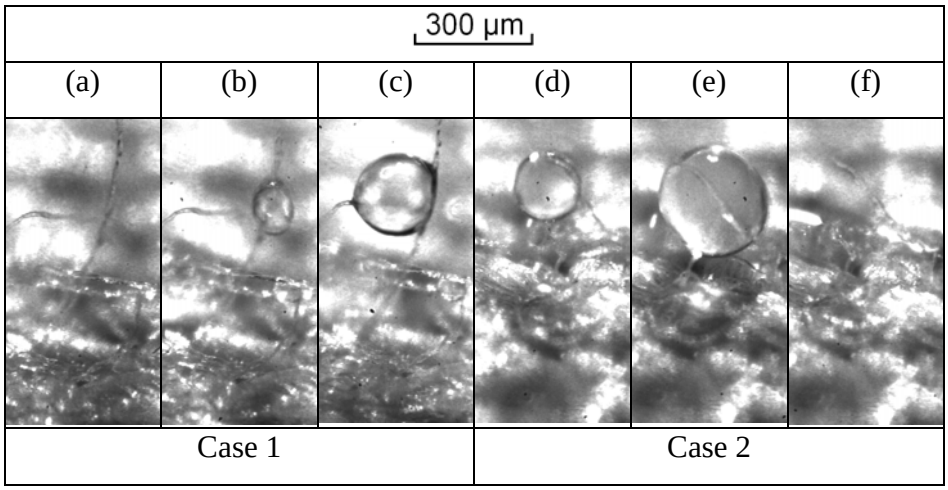

Figure 6-12: DOD drops captured by surface fiber on the cotton fabric. Case 1: images (a), (b) and (c) show before, intermediate and after the accumulation of captured drops on a fiber, respectively. Case 2: images (d), (e) and (f) show intermediate, state of maximized captured drop volume, and state after captured drop fallen down onto the cotton fabric, respectively.

Number of drops	Drops captured by surface fiber	Drops not captured by surface fiber
4	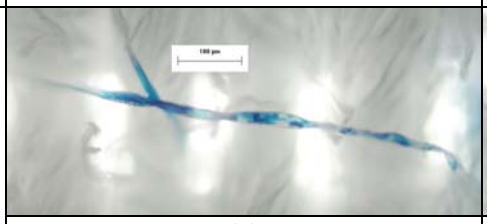	
	(a)	(b)
6	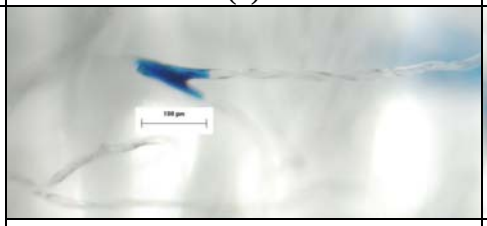	
	(c)	(d)
8	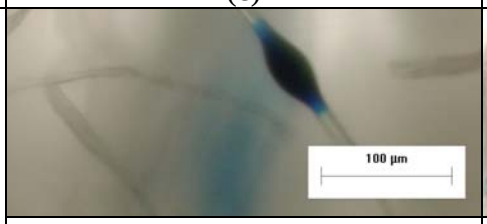	
	(e)	(f)

Figure 6-13: Effect of surface fiber on final ink distribution on cotton fabric. All the scale bars shown in the images represent 100 µm.

6.5 Conclusions

A high-speed high-magnification continuous imaging system was developed for imaging multi-DOD drop impaction on textile substrates. Various numbers of drop-on-demand inkjet drops were deposited on textile fabrics, and the process was visualized. As a comparison, experiments were also conducted on a high quality inkjet paper under the same conditions. Dynamics of DOD drops accumulation and spreading on the substrates and final ink distribution show drastic differences between digital printing on textiles and paper. The final ink distribution on inkjet paper resembled irregular circles, with their size increasing as the number of drops increased. The final ink distribution on fabric was greatly affected by the fabric structure, that is, the yarn direction and intersections. The ink tended to stay on one yarn as drops accumulated until excess ink moved to neighboring yarns. As the number of drops increased, the primary change in the ink distribution on the cotton fabric was the increasing distance over which the ink spread along the yarns. Fibers protrude from the surface of the cotton yarns, creating a "hairy" fabric. These fibers can affect the distribution of ink on the fabric.

6.6 References

1. Worthington, A. M., Proc. R. Soc. Lond. 25, 261 (1876).
2. Yarin, A. L., Annu. Rev. Fluid Mech. 38, 159 (2006).
3. Range, K. and Feuillebois, F., J. Colloid Interface Sci. 203, 16 (1998).
4. Park, H., Carr, W. W., and Zhu, J., Final Program and Proceedings of IS&T's NIP 18, 620 (2002).
5. Park, H., Drop Impingement and Interaction with a Solid Surface, Doctorial dissertation, Georgia Institute of Technology, Atlanta, (2003).
6. Minor, F.W., Schwartz, A.M., Wulkow, E.A., and Buckles, L. C., Textile Res. J. 29, 931 (1959).
7. Minor, F.W., Schwartz, A.M., Buckles, L. C., Wulkow, E.A., Marks, M. P., and Fielding, G. H., Textile Res. J. 31, 525 (1961).
8. Minor, F.W., Schwartz, A.M., Buckles, L. C., Wulkow, E.A., Marks, M. P., and Fielding, G. H., Textile Res. J. 32, 140 (1962).
9. Tippett, B.G., International Conference on Digital Production Printing and Industrial Applications: Final Program and Proceedings, 276 (2003).
10. Sarma, D., Textile World 154, 42 (2004).
11. Hees, U., Freche, M., Kluge, M., Provost, J., and Weiser, J., Final Program and Proceedings of IS&T's NIP 19, 626 (2003).
12. Kiatkamjornwong, S., Putthimai, P., and Noguchi, H., Surface Coatings International Part B: Coatings Transactions 88, 25 (2005).
13. Sarma, D. and Liker, S., Final Program and Proceedings of IS&T's NIP 21, 245 (2005).
14. Le, H., International Conference on Digital Production Printing and Industrial Applications: Final Program and Proceedings, 159 (2005).

15. Kruger, C., Dieleman, C., Kluge, M., Provost, J., and Weiser, J., Final Program and Proceedings of IS&T's NIP20, 610 (2004).
16. Ray, S. F. and British Association for High Speed Photography, High speed photography and photonics, Bellingham, Wash.: SPIE Press. xxi, 402 (2002).
17. McHale, G. and Newton, M. I., Colloid Surf. A: Physicochem. Eng. Asp. 206, 79 (2002).
18. Dong, H., Drop-on-demand inkjet drop formation and deposition, Doctorial dissertation, Georgia Institute of Technology, Atlanta, (2006).
19. Dong, H., Carr W. W., Bucknall D. G., and Morris, J. F., AICHE J. 53, 2606 (2007).
20. Sawhney A, Agrawal A, Lo T. C, et al., AATCC Rev. 7, 42 (2007).
21. Bidoki S. M., McGorman D., Lewis D. M., et al., AATCC Rev. 5, 11 (2005).
22. Dong, H., Carr, W. W., and Morris, J. F., Rev. Sci. Instrum.77, 85101 (2006).
23. Lorenceau, E., Clanet, C., and Quéré, D., J. Colloid Interface Sci. 279, 192 (2004).
24. Park, H., Carr, W.W., Ok, H., and Park, S., Textile Res. J. 76, 720 (2006).

CHAPTER 7

CONCLUSIONS AND RECOMMENDATIONS

7.1 Conclusions

The first part of the study was focused on the rheological properties and DOD drop formation dynamics of surface-modified carbon-black pigmented water-based inkjet inks. A capillary viscometer was designed, constructed, and used to measure the shear rate dependent viscosity of inkjet inks with shear rates up to $2\times10^5\ s^{-1}$. The inkjet ink samples with similar low-shear-rate viscosity exhibited significantly different shear viscosities at high shear rates depending on particle loading. A commercially available Couette viscometer was utilized to measure the temperature and time dependent viscosities of inkjet inks. The temperature dependent viscosity data indicate that the viscous heating effect was insignificant in the measurement of the shear rate dependent viscosity of the tested samples. The inkjet ink samples with sufficiently high pigment loading (~ 18.0 vol%) were found to show time-dependent shear viscosity. The shear rate and time dependent viscosity is attributed to the change of suspension microstructure. It is conjectured that weakly structured agglomerates exist in the suspension and they break down under shearing.

The high-speed imaging system based on flash photography technique originally developed by Dong *et al.* [1] was modified to study DOD drop formation dynamics of pigmented inkjet inks. Although the jettability of pigmented inkjet inks was much lower than that of the pure fluid, once they were jetted successfully, the reproducibility of DOD drop formation was very high. The overall DOD drop formation dynamics of a inkjet ink with pigment loading of 15.0 vol% was compare with those of a pure Newtonian fluid and a pigmented ink with pigment loading of 4.7 vol%. The three inks had similar low-

shear-rate shear viscosities, but significantly different high-shear-rate shear viscosities. Overall DOD drop formation dynamics were very similar. A proposed explanation for these observations is that the shearing time during DOD drop ejection is insufficient for changing and stabilizing the microstructure of the suspension. Thus the shear viscosity exhibited during DOD drop formation is similar to the low-shear-rate shear viscosity.

DOD drop formation involves temporally and spatially highly unsteady flow field with 1) time scale less than 100 μs, 2) length scale less than 100 μm, and 3) temporally fast varied high shear rate and rate of surface dilatational deformation. Fluid properties/behavior obtained using instruments/devices, such as rheometer, bubble pressure tensiometry, and liquid bridge, may not be applicable to DOD drop formation dynamics because the time scales of the measurements may be quite different from those occurring in DOD drop formation. Thus direct observation using the high-speed imaging system is necessary to determine the effects of complex fluids on DOD drop formation dynamics.

The second part of the research contributed to the understanding of the effects of signal amplitude and jetting frequency of actuating waveform on DOD drop formation of a Newtonian fluid with shear viscosity of 6.3 cP and surface tension of 32 mN/m. As signal amplitude was increased, the evolution of the shape of the ejected liquid thread was the same except that the thread length was longer when the signal amplitude was higher. It was found that both the first and second breakup times and the primary drop size were independent of signal amplitudes. The satellite formation was due to end-pinching at the lower voltage amplitudes, but as voltage amplitude was increased, the ligament length increased, and multiple breakup occurred, apparently due to wave-like instability. The reproducibility of evolution of the secondary liquid thread became very low once voltage amplitude was increased to a level where the wave-like instability breakup occurred. When jetting frequency is sufficiently high, it affected the volume and speed of the ejected liquid body.

When the nozzle went from idle to jetting for frequencies lower than 6.7 kHz, the drop triggered by the first pulse was found to be identical to subsequent drops in the sequence and independent of jetting frequency. However, at jetting frequencies higher than 6.7 kHz, DOD drop formation after idle varied over the first four pulses. A modulating pulse added before the first pulse eliminated the variation in drop formation at the higher jetting frequencies.

In the last part of the research, the important features of impaction and post-impaction dynamics of multi-DOD drop on inkjet paper and textiles were investigated. The final ink distribution on inkjet paper resembled irregular circles, with their size increasing as the number of drops increased. The final ink distribution on fabric was greatly affected by the fabric structure, that is, the yarn direction and intersections. The ink tended to stay on one yarn as drops accumulated until excess ink moved to neighboring yarns. As the number of drops increased, the primary change in the ink distribution on the cotton fabric was the increasing distance over which the ink spread along the yarns. Fibers protrude from the surface of the cotton yarns, creating a "hairy" fabric. These fibers can affect the distribution of ink on the fabric.

7.2 Recommendations

In this dissertation research, surface-modified carbon-black pigmented water-based inkjet inks were used for studying DOD drop formation of complex fluids. For this particular colloidal suspension, we conjecture that the DOD drop formation process imposes insufficient shearing time for changing and stabilizing the microstructure of the suspension. It is extremely hard to verify this conjecture directly by experiments. We recommend utilizing other complex fluids systems including steric-dispersed colloidal particle suspension and dilute or semi-dilute polymeric solutions for further investigation. The strength of the forces holding the microstructure together is different for various

complex fluids, leading to differences in response of microstructure to shear stress and shearing time. As a result, the bulk response of complex fluids to inkjet jetting process may vary. For example, the elongation viscosity of polymeric solution is affected by molecular weight and structure. Industrial studies [6] indicate that for polymers with linear chain morphology, higher molecular weight leads to longer length of ejected liquid thread and higher irregularity of satellite formation. We recommend studying the effect of molecular weight and polymer structure on DOD drop formation dynamics of polymeric solution.

The average rate of surface dilatational deformation was found to be between 20,000 and 30,000 s^{-1} during the ejection process, indicating the surface of the ejected liquid thread is under highly dynamic conditions. Typical inkjet inks contain surfactants for adjusting surface tension; however, with such a high average rate of surface dilatational deformation, significant change of surface concentration of surfactant may be expected. As a result, it is conjectured that dynamic surface tension (DST) could be significantly different for different inkjet inks. Although DST can be measured with bubble pressure tensiometry [2, 3, 4] with surface aging to the sub-millisecond range, it is still not compatible to the average rate of surface dilatational deformation occurred during DOD drop formation. We recommend comparing DOD drop formation dynamics of three Newtonian fluids which have similar shear viscosity, density, and acoustic wave speed, yet different static/dynamic surface tensions. Fluid 1 can be prepared using water, glycerin, and 1-propanol; as a result, its DST is independent of surface aging and is the same as static surface tension (~ 30 mN/m). Fluid 2 can be prepared using water, glycerin, and surfactant such as Tergital®, which has a DST different from static surface tension (~ 30 mN/m). Fluid 3 can be prepared using water and glycerin, which has the same DST as its static surface tension (~ 70 mN/m).

The multi-drop deposition study in Chapter VI indicates three key stages exist in different time scales: 1) impaction and accumulation of inkjet drops (~ O(1 ms)), 2)

capillary spreading in the open microfluidic grooves (~ O(10 ms)), and 3) drying of deposited inkjet inks (~ O(1000 ms)). Studying the impaction dynamics on textiles is difficult due to poor reproducibility of observations resulting from the variability of the textile structure. We recommend using the continuous imaging system discussed in Chapter VI to study the dynamics of capillary spreading of inkjet deposited drops on textile-like structures and open microfluidic channels. Surfaces with well defined morphology such as trenches and wells can be fabricated on silicon wafer based on lithography technique. For the effect of surface energy on capillary spreading, the surface of the structured rough surface can be coated with gold and then treated with self assembled monolayers (SAMs) [5] to adjust surface energy.

7.3 References

1. Dong, H., Carr, W. W., and Morris, J. F., Rev. Sci. Instrum.77, 85101 (2006).
2. Fainerman, V. B., Makievski, A. V., and Miller, R., Rev. Sci. Instrum. 75, 213 (2004).
3. Fainerman, V. B. and Miller, R., Adv. Colloid Interf. Sci., 108-109, 287 (2004).
4. Miller, R., Private communication.
5. Dong, H., Drop-on-demand inkjet drop formation and deposition, Doctorial dissertation, Georgia Institute of Technology, Atlanta, (2006).
6. Letendre, W., Private communication.

APPENDIX A

SIGNIFICANCE OF VISCOUS DISSIPATION DURING CAPILLARY VISCOMETRY MEASUREMENTS

In this appendix, a simple analysis is made to estimate the maximum temperature increase over the length of the capillary due to viscous dissipation.

In the capillary viscometer designed and constructed in this dissertation research, capillary dies with varied lengths and diameters were used. In Figure A-1, a schematic of the geometry of a capillary die is shown. The inkjet ink flows through the capillary as indicated by the arrow.

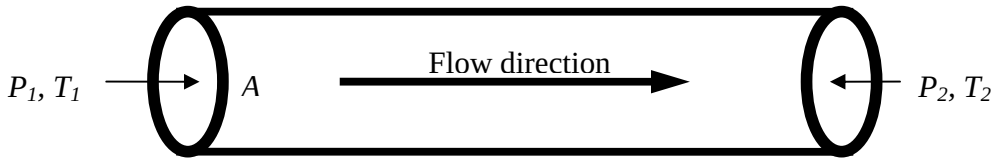

Figure A-1: Schematic of the capillary die.

The following assumptions are made: 1) the capillary die does not lose heat to the surrounding air; 2) conduction in the direction of flow is negligible compared with convection; 3) the heat capacity of the capillary die is negligible; 4) end effects are negligible; and 5) the fluid temperature is constant over the cross section of the capillary die. Using these assumptions, the following energy balance can be derived for the fluid flowing through the capillary:

$$Rate\ of\ energy\ flowing\ in + Rate\ of\ energy\ generated = Rate\ of\ energy\ flowing\ out$$

where

$$Rate\ of\ energy\ flowing\ in = \dot{m}C_P T_1,$$

$$Rate\ of\ energy\ flowing\ out = \dot{m}C_P T_2,$$

$$Rate\ of\ energy\ generated = Q(P_1 - P_2),$$

where $\dot{m}$ is the mass flow rate, C_P is the heat capacity of the fluid, Q is the volumetric flow rate, T is fluid temperature and P is fluid pressure.

By using $\dot{m} = \rho Q$, where ρ is the density of the fluid, substituting the relationships given above, and rearranging, the following equation can be obtained:

$$\Delta T = T_1 - T_2 = \frac{(P_1 - P_2)}{\rho C_p} = \frac{\Delta P}{\rho C_p}$$

In the above derivation, we assumed that C_P and ρ do not vary with temperature, and they were evaluated at room temperature.

For the tests conducted in this study, the maximum pressure across the capillary die was 2.4×10^6 Pa (345 psi). Using this value of ΔP, ΔT was determined to be less than 1 K or 1 °C. According to Figure 2-12, the decrease of shear viscosity is insignificant for a temperature change of 1 K.